ARMY RESEARCH LABORATORY

Extended Desert Calculation Results With Comparisons to PRISCILLA Experimental Data and a Near-Ideal Calculation

Charles E. Needham
Robert G. Ekler
Lynn W. Kennedy

ARL-CR-235 July 1995

prepared by

S-Cubed, a Division of Maxwell Laboratories, Inc.
2501 Yale Boulevard, SE, Suite 300
Albuquerque, NM 87106

under contract

DAAL01-94-P-1217

NOTICES

Destroy this report when it is no longer needed. *DO NOT return it to the originator.*

Additional copies of this report may be obtained from the National Technical Information Service, U.S. Department of Commerce, 5285 Port Royal Road, Springfield, VA 22161.

The findings of this report are not to be construed as an official Department of the Army position, unless so designated by other authorized documents.

The use of trade names or manufacturers' names in this report does not constitute endorsement of any commercial product.

REPORT DOCUMENTATION PAGE

Form Approved
OMB No. 0704-0188

1. AGENCY USE ONLY (Leave blank)	2. REPORT DATE	3. REPORT TYPE AND DATES COVERED
	July 1995	Final, Jan 94–Mar 95

4. TITLE AND SUBTITLE

Extended Desert Calculation Results With Comparisons to PRISCILLA Experimental Data and a Near-Ideal Calculation

5. FUNDING NUMBERS

C: DAAL01-94-P-1217
4G061-415-U2
4G061-515-U2

6. AUTHOR(S)

Charles E. Needham, Robert G. Ekler, and Lynn W. Kennedy

7. PERFORMING ORGANIZATION NAME(S) AND ADDRESS(ES)

S-Cubed, a Division of Maxwell Laboratories, Inc.
2501 Yale Boulevard, SE, Suite 300
Albuquerque, NM 87106

8. PERFORMING ORGANIZATION REPORT NUMBER

SSS-DFR-94-14920

9. SPONSORING/MONITORING AGENCY NAME(S) AND ADDRESS(ES)

U.S. Army Research Laboratory
ATTN: AMSRL-WT-NC
Aberdeen Proving Ground, MD 21005-5066

10. SPONSORING/MONITORING AGENCY REPORT NUMBER

ARL-CR-235

11. SUPPLEMENTARY NOTES

The point of contact for this report is Richard E. Lottero, U.S. Army Research Laboratory, ATTN: AMSRL-WT-NC, Aberdeen Proving Ground, MD 21005-5066. Computer time supplied by Headquarters, Defense Nuclear Agency.

12a. DISTRIBUTION/AVAILABILITY STATEMENT

Approved for public release; distribution is unlimited.

12b. DISTRIBUTION CODE

13. ABSTRACT *(Maximum 200 words)*

An extended calculation of the non-ideal airblast environment resulting from the PRISCILLA nuclear detonation has been completed. This calculation used the most recent, accepted interpretation of the experimentally determined thermal layer model.[1] The calculation included the effects of turbulence, surface roughness, and dust sweep-up in determining the near-surface blast environment. Full hydrodynamic definition of the precursor environment is now available from ground zero to a distance of over two kilometers. Information includes full spatial definition at selected times (about 25) and full-time, resolved waveforms at over 1,000 locations. the results of the calculation are compared with experimental data and show good to excellent agreement in all measured parameters.

An accompanying calculation without a thermal layer was also extended to over a two-kilometer range. This calculation served as the "ideal" case. The "ideal" calculation included the effects of surface roughness and turbulence but not an interaction with a thermal layer or dust sweep-up. Results of this calculation are used to quantify the differences specifically caused by thermal and dust interactions.

The excellent agreement between experiment and calculation demonstrates the degree of understanding of the physics involved in blast propagation over real surfaces. This understanding of the free-field environment is the necessary first step to predicting loads and response of vehicles or other targets subjected to such an environment.

14. SUBJECT TERMS	15. NUMBER OF PAGES
non-ideal blast, dynamic pressure impulse, nuclear blast, airblast, dust, turbulence, thermal precursor	108
	16. PRICE CODE

17. SECURITY CLASSIFICATION OF REPORT	18. SECURITY CLASSIFICATION OF THIS PAGE	19. SECURITY CLASSIFICATION OF ABSTRACT	20. LIMITATION OF ABSTRACT
UNCLASSIFIED	UNCLASSIFIED	UNCLASSIFIED	UL

INTENTIONALLY LEFT BLANK.

FOREWORD

This work was performed for the U.S. Army Research Laboratory (ARL) under Contract DAAL01-94-P-1217. The calculations were made using the latest version of the S-Cubed Hydrodynamic Advanced Research Code (SHARC). This code has been upgraded to include a version of a K-ε turbulence model, which has been modified by S-Cubed[2] for non-steady, compressible fluid flow. The turbulence model has a rough law of the wall boundary layer model[3] and a dust sweep-up model,[4] both of which were used for the desert calculation. The K-ε model and the rough law-of-the-wall were also used in the near-ideal calculation. It is the combination of high-order differencing, efficient computer algorithms, and realistic physical models that has made the agreement with experimental data possible.

We would like to acknowledge the efforts of Rich Lottero, Klaus Opalka, and Bud Raley of ARL for making this work possible, and John Keefer and Noel Ethridge of ARA for their guidance in matters of thermal layer development and experimental data interpretation.

INTENTIONALLY LEFT BLANK.

TABLE OF CONTENTS

INTENTIONALLY LEFT BLANK.

SECTION 1
BACKGROUND

This calculation is the product of over four decades of research into thermally-precursed airblast. It has been made possible by significant advances in numerical differencing techniques, physical modeling development, and computer hardware improvement. The importance of turbulence and a good boundary layer model were demonstrated during the DIAMOND ARC experiments in 1989[5].

The role of pre-shock dust has been debated for many years. The most recent calculations assume that pre-shock dust loading of the air is negligible. This is supported by several different types of observations. First, measurements of the temperature and sound speed as a function of height above desert surfaces[6] clearly show that the peak temperature occurs near the ground and decreases rapidly with height above the surface. If significant dust had been lofted, this dust would have absorbed incident radiation and caused heating of the air well above the ground. Second, photography from cameras located over two kILOMETERS from bus and truck targets[7] clearly show the buses and trucks until shock arrival. This means that the visible light, mean free-path is in excess of one kilometer and therefore, no significant absorption of radiated energy can occur in the three-meter depth of the observed dust height. Third, shock photography indicates that the precursor shock is linear and extends to very near the ground. If there were any significant enhancements of sound speed above the ground, the precursor shock would reflect the structure of the thermal layer with the front traveling faster in the highest sound speed region. This is further evidence that the thermal layer is hottest near the ground and cools rapidly with height. Fourth, arrival times measured by free-field gages and gages on structures[8] show that the signal arrival at ground level is earlier than at the three-foot elevation. Some gages on structures were only six inches above the surface. Even these gages show arrival after the ground-level gages. The shock is traveling faster at ground level than at six inches above the ground. The implication is that the hottest part of the thermal layer is less than six inches thick and that temperature decreases rapidly above that height. All of this points to negligible dust lofting prior to shock arrival.

One continuing subject for study is the observed fact that a precursor signal can and does travel subsonically at ranges beyond the 30-psi ideal overpressure range. This observation has not been fully utilized in this calculation and could lead to even better agreement with experiment at distances greater than one kilometer. The DIAMOND ARC arrival time data[5] indicate that the leading measured disturbance is traveling below the sound speed in the helium bag by about 30 % for all ranges beyond the 30 psi range. The implication is that sound speeds in the pre-shock thermal layer may be 30 to 50 percent greater than the measured signal velocity at ranges greater than 3500 feet for PRISCILLA. This phenomenon has been studied and reported in Reference 10 by Barthel at S-CUBED. Such an extended hot layer has not yet been used in a calculation.

SECTION 2
INITIAL CONDITIONS

The calculations described in Reference 9 were used as initial conditions for the extended calculations reported here. The "ideal" calculation was started from a time of two seconds and run to a time of four seconds.

The desert thermal layer calculation was restarted when the shock reached about 1,450 feet in ground range. The thermal layer temperature was increased to match a sensible upper bound of the experimentally-determined pre-shock thermal layer temperature and was run to a distance of 3,000 feet. The calculation indicated a shorter precursor prior to "main shock" arrival at the 3,000-foot range than was seen in the experiment, indicating that the thermal layer used in the calculation was not as hot as that which existed in the experiment. The thermal layer temperature for distances beyond 3,000 feet was re-evaluated, based on measurements interpreted from several nuclear events. The thermal layer was extended to a range of 4,300 feet. The calculation was restarted a second time at a distance of 2,500 feet and continued to four seconds and a distance of 6,000 feet. Figure 1 shows the three temperature/sound speed curves used for the three calculations. The results given in this report used the maximum of the three curves at any given distance.

Both calculations (ideal and precursed) used the S-CUBED K–ε turbulence model. This model is an extension of the usual K–ε model which uses a variable coefficient for formation and dissipation of turbulence, based on local conditions and the history of the flow. The S-CUBED modifications extend the K–ε model to compressible, non-steady flows. Both calculations used a law-of-the-wall for real surfaces in conjunction with the turbulence model. The ideal calculation used a smooth wall Clauser law-of-the-wall and the desert used a smooth wall Rubesin law-of-the-wall to represent the surface interaction.

The ideal calculation used a shock-following subgrid with 10-centemeter zones throughout most of the calculation. The precursor calculation used a similar shock following subgrid, but had 30-centemeter zones for most of the calculation duration.

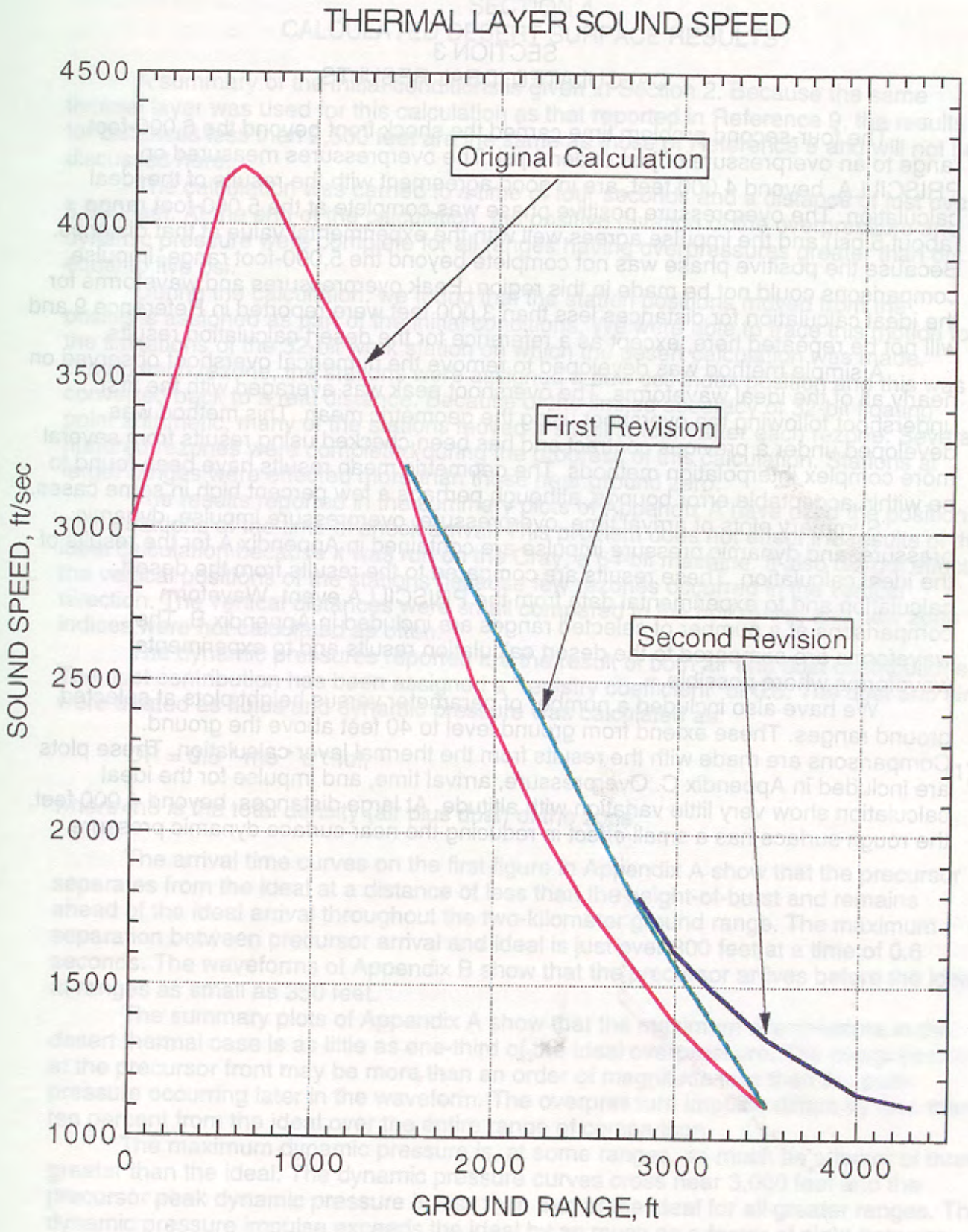

Figure 1. PRISCILLA sound speed vs. range.

SECTION 3
CALCULATED IDEAL RESULTS

The four-second problem time carried the shock front beyond the 6,000-foot range to an overpressure of just under 4 psi. The overpressures measured on PRISCILLA, beyond 4,000 feet, are in good agreement with the results of the ideal calculation. The overpressure positive phase was complete at the 5,000-foot range (about 5 psi) and the impulse agrees well with the experimental value at that distance. Because the positive phase was not complete beyond the 5,000-foot range, impulse comparisons could not be made in this region. Peak overpressures and waveforms for the ideal calculation for distances less than 3,000 feet were reported in Reference 9 and will not be repeated here, except as a reference for the desert calculation results.

A simple method was developed to remove the numerical overshoot observed on nearly all of the ideal waveforms. The overshoot peak was averaged with the first undershoot following the overshoot using the geometric mean. This method was developed under a previous contract and has been checked using results from several more complex interpolation methods. The geometric mean results have been found to be within acceptable error bounds, although perhaps a few percent high in some cases.

Summary plots of arrival time, overpressure, overpressure impulse, dynamic pressure, and dynamic pressure impulse are contained in Appendix A for the results of the ideal calculation. These results are compared to the results from the desert calculation and to experimental data from the PRISCILLA event. Waveform comparisons at a number of selected ranges are included in Appendix B. The waveforms are compared to the desert calculation results and to experimental waveforms where possible.

We have also included a number of parameter versus height plots at selected ground ranges. These extend from ground level to 40 feet above the ground. Comparisons are made with the results from the thermal layer calculation. These plots are included in Appendix C. Overpressure, arrival time, and impulse for the ideal calculation show very little variation with altitude. At large distances, beyond 4,000 feet, the rough surface has a small effect in reducing the near surface dynamic pressure.

SECTION 4
CALCULATED DESERT SURFACE RESULTS

A summary of the initial conditions is given in Section 2. Because the same thermal layer was used for this calculation as that reported in Reference 9, the results for distances less than 2,500 feet are the same as those of Reference 9 and will not be discussed here.

The calculation was carried to a time of four seconds and a distance of just over 6,000 feet. At the end of the calculation, the positive duration of the overpressure and dynamic pressure were complete for all ranges having overpressures greater than or equal to five psi.

During the calculation, we found that the station positions moved from the positions assigned as part of the initial conditions. We were able to trace this motion to the limitations of the 32-bit work station on which the desert calculation was made. During each rezone, the stations were assigned a new cell index position and this was converted back to a real distance. Because of the limited accuracy of 32-bit floating point arithmetic, many of the stations moved a small amount after each rezone. Several hundred rezones were completed during the progress of this calculation. Stations at larger ranges were effected more than those near ground zero.

The results reported in the summary plots of Appendix A have used the positions of the stations at the time of shock arrival. This problem does not effect the results of the ideal calculation because it was run on the Cray, a 64-bit machine. It also did not effect the vertical positions of the stations because few rezones occurred in the vertical direction. The vertical distances were small compared to the horizontal, and new zone indices were not calculated as often.

The dynamic pressures reported are the result of both air and dust contributions. The dust contribution has been assigned a "registry coefficient" of 0.5. The dust and air were treated as fluids and dynamic pressure was calculated as:

$$DP = 0.5 * rho * u * |u|, \quad (1)$$

where rho is the total density (air plus dust) of the zone.

The arrival time curves on the first figure in Appendix A show that the precursor separates from the ideal at a distance of less than the height-of-burst and remains ahead of the ideal arrival throughout the two-kilometer ground range. The maximum separation between precursor arrival and ideal is just over 300 feet at a time of 0.6 seconds. The waveforms of Appendix B show that the precursor arrives before the ideal at ranges as small as 350 feet.

The summary plots of Appendix A show that the maximum overpressure in the desert thermal case is as little as one-third of the ideal overpressure. The overpressure at the precursor front may be more than an order of magnitude less than the peak pressure occurring later in the waveform. The overpressure impulse differs by less than ten percent from the ideal over the entire range of comparison.

The maximum dynamic pressure is, at some ranges, as much as a factor of three greater than the ideal. The dynamic pressure curves cross near 3,000 feet and the precursor peak dynamic pressure is less than that of the ideal for all greater ranges. The dynamic pressure impulse exceeds the ideal by as much as a factor of eight between

ground ranges of 2,000 and 3,500 feet, then falls below the ideal values at greater ranges.

The waveforms of Appendix B show the details of many of the features described above. At a range of 2,500 feet, the ground-level overpressure waveform has a rounded front, with the peak overpressure near the front. Only a single peak is evident. The peak overpressure is about one-third of that for the ideal calculation. Overpressures at three and ten feet are very close to those at ground level. The dynamic pressure waveform shows that the maximum pressure occurs in a secondary peak some 300 milliseconds behind the precursor wave. The peak is about two and one-half times the ideal peak.

At a range of 3,000 feet, the overpressure waveforms are similar but the non-ideal peak is about half that of the ideal. The increase relative to the ideal is a sign of the precursor front slowing and decreasing in extent. The dynamic pressure waveform at this range shows two major rounded peaks, with the second occurring about 150 milliseconds after arrival. The peak is about twice that of the ideal. The decrease in separation time of the two peaks beyond 2,500 feet is a further indication of the beginnings of precursor clean-up.

By 3,500 feet, the calculation shows a rounded front, an inflection, and a sharp rise to a peak overpressure which is about 75 percent that of the ideal. The sharp rise to the second peak is an indication of precursor clean-up. The dynamic pressure waveform shows multiple peaks and a slow rise after first arrival. The peak dynamic pressure is comparable to the ideal peak. The decay after the peak is reached is much slower than in the ideal case and leads to a dynamic pressure impulse of about three times the ideal.

At a range of 4,000 feet, the overpressure waveform is nearly ideal. The major difference between precursed and ideal at this range is that the peak overpressure is a few percent lower than the ideal. The dynamic pressure waveform shows that the precursed waveform falls below the ideal at all times, thus causing a lower dynamic pressure impulse.

For ranges beyond 4,000 feet, the non-ideal waveforms are very close to the ideal but the arrival times are somewhat smaller and the peaks remain a few percent lower than ideal.

Appendix C contains comparisons of various parameters as a function of height at selected ground ranges. The plots cover the variation with altitude from ground level to 40 feet above the ground. At the 2,100-foot ground range, the peak precursor overpressure is about one-third that of the ideal with the near ground-level pressure as much as 50 percent greater than that above 10 feet in altitude. The ideal does not vary with altitude to less than one percent.

At 2,300 feet, some variation in peak overpressure is seen in the lower 10 feet, but the variations are less than 30 percent in the precursor case. In general, the precursed maximum overpressures are about one-third those of the ideal. The ideal shows no variation with altitude.

The comparison at 2,550 feet shows the precursor pressures to be less than half those of the ideal case. Variations with altitude are less than ten percent for the precursor and less than one percent for the ideal. This trend continues through the 2,950-foot ground range.

The temperature and sound speed in the thermal layer decrease rapidly beyond a range of 3,000 ft. This marks the clean-up phase of precursor propagation. The variation with height at 3,250 and 3,650 shows dramatic changes as the layer cools. At

3,250 feet the peak overpressure at 40 feet above the surface is about 30 percent greater than near the surface, but is still about 75 percent of the ideal. The ideal remains unchanged with height. By 3,650 feet, the overpressure above 20 feet differs from the ideal by less than 10 percent, while near ground level the overpressures are about 80 percent of ideal.

The thermal layer terminated at the 4,300-foot range; no pre-shock heating was present beyond this range. The variations with height beyond the end of the thermal layer are caused by residual differences in energy distribution in the shock and transient flows which are attempting to equilibrate along the shock front. Variations in height are small, of the order of two percent, and the differences between precursed and ideal are less than ten percent.

The arrival time as a function of height plots show no surprises. The curves are very smooth and show that the arrival at ground level is earlier than at any other height. This is in agreement with observed arrival times on structures from the PRISCILLA event. The precursor arrival times are earlier than the ideal for all ground ranges. Beyond the 4,300-foot range, the arrival time does not change with height.

The dynamic pressure plots of Appendix C show that the dynamic pressure nearest ground level is about a factor of two higher than at an elevation of three feet at the 2,100-foot ground range. This characteristic decays rapidly as the boundary layer grows behind the precursor front. By 2,500 feet, the maximum dynamic pressure occurs three to six feet above the ground. For all ground ranges less than about 3,200 feet, the precursed dynamic pressure exceeds that of the ideal near ground level. At 2,950 feet, the dynamic pressure near ground level is more than twice the ideal but falls below the ideal above 35 feet from the surface.

As with the overpressure, several oscillations are present in dynamic pressure as the precursor cleans up. Apparently, energy is exchanged between dynamic pressure and overpressure as the shock front adjusts to the absence of a thermal layer.

The most dramatic effect is seen in the dynamic pressure impulse. At a range of 2,100 feet, the near-surface dynamic pressure impulse from the precursor calculation exceeds the ideal by more than an order of magnitude, while at the three-foot elevation, the ideal is exceeded by about a factor of five. The impulse remains greater than the ideal for all heights. Some effect of the boundary layer can be seen in the reduction of dynamic pressure impulse for the ideal case also.

The effect of the boundary layer is evident in the 2,300-foot plot. The impulse for the precursed calculation changes from being greatest at ground level to being reduced such that the maximum occurs near the three-foot height. The ideal impulse is also reduced near ground level.

The maximum impulse of the precursor is greater than the ideal at all heights, but approaches the ideal near the 40-foot height throughout the clean-up phase, to a distance of nearly 4,000 feet. The impulse drops sharply beyond 4,000 feet and falls below the ideal for the remainder of the calculated range.

SECTION 5
COMPARISONS OF CALCULATIONS WITH EXPERIMENTAL DATA

The summary plots of Appendix A contain comparisons of calculations with nearly all available data from the PRISCILLA event.

The arrival time curve shows excellent agreement with the majority of the data. Some data have been questioned (Keefer private communication) because of the type of instrumentation used. In general, the desert calculation shows good agreement with the measured data and its wave front always arrives earlier at any given range than does that of the ideal case. The data indicates a faster propagation at ranges beyond 3,500 feet than was calculated. This is one of many indications that a significant thermal layer existed well beyond the 4,000-foot range in the PRISCILLA test.

The overpressure summary plot includes experimental data from ground level, three-foot and ten-foot heights. The three- and ten-foot elevation data agree better with the ideal overpressures than with the precursor values. The calculated overpressures are for ground level only. Two overpressures are plotted for each calculation: the first peak and the maximum. The only range for which these curves differ in the ideal case is during double and complex Mach reflection. This limited region extends from about 600 to 1,400 feet. For the precursor calculation, the peak overpressure falls below the ideal almost immediately. As the precursor forms and generates a double peaked waveform, the two curves diverge. At a range of 350 feet, only one peak is present, but by 500 feet a weak shock having a peak of about 10 percent [1] of the maximum leads the so-called "main wave". The precursed overpressure peaks fall below those of the ideal to a range of just over 4,000 feet, the end of the thermal layer. The first peak may be as little as 10% of the maximum overpressure at a given range.

The calculated precursor overpressure is in good agreement with all of the experimental data. It should be noted that the overpressure reaches a relative minimum at a range of just over 2,500 feet, then rises to a relative maximum at about 4,000 feet. This maximum is slightly higher than the ideal at this range. The peak then falls back to the ideal level for the remainder of the calculated ranges. This behavior is in agreement with the experimental data from several nuclear shots, including PRISCILLA.

The increase in overpressure as a function of ground range, beyond the 2,500-foot range, has been observed experimentally and is now confirmed by calculation. The rise and fall of the overpressure with range leads to a triple valued function for the range of a given overpressure; *e.g.*, there are three ranges at which 8 psi occurs. The calculation indicates 2,200, 3,200, and 4,100 feet all had a peak overpressure of 8 psi. This triple valued function is the cause of the non-ideal height-of-burst curves having loops and multiple values as a function of ground range and height of burst. These characteristics are real, calculable, and we believe that we now understand them.

The overpressure impulse data have considerably more scatter than the peaks. The calculations fall near the high side of the data. The causes for this scatter can be seen in the waveforms of Appendix B. Some waveforms fall below ambient at a relatively early time after shock arrival, while others do not return to ambient for an extended period. Such scatter is an indication of the difficulty of making measurements in the nuclear environment and the variety of waveforms measured at the same ground

[1] The agreement of the computation with the BRL waveform at 1650 feet is apparently fortuitous. The timing on the BRL waveform is now believed to be in error; the BRL waveform should be expanded so that the maximum peak coincides with that on the SRI peak. The BRL self-recording gages used in PRISCILLA did not have a timing-mark generator.

range. The waveforms depend on the integrated history of the interaction of the shock with the thermal layer, and surface irregularities contribute significantly to variations in this history.

The peak dynamic pressure summary plot shows that the peak measured values differ, in general, by about a factor of two to three from the ideal. The data are above the ideal for ground ranges between 1,200 feet and 3,200 feet. The calculated precursor results show this range of variation and agree with the range at which the dynamic pressure falls below the ideal.

The dynamic pressure impulse data, taken three feet above the surface, are in good agreement with the precursor calculated results. When viewed as in the sixth figure of Appendix A, the data fall onto two lines. The first line is very near the ideal, while the second closely follows the precursor calculation. The data and the calculation indicate that for some ranges the dynamic pressure impulse may exceed the ideal by more than an order of magnitude.

The waveforms of Appendix B include all available desert line waveforms. No effort has been made to edit, delete, or emphasize any particular waveform or comparison. Many of the gages did not have associated arrival times, but times were given as relative to first signal arrival. We have shifted all desert waveforms so that the first signal arrives at the time of the calculated precursor waveform. Because the current calculation differs from that of Reference 9, only at distances greater than 1,450 feet, the discussion of waveform comparisons will be limited to those beyond the 1,450 foot range.

The calculated waveforms of Appendix B represent the mean flow parameters at the positions given. The calculations include the turbulent contribution as a separate parameter. Waveforms using a combination of the mean parameters and the turbulent contribution can be reconstructed from the calculations. This reconstruction includes a full frequency distribution of the Kolmogorov spectrum. The resulting waveforms must then be low-pass filtered to the characteristics of a given gage before comparisons can be made; this has not been done here. The calculated waveforms are therefore somewhat smoother than the data because of the lack of the turbulent component. The turbulence will add oscillations on the waveforms, but impulse values will not be changed.

At 1,650 feet, the agreement between the calculated precursor and the BRL measured overpressure waveforms is excellent. The SRI gage shows greater separation between first and second peaks and a somewhat higher second peak.

At 2,000 feet, the two SRI gages show high, spiking secondary peaks which are as high as those measured at the 1,650-foot range and above the ideal at this range. The calculation shows excellent agreement with the rise and shape of the first peak and agrees with the timing between first and second peaks, but falls well below the second peak pressure. This comparison must be weighed against the measurements taken before and after this ground range.

Some 250 feet further, at 2,250 feet, the BRL waveform indicates no such secondary spike. The calculated precursor waveform is again in excellent agreement with the data.

By 2,500 feet, the second peak is no longer apparent in the waveform. The SRI and BRL gages are in agreement, and the calculated waveform follows the same pattern.

At 3,000 feet, the BRL, SRI, and calculated precursor waveforms are essentially overlays. The two data waveforms show a small spike near 1.25 seconds. The spike

indicates the formation of a secondary shock as precursor clean-up begins. This is not apparent in the calculation.

The clean-up continues, as seen at the 3,500-foot range. The calculation has a shorter, rounded front and a higher second peak than the experimental waveform. This is a further indication that the thermal layer used in this calculation is cooler than existed in the experiment at this range. The experimental waveform falls more quickly after the peak, but this should be compared with the waveform measured just three feet above the ground. Here, the SRI data merges with the calculated waveforms after about 1.7 seconds.

The premature clean-up of the calculation is further demonstrated in the waveforms compared at 4,000 feet. The experiment shows a separation of about 30 ms between the first and second peaks, but the calculation has a single, rapid rise indicates nearly complete clean-up at this range.

SECTION 6
CONCLUSIONS

The results of the "ideal" calculation serve as a benchmark for the definition of the entire airblast flowfield over a realistic surface. This calculation is being and will be used to compare and quantify the effects of dust and thermal layers. The zone size remained at 10 centimeters in the shock following sub-grid to a distance of over 1.2 kilometers. The zone size in the subgrid was then gradually increased to a maximum of 30 centimeters as the shock approached 2 kilometers. The resolution is adequate for this calculation to be considered state-of-the-art.

The desert calculation required some compromise on resolution. The moving subgrid contained zones with dimensions of 30 centimeters throughout the calculation. This compromise was necessary in order to assure completion of the calculation within cost constraints. A desert thermal layer calculation with 10-centimeter resolution at the PRISCILLA scale is still a very desirable goal. This calculation has sufficient resolution to answer many of the questions about thermal layer temperature distribution and the role of dust in the overall flowfield. A higher resolution calculation will require careful reconsideration of the temperature distribution in the thermal layer, the extent of the high sound-speed region, and the consequences of temperature gradients on precursor cleanup.

The desert precursor calculation results, presented here, show the best agreement with experimental data of any calculation by any organization done to date. This comparison includes arrival times, overpressures, dynamic pressures, impulses, and waveform details. We now have defined the flowfield for the PRISCILLA event in sufficient detail to provide high quality environment descriptions, above 25 psi but with less fidelity at lower pressures.

The results of this calculation are being transferred to magnetic media and will be available for further detailed analysis in the future. Some questions about the role of dust versus air in the measurement of dynamic pressure have already been addressed during the comparisons between calculational results and experimental data. The growth of a boundary layer and the interaction of the precursor with the boundary layer can be more fully examined. The role of turbulence in dust lofting and dust distribution behind the precursor is yet to be addressed in detail. Many insights into these associated phenomena and some answers are now available, but further analysis is required to exploit fully this pair of computations.

INTENTIONALLY LEFT BLANK.

REFERENCES

1 Carpenter, H.J., Engler, M.J., McCaffree, L.A., "Pre-Shock Thermal Layer Sound speeds Developed from Nuclear Test Data", DNA-TR-89-190, Defense Nuclear Agency, Alexandria Va., August, 1991.

2 Pierce, T.H., "Numerical Boundary Layer Analysis with K-E Turbulence Model and Wall Functions," Defense Nuclear Agency Report DNA-TR-87-15, September 1986.

3 Barthel, J.R., Needham, C.E., Pierce, T.H., and Schneyer, G.P., "A Computational Model for Precursed Airblasts Over Rough Surfaces," S-Cubed Report SSS-R-89-10003, August 1989.

4 Pierce, T.H., "Turbulence and Real-Surface Sub-Models in S-Cubed Hydrocodes," S-Cubed Draft Report DTR-91-12671, 1991.

5 Needham, C.E., et. al., "Theoretical Calculations for Precursor Definition," Defense Nuclear Agency Report DNA-TR-90-18, September 1990.

6a Swift, L.M., Sachs, D.C., and Kriebel, A.R., "Operation PLUMBBOB, Project 1.3: Air-Blast Phenomena in the High Pressure Region," WT-1043, Stanford Research Institute, Menlo Park, CA, December 1960.

6b Bryant, E.J., Keefer, J.H., Swift, L.M., and Sachs, D.C., "Operation PLUMBBOB, Projects 1.8a and 1.8c: Effects of Rough and Sloping Terrain on Airblast Phenomena", WT-1407, Ballistic Research Laboratories, Aberdeen, MD, July 1962.

7 Operation PLUMBBOB, Event PRISCILLA, documentary photography, available from DASIAC film archives, Kaman Sciences, Corp., P.O. Box 1479, Santa Barbara, CA 93102-1479.

8 Banister, J.R., and Vortman, L.J., "Operation PLUMBBOB, Project 34.1: Effects of a Precursor Shock Wave on Blast Loading of a Structure," WT-1472, Sandia Corporation, Albuquerque, NM, October 1960.

9 Crepeau, J.E., Ekler, R.G., Kennedy, L.W., Needham, C.E., and Rogers, S.H., "SHARC Hydrocode Calculations of the PRISCILLA Event," S-Cubed Report SSS-DFR-93-14283, October 1993.

10 Barthel, J., "On the Relationship Between Thermal Layer Sound Speed and Precursor Observables," Defense Nuclear Agency Report DNA-TR-88-241, January 1992.

INTENTIONALLY LEFT BLANK.

APPENDIX A
PARAMETER SUMMARY PLOTS

This Appendix contains summary plots of hydrodynamic parameters as a function of ground range. Each plot contains the results of the ideal calculation, the desert calculation, and experimental data. No dynamic pressure measurements were made at ground level. All the experimental dynamic pressure data were taken at least three feet above the surface. Many of the dynamic pressures from the experiment were derived from stagnation pressure measurements at a 3-foot elevation and the overpressure measurements at ground level. The results from the PRISCILLA calculation show that the overpressure varies between ground level and three feet in the region of strong precursor and the assumption of equal overpressures may be in error by 10% or so.

All measured dynamic pressures are taken without regard to the type of gage or its dust registry coefficient. The calculated dynamic pressures include the dust dynamic pressure contribution. In the plots from these calculations, the dust is treated as a fluid and has a registry coefficient of 0.5.

PRISCILLA
ARRIVAL TIME AT GROUND LEVEL

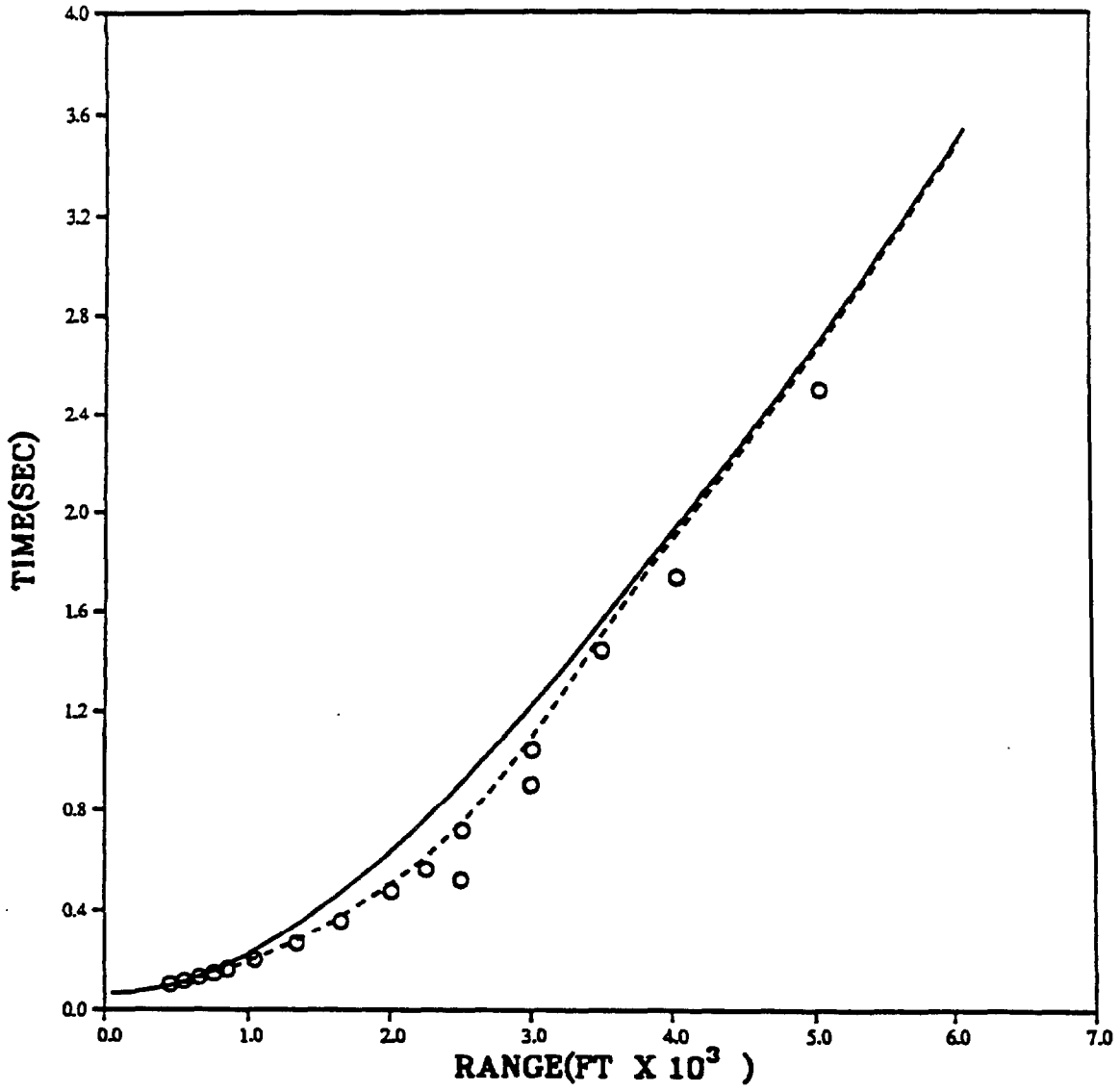

IDEAL
DESERT THERMAL LAYER JULY 6 REV.
DATA

PRISCILLA DESERT
OVERPRESSURE AT GROUND LEVEL

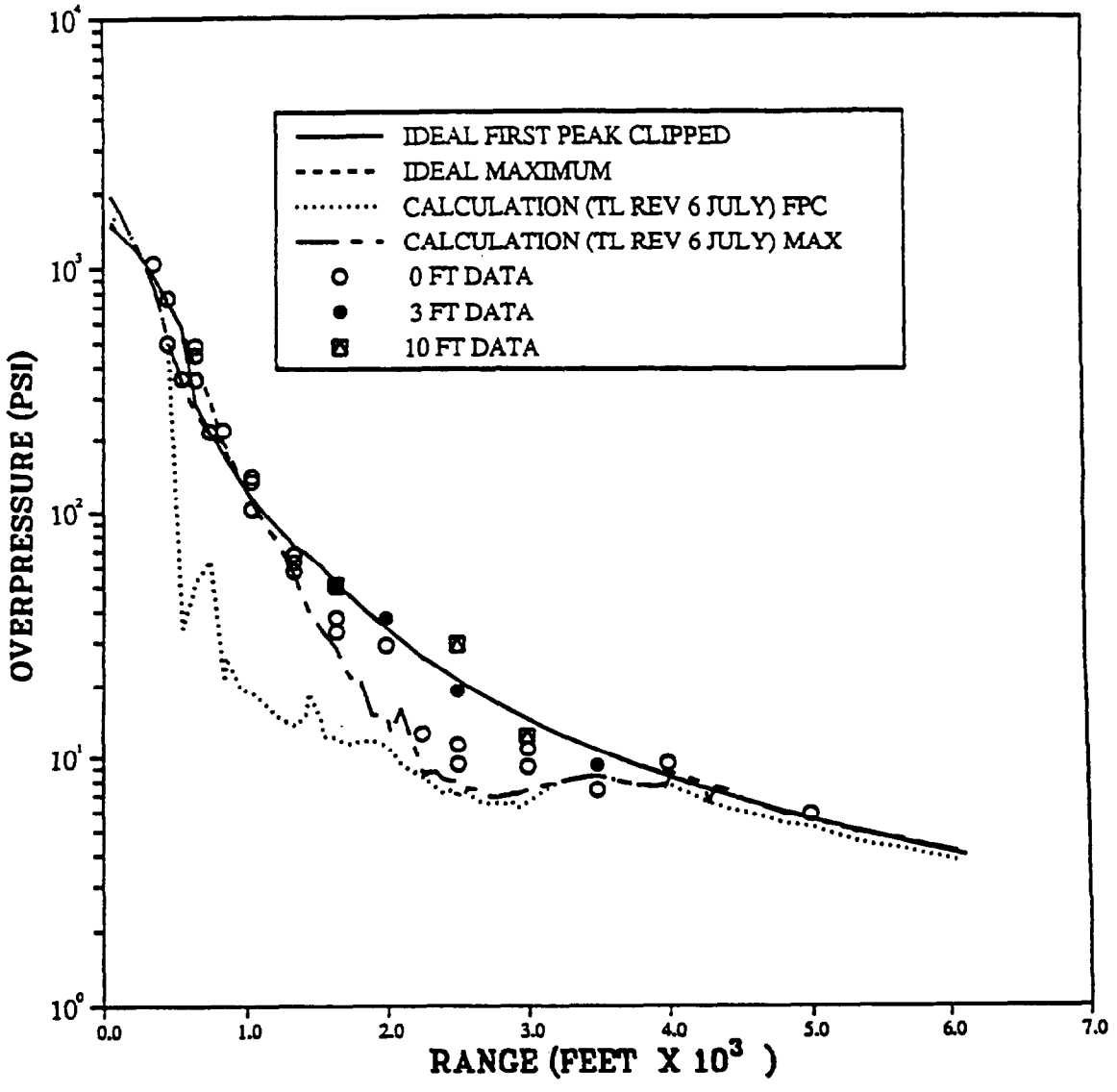

PRISCILLA DESERT
OVERPRESSURE IMPULSE
GROUND LEVEL

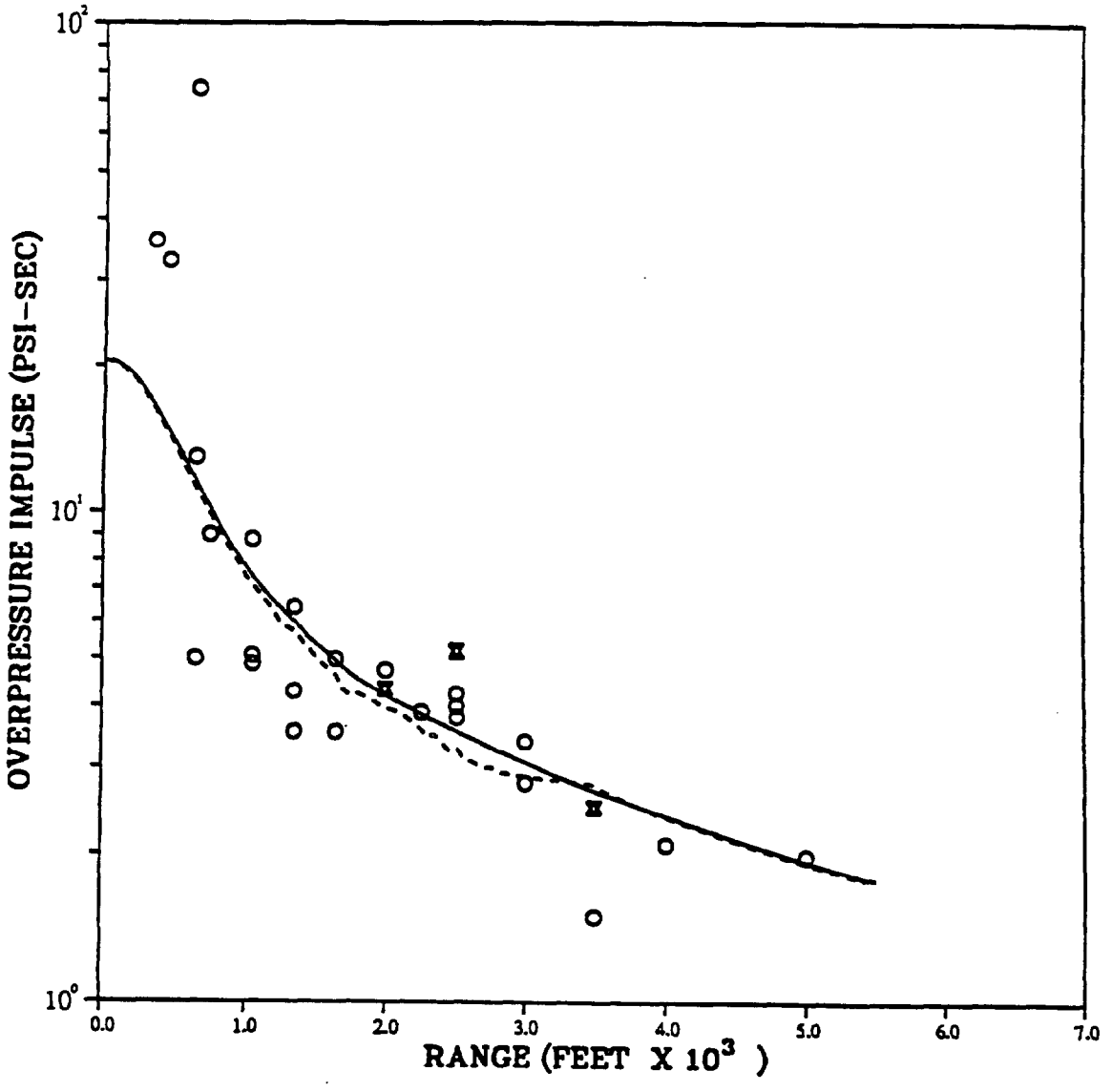

IDEAL 0 FT
CALCULATION 0 FT (TL REV 6 JULY)
DATA 0 FT
DATA 3 FT

PRISCILLA DESERT
HORIZONTAL DYNAMIC PRESSURE PEAKS
91.44 CM LEVEL (3 FEET)

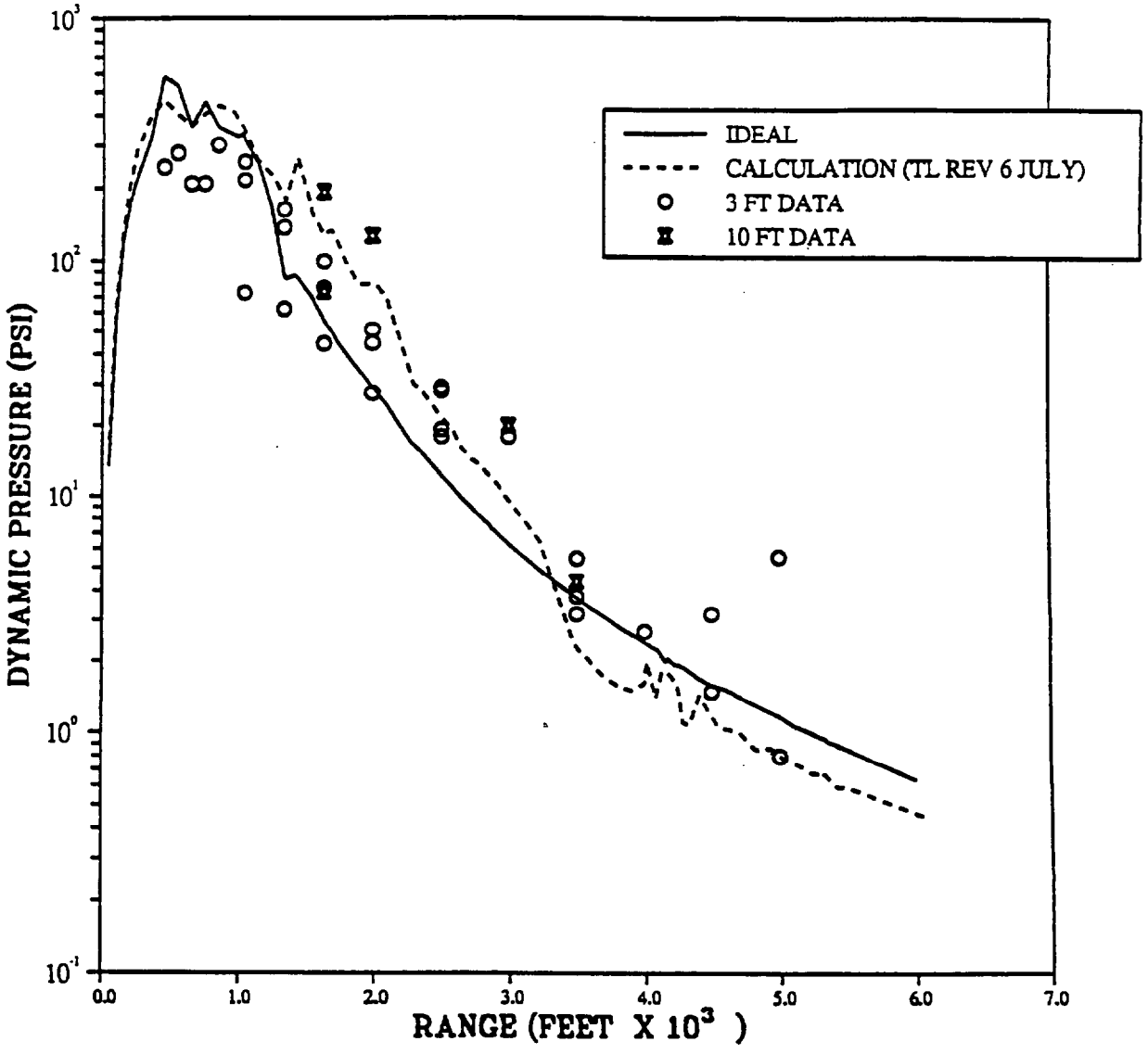

PRISCILLA DESERT
HORIZONTAL DYNAMIC PRESSURE PEAKS
304.8 CM LEVEL (10 FEET)

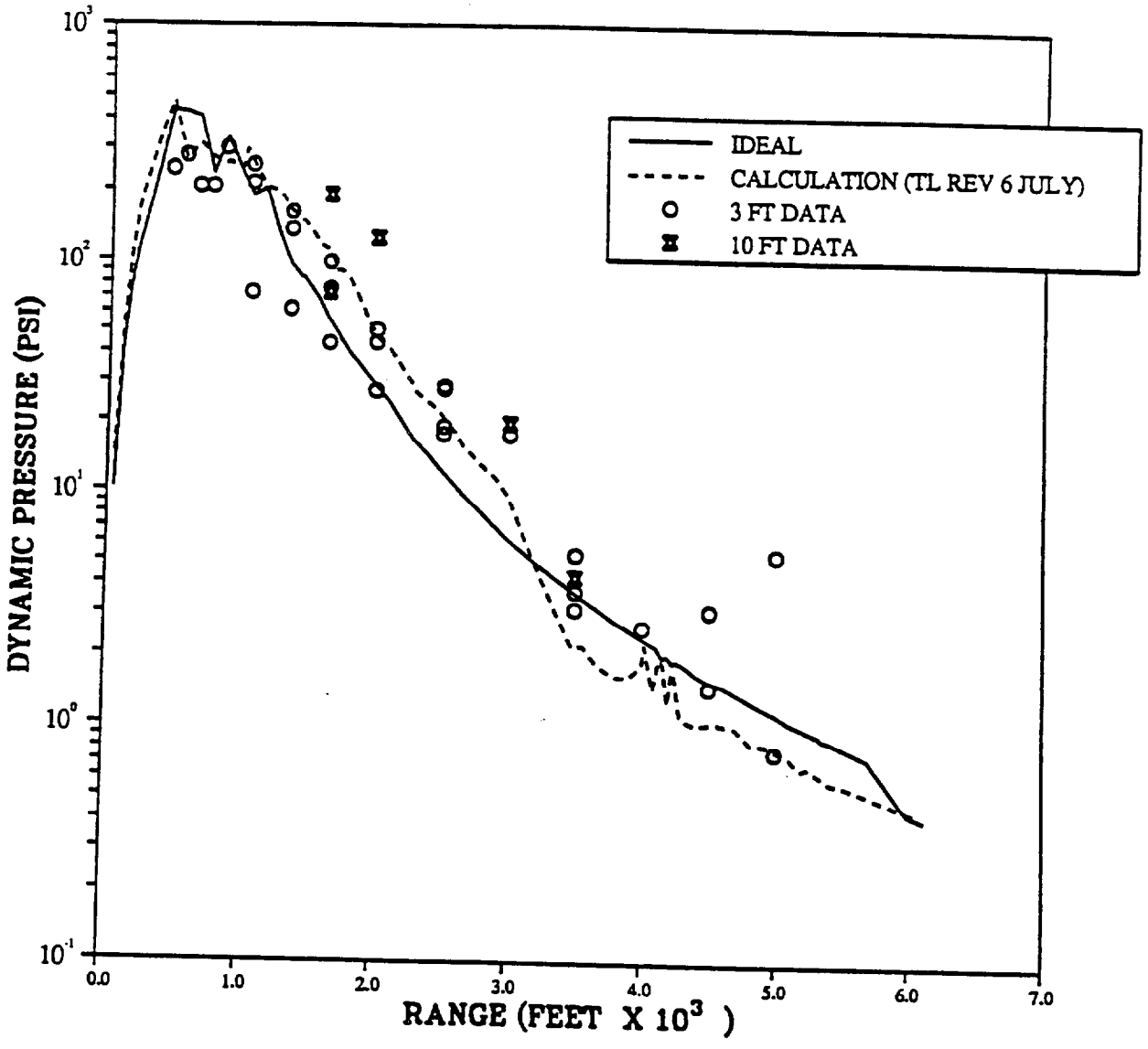

DESERT PRISCILLA
HORIZONTAL DYNAMIC PRESSURE IMPULSE
AT 91.44 CM LEVEL (3 FEET)

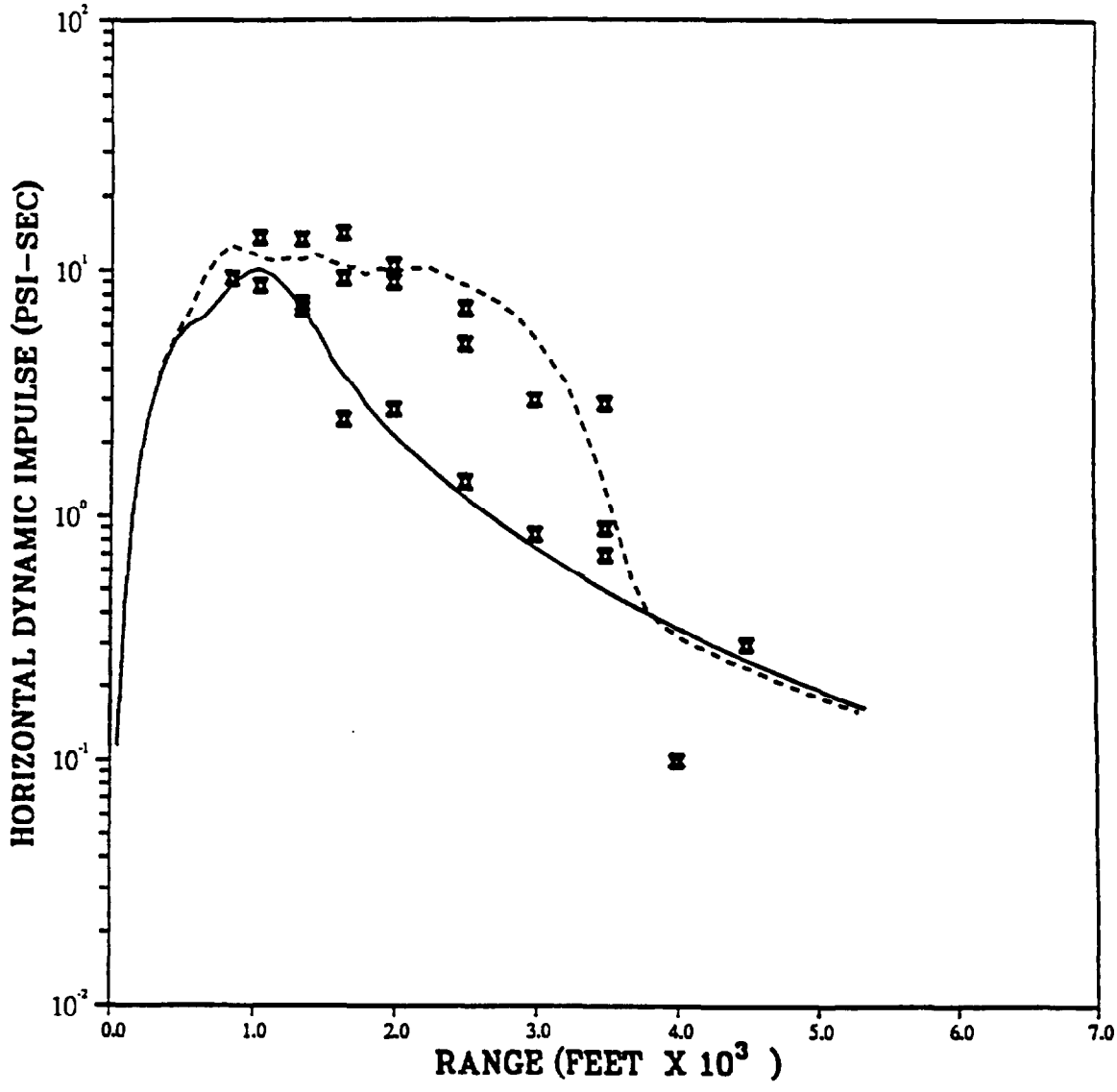

IDEAL
DESERT CALC (TL REV 6 JULY)
GAGE DATA AT 3 FT

DESERT PRISCILLA
HORIZONTAL DYNAMIC PRESSURE IMPULSE
AT 304.8 CM LEVEL (10 FEET)

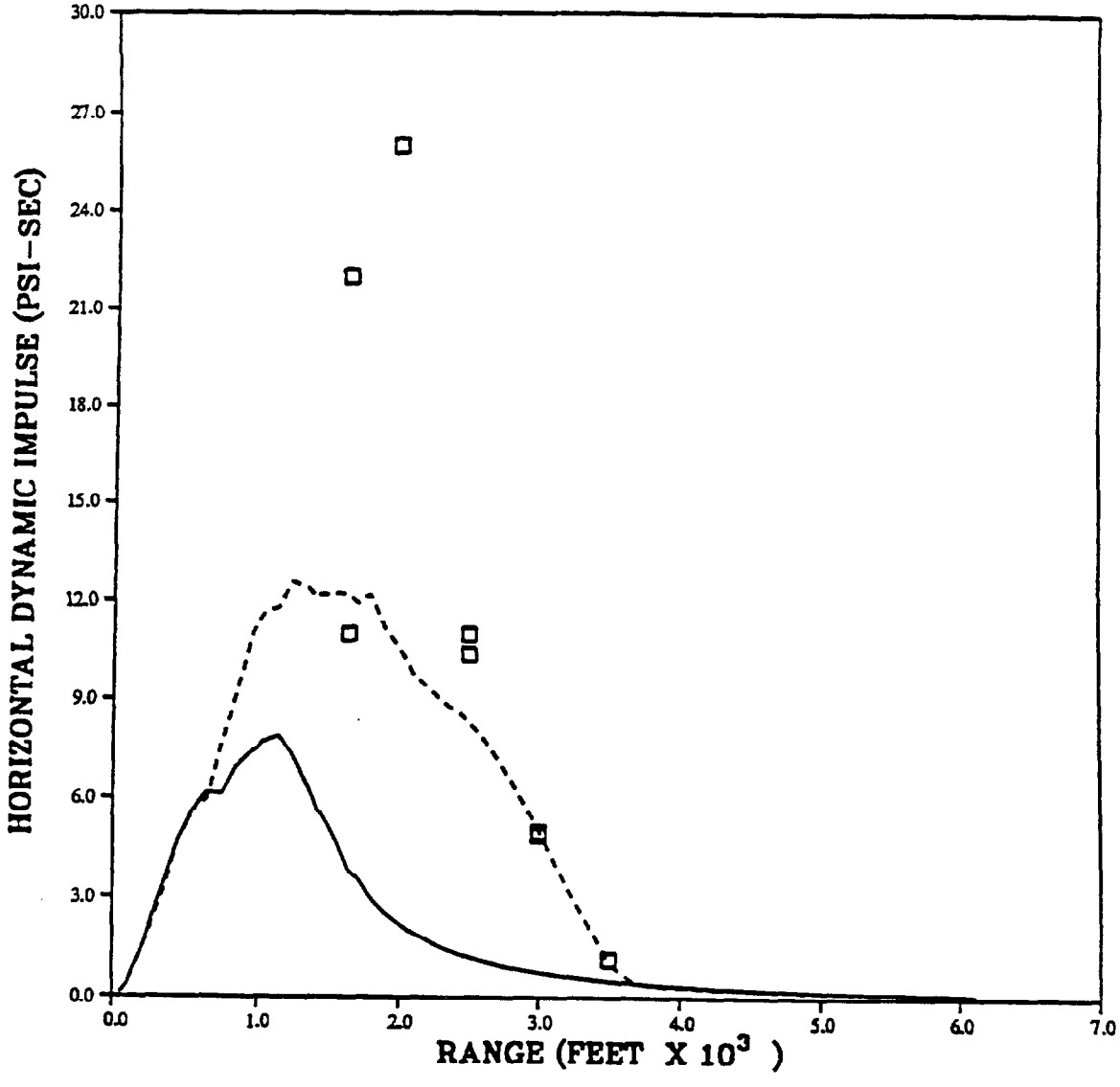

APPENDIX B
WAVEFORM COMPARISONS

This Appendix contains waveform comparisons of overpressure, dynamic pressure, and their impulses. Each plot contains the ideal waveform, the calculated precursor waveform, and at least one measured waveform at the corresponding distance. Arrival time of the measured waveform has been shifted to agree with the precursor calculation.

More information is available. The dust density as a function of time has been calculated and saved. It is possible to determine the calculated air and dust dynamic pressures independently. Any desired dust registry coefficient or a functional form of the dust registry coefficient may be used. Mach number of the flow as a function of time is also available at any of the station positions. Full descriptions of the turbulence environment are also available at each station, including the turbulent energy and the rate of turbulence dissipation.

PRISCILLA
CALCULATION - DATA COMPARISONS
OVERPRESSURE AT 350 FEET (107 M)

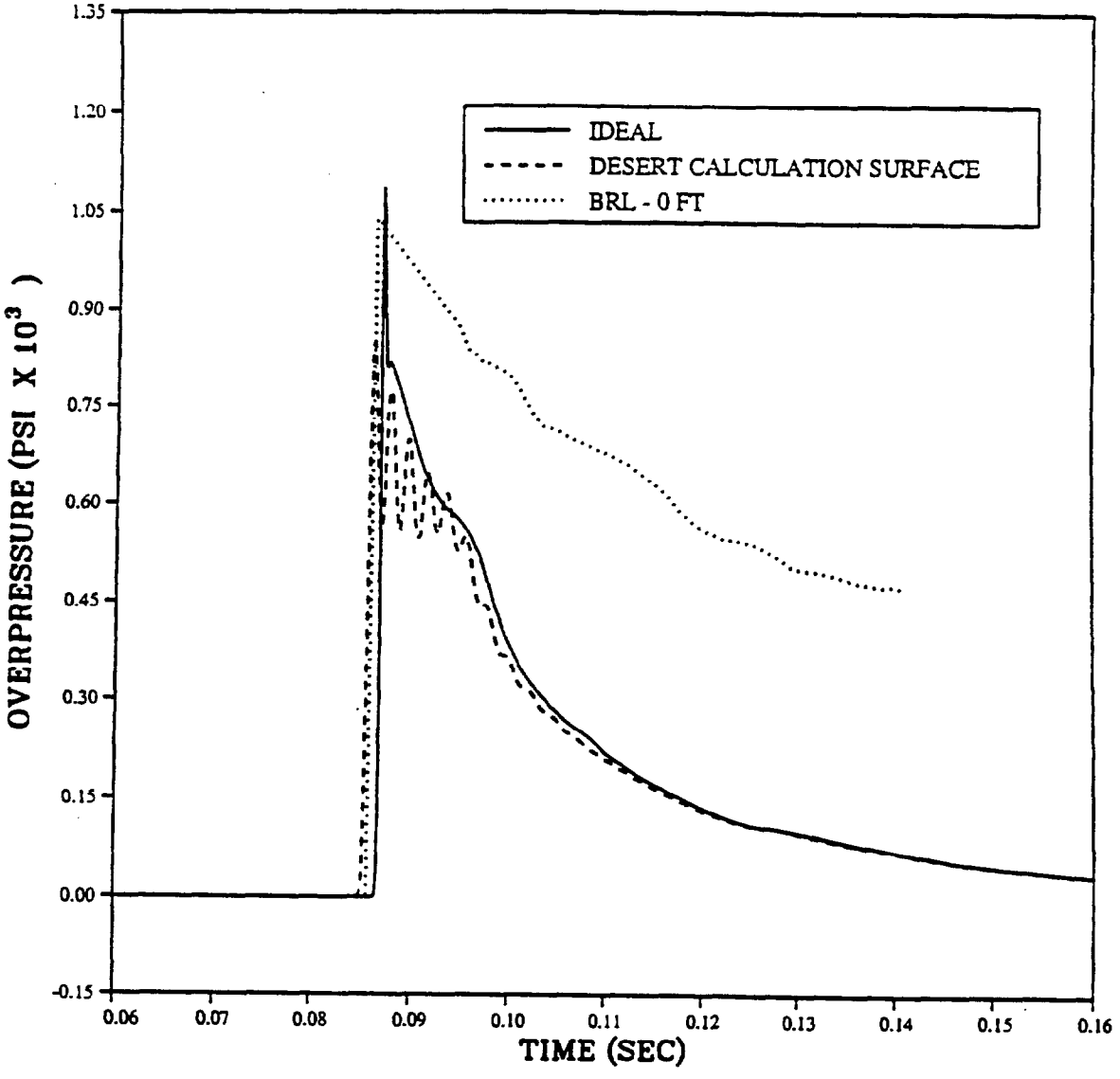

PRISCILLA
CALCULATION - DATA COMPARISONS
OVERPRESSURE AT 450 FEET (137 M)

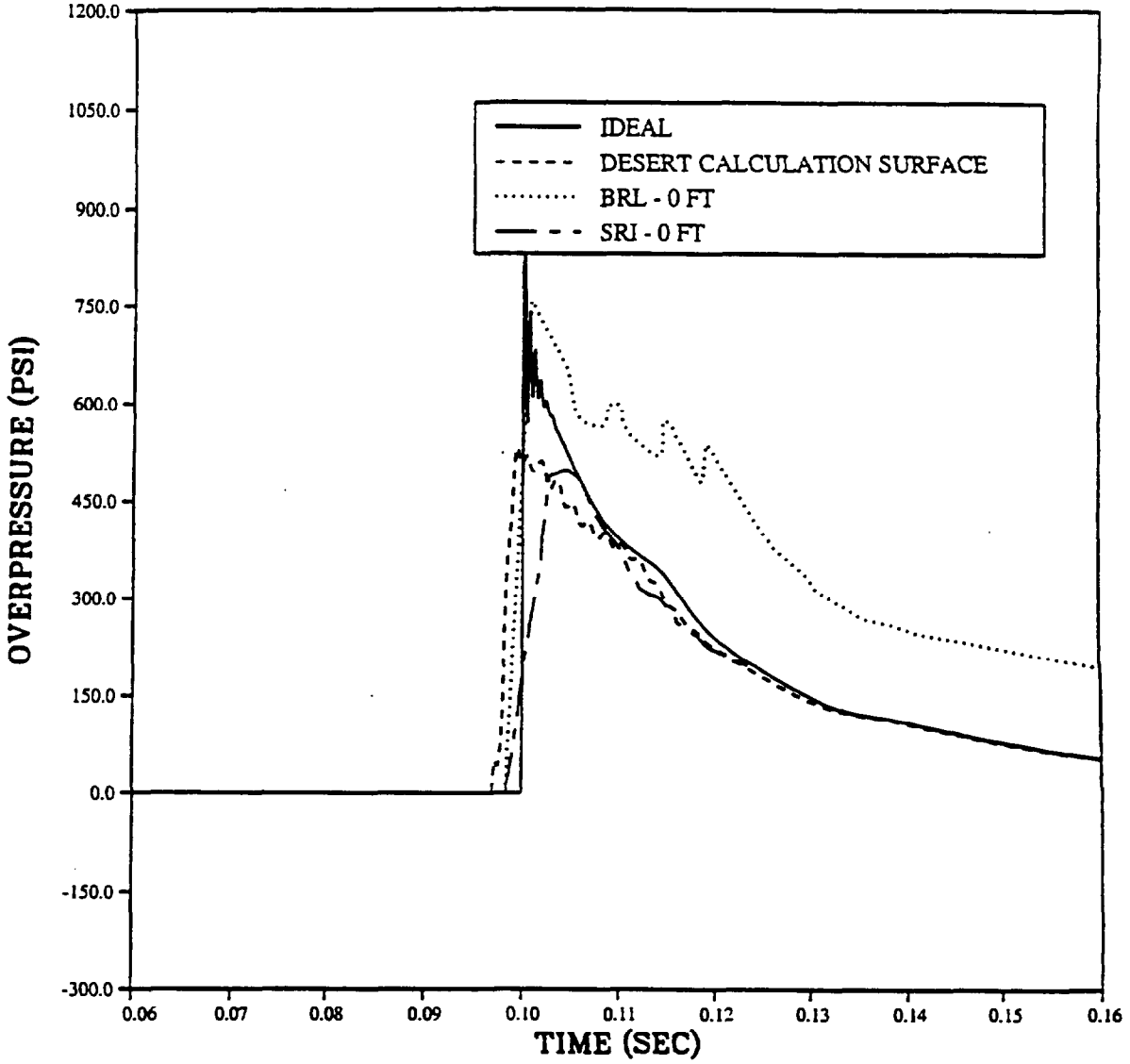

PRISCILLA
CALCULATION - DATA COMPARISONS
OVERPRESSURE AT 550 FEET (168 M)

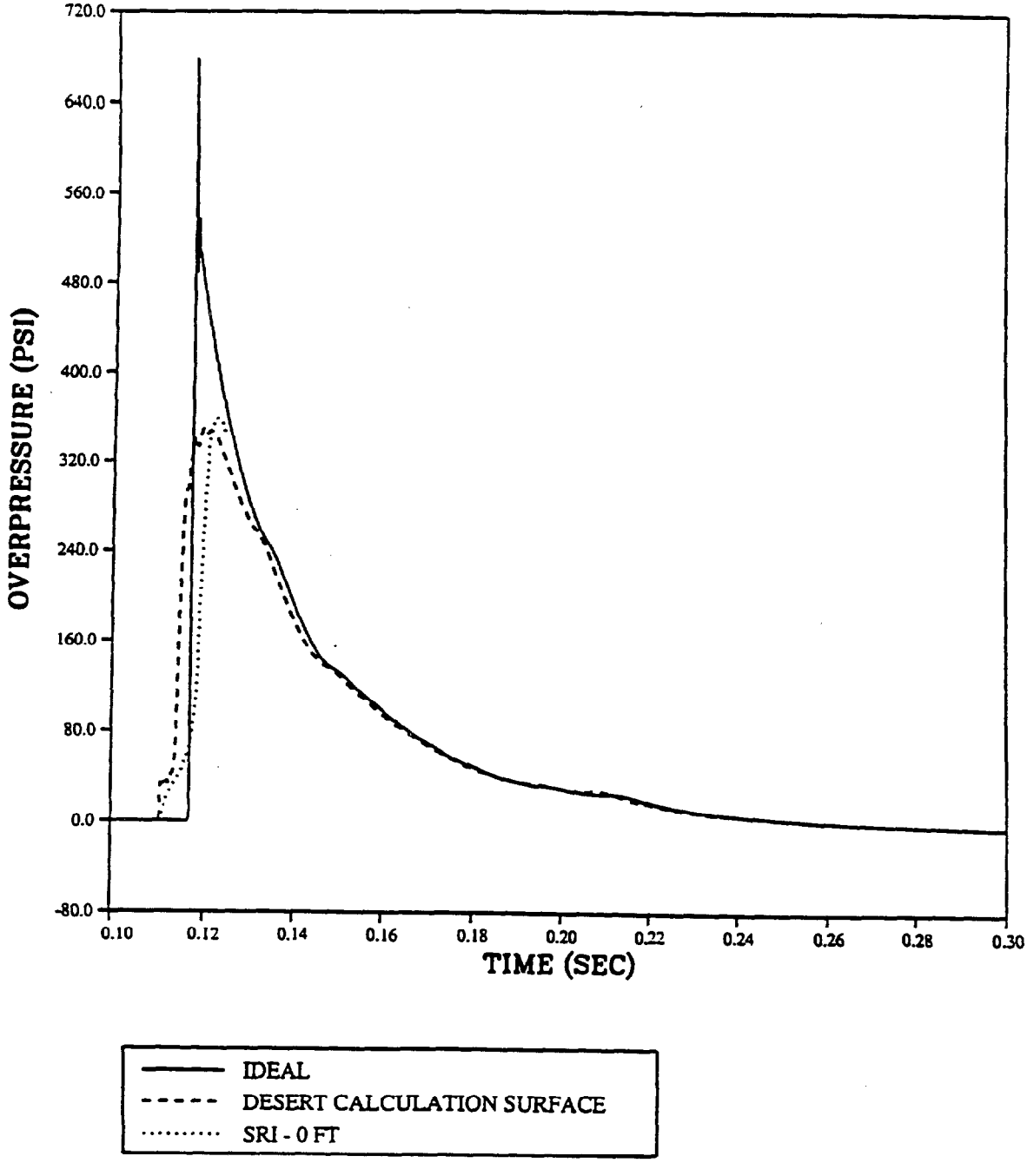

PRISCILLA
CALCULATION - DATA COMPARISONS
OVERPRESSURE AT 650 FEET (198 M)

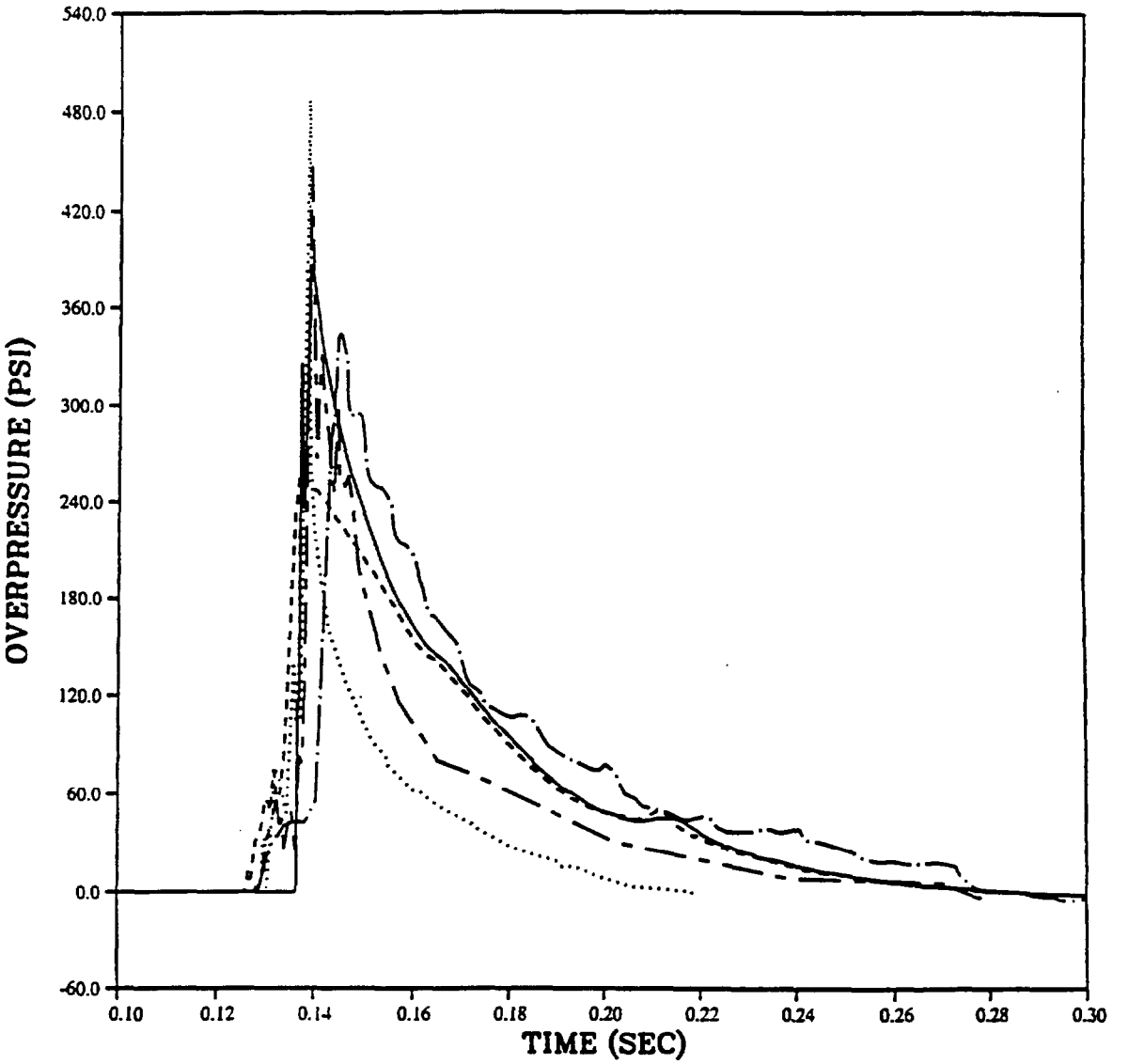

PRISCILLA
CALCULATION - DATA COMPARISONS
OVERPRESSURE AT 750 FEET (229 M)

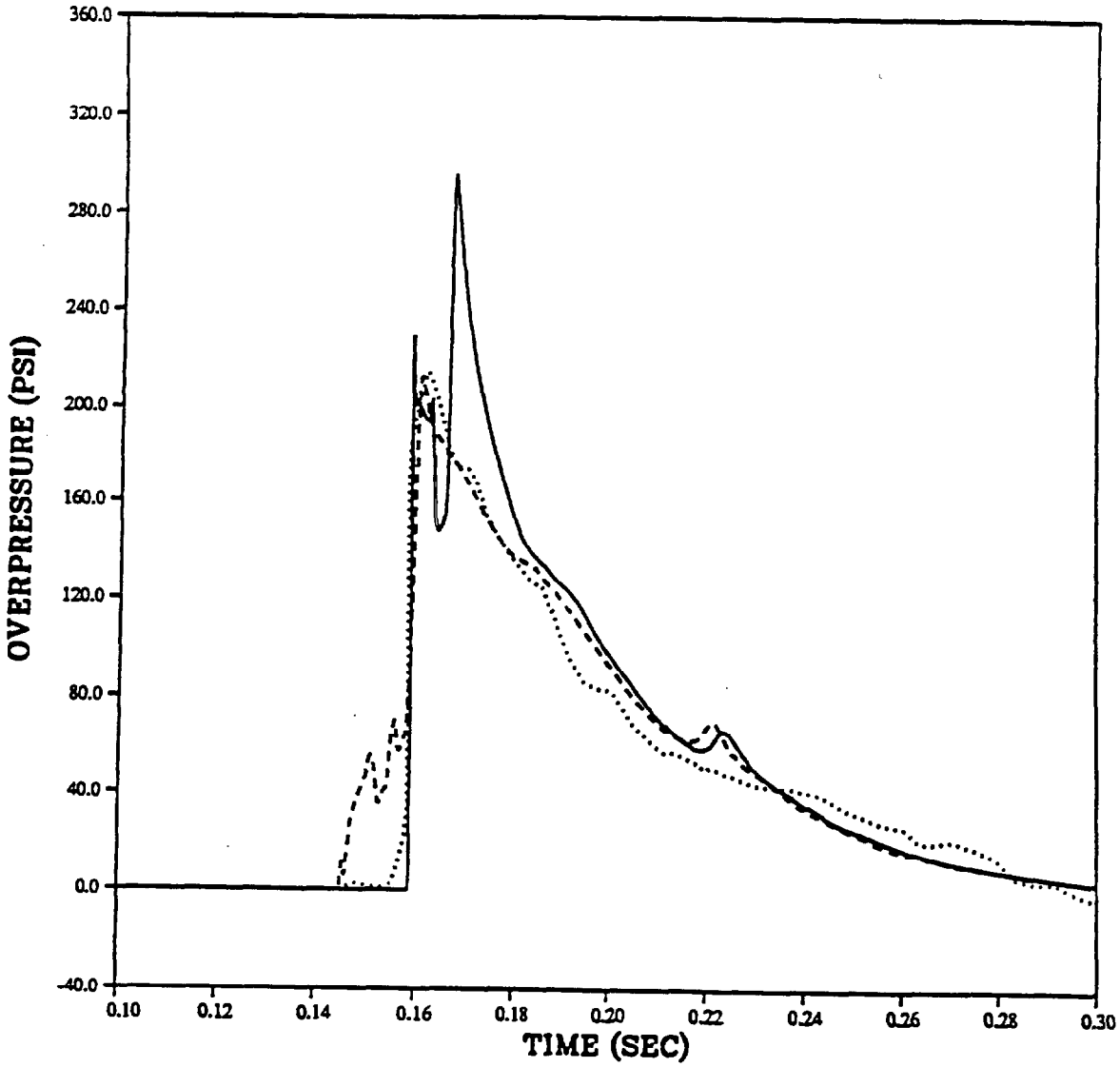

PRISCILLA
CALCULATION - DATA COMPARISONS
OVERPRESSURE AT 850 FEET (260 M)

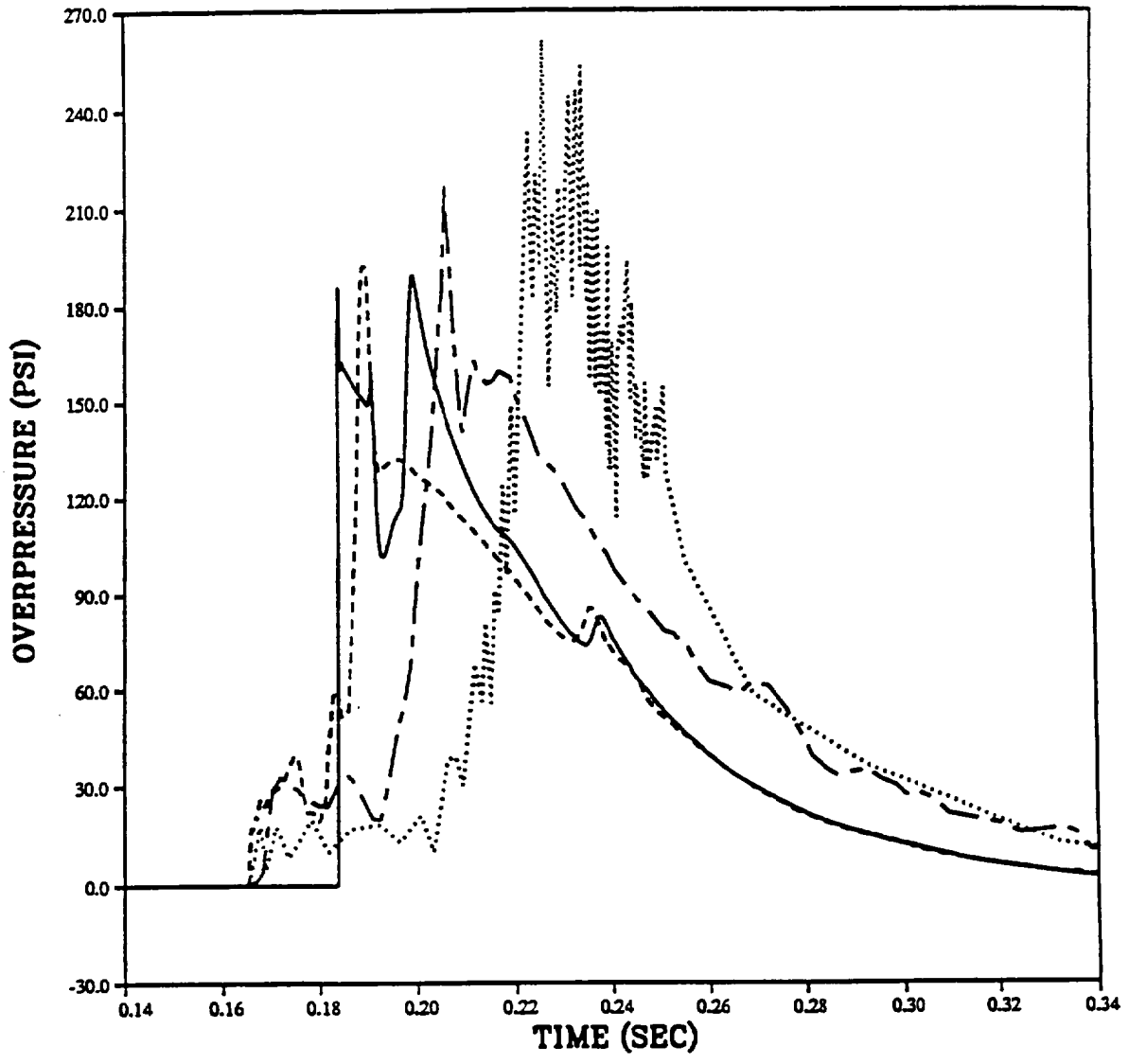

PRISCILLA
CALCULATION - DATA COMPARISONS
OVERPRESSURE AT 1050 FEET (320 M)

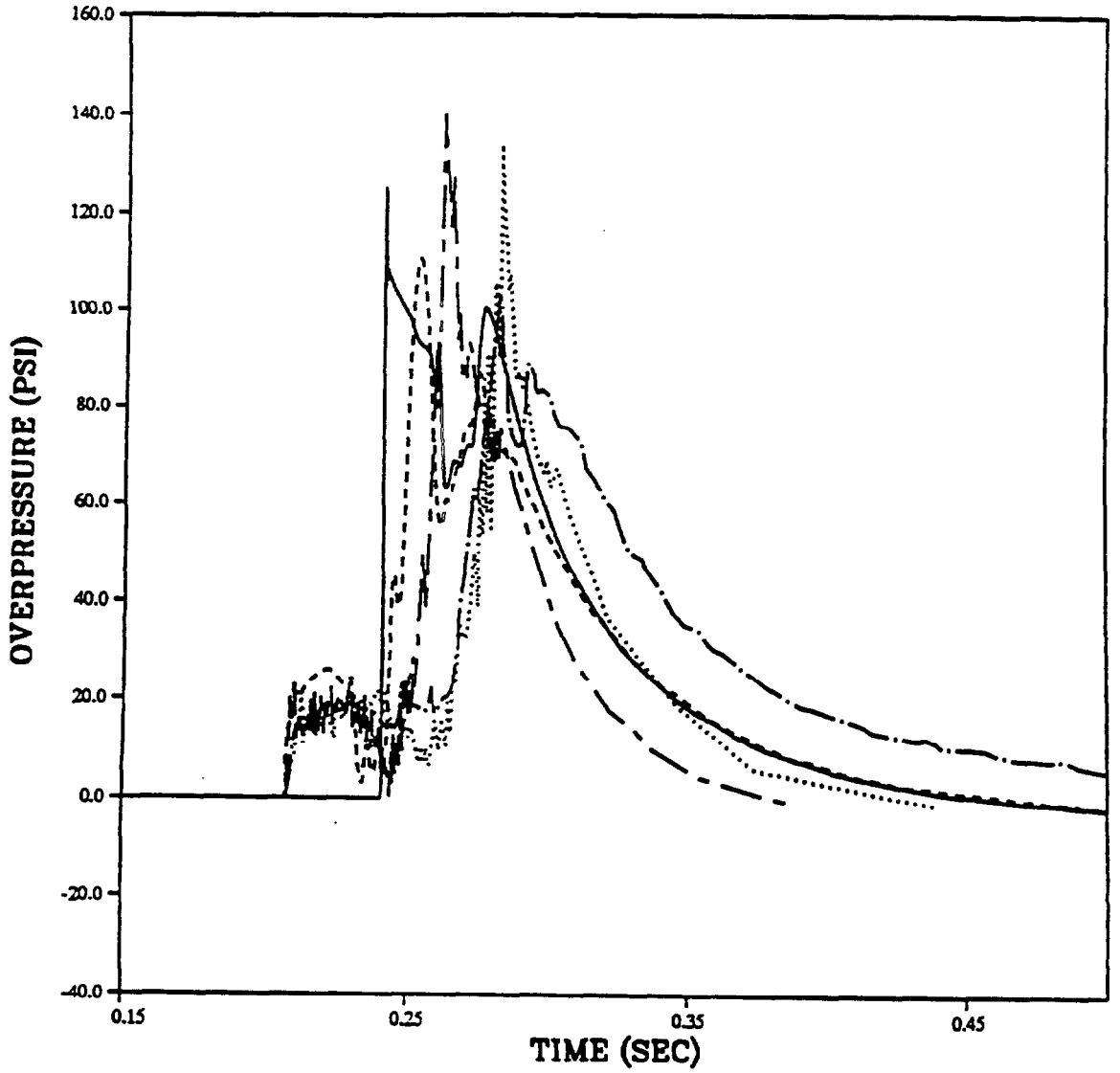

IDEAL
DESERT CALCULATION SURFACE
BRL - 0 FT
BRL - 0 FT
SRI - 0 FT

PRISCILLA
CALCULATION - DATA COMPARISONS
OVERPRESSURE AT 1350 FEET (410 M)

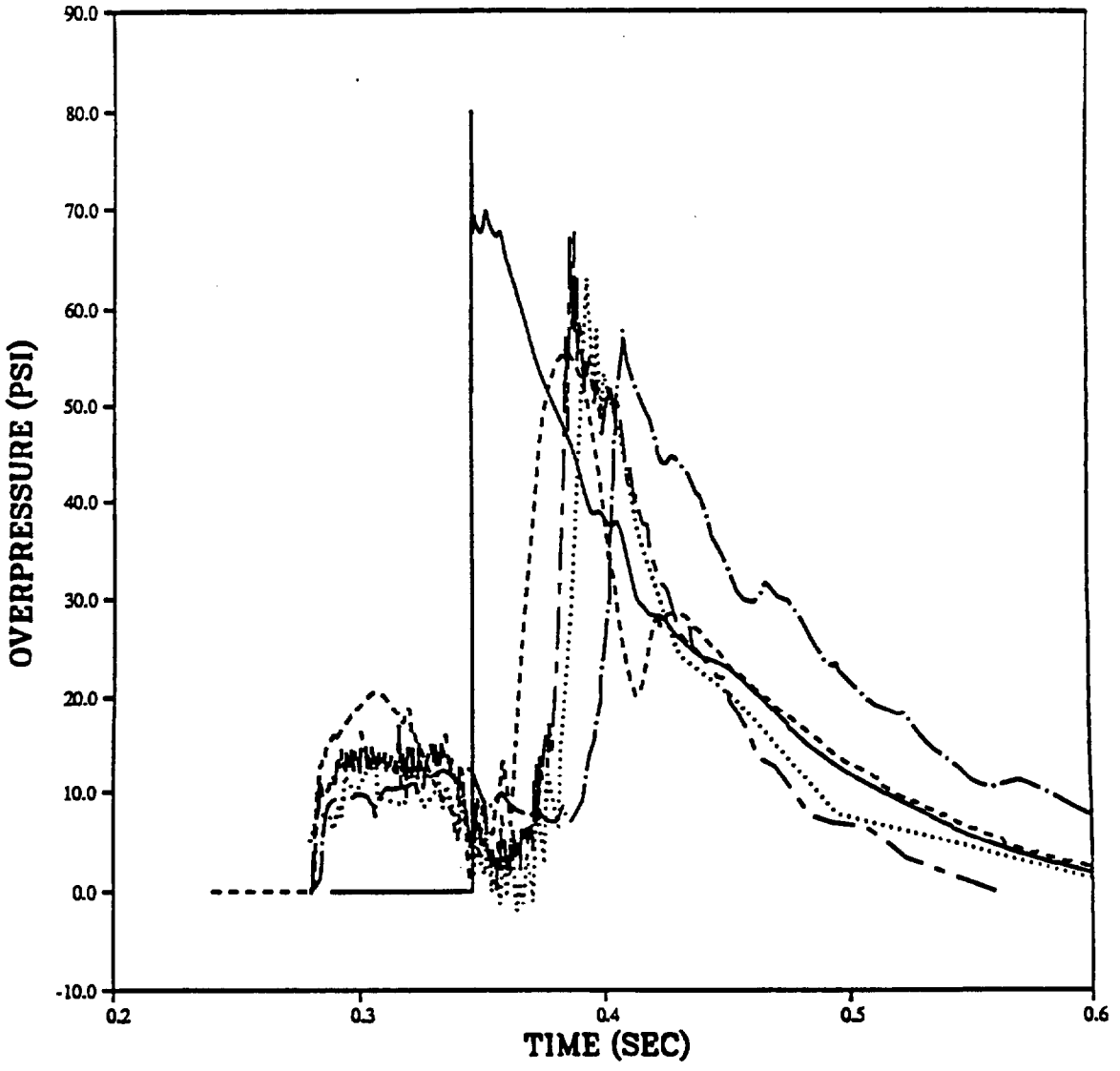

IDEAL
DESERT CALCULATION SURFACE
BRL - 0 FT
BRL - 0 FT
SRI - 0 FT

PRISCILLA
CALCULATION - DATA COMPARISONS
OVERPRESSURE AT 1650 FEET (503 M)

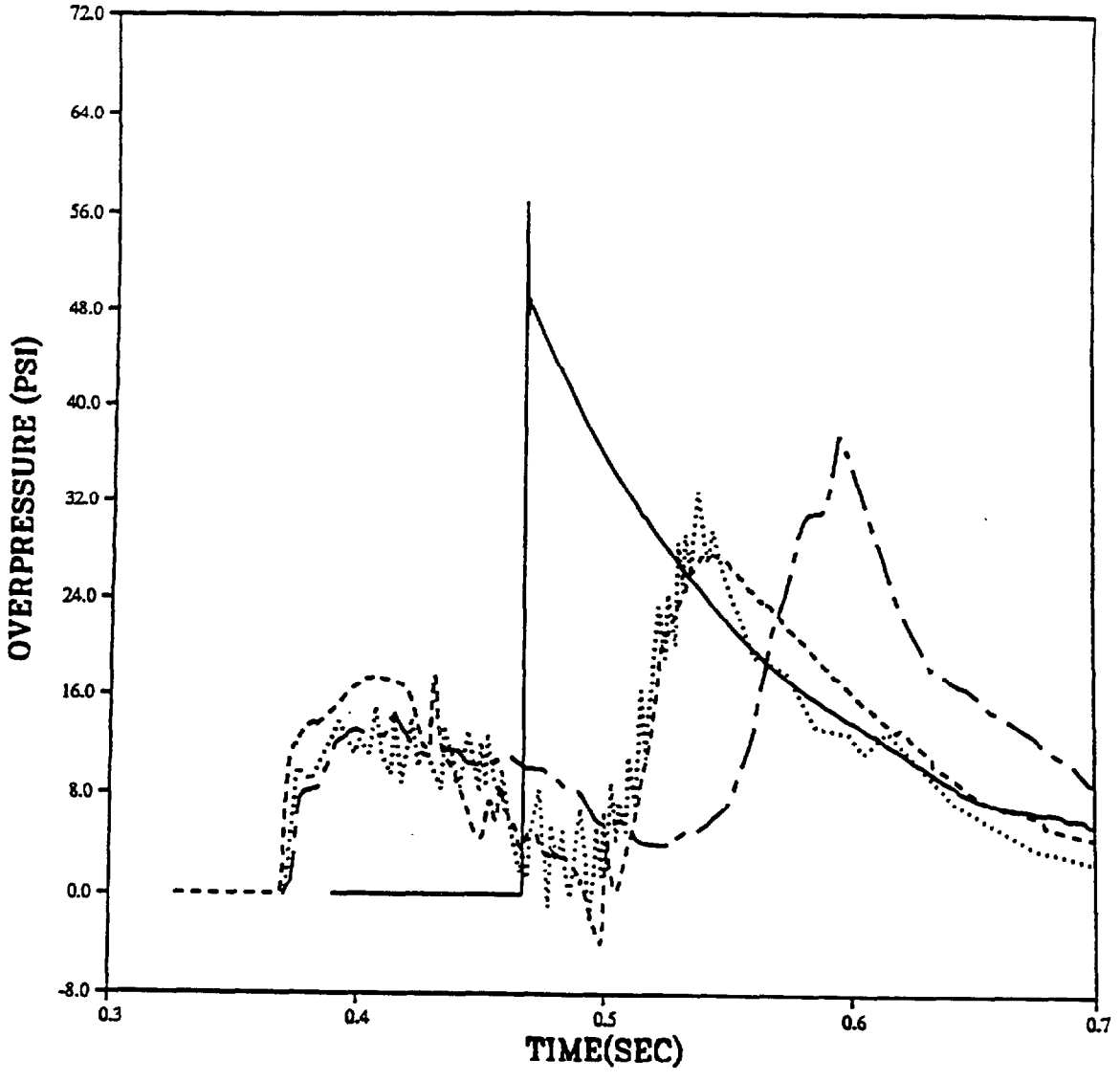

IDEAL
DESERT CALCULATION SURFACE
BRL - 0 FT
SRI - 0 FT

PRISCILLA
CALCULATION - DATA COMPARISONS
OVERPRESSURE AT 2000 FEET (610 M)

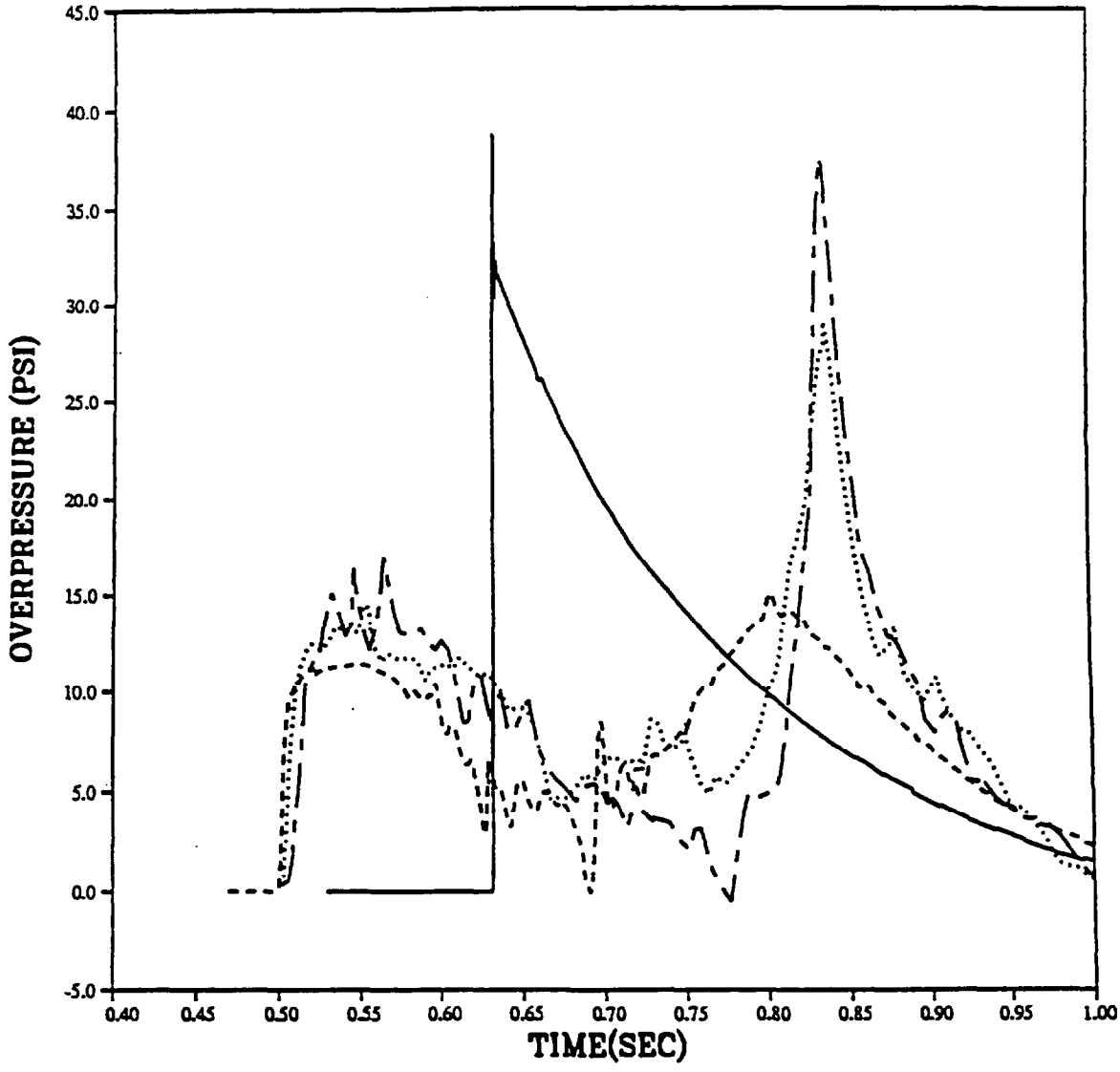

PRISCILLA
CALCULATION - DATA COMPARISONS
OVERPRESSURE AT 2250 FEET (686 M)

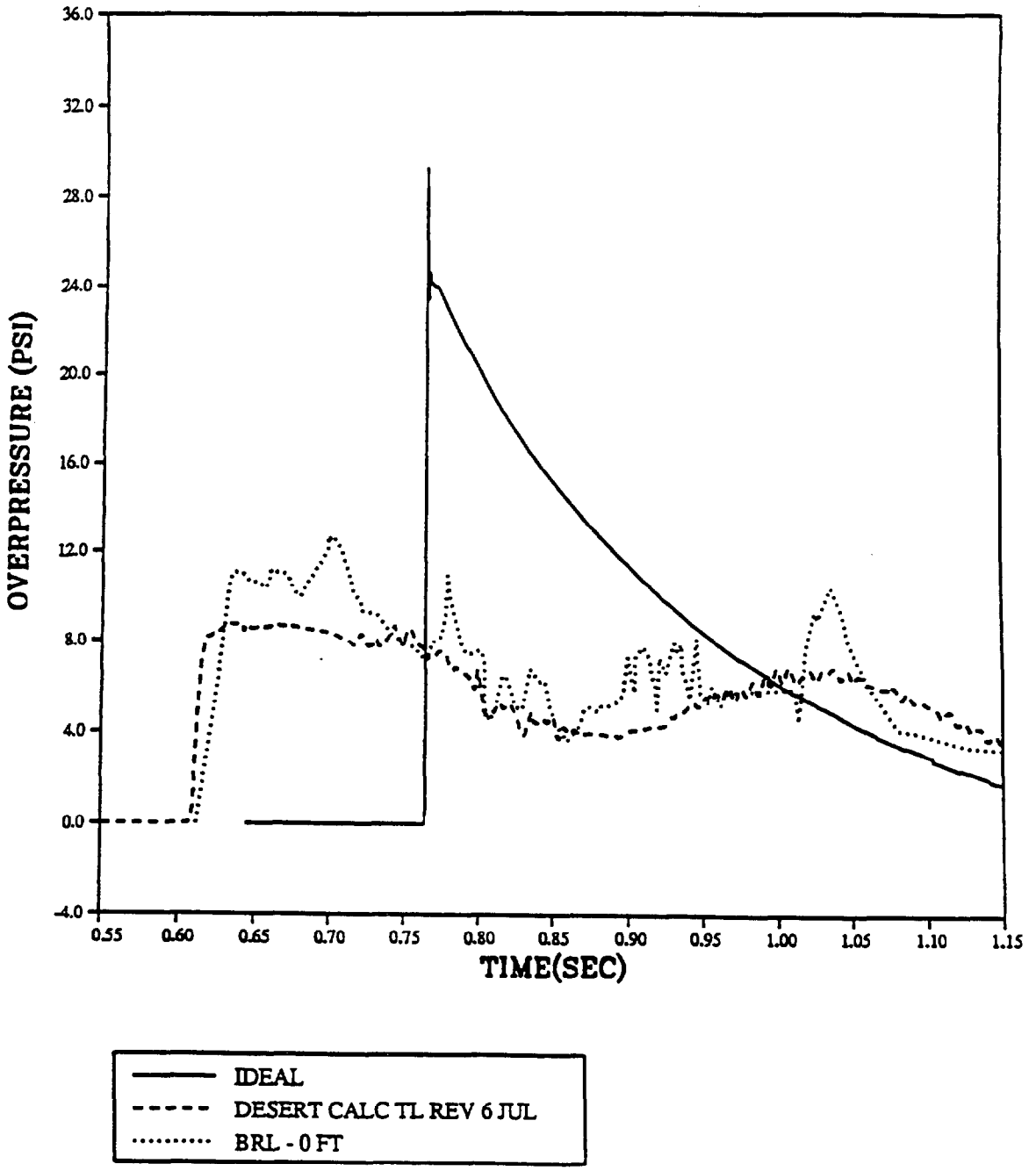

PRISCILLA
CALCULATION - DATA COMPARISONS
OVERPRESSURE AT 2500 FEET (762 M)

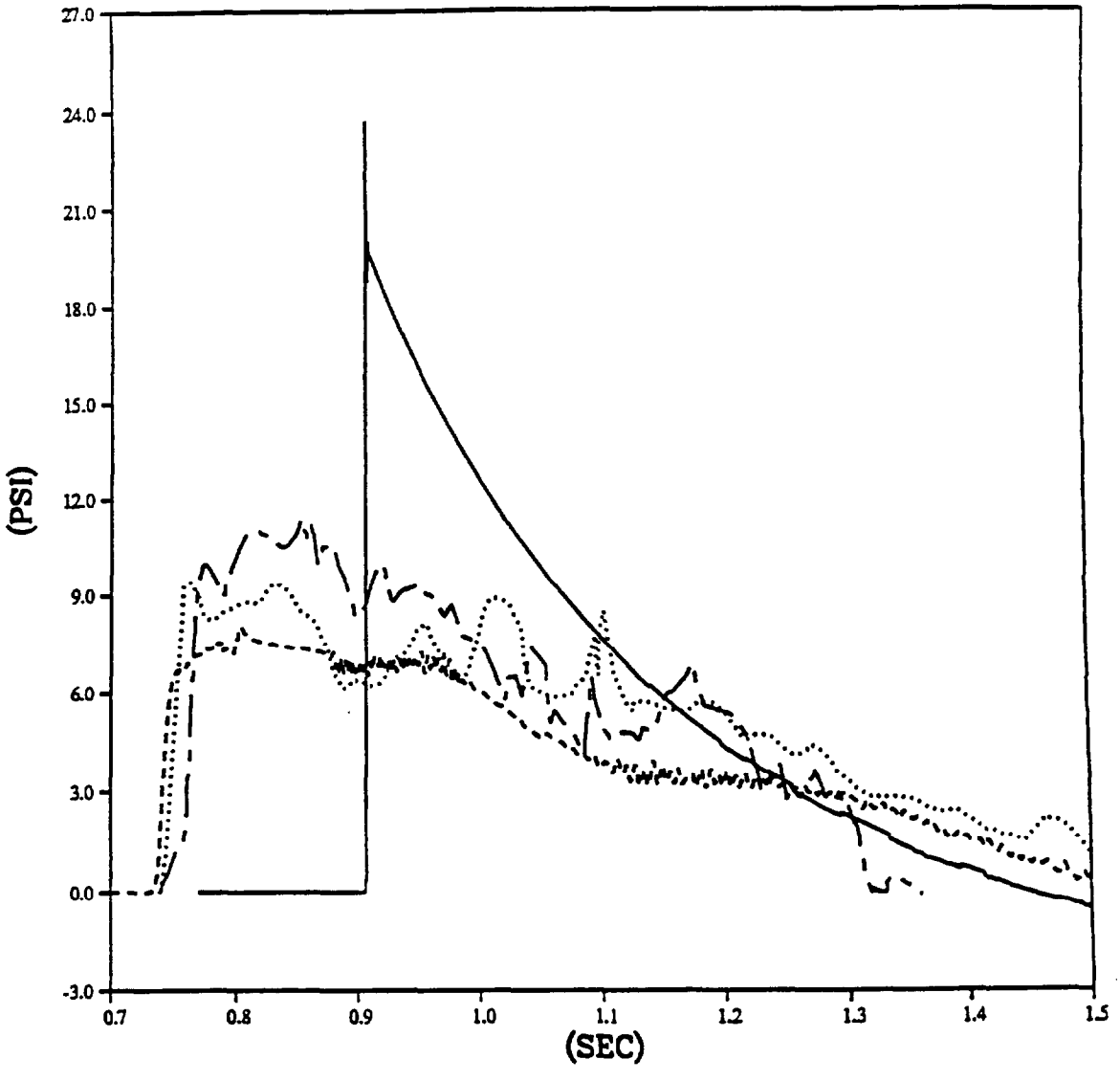

PRISCILLA
CALCULATION - DATA COMPARISONS
OVERPRESSURE AT 2500 FEET (762 M)

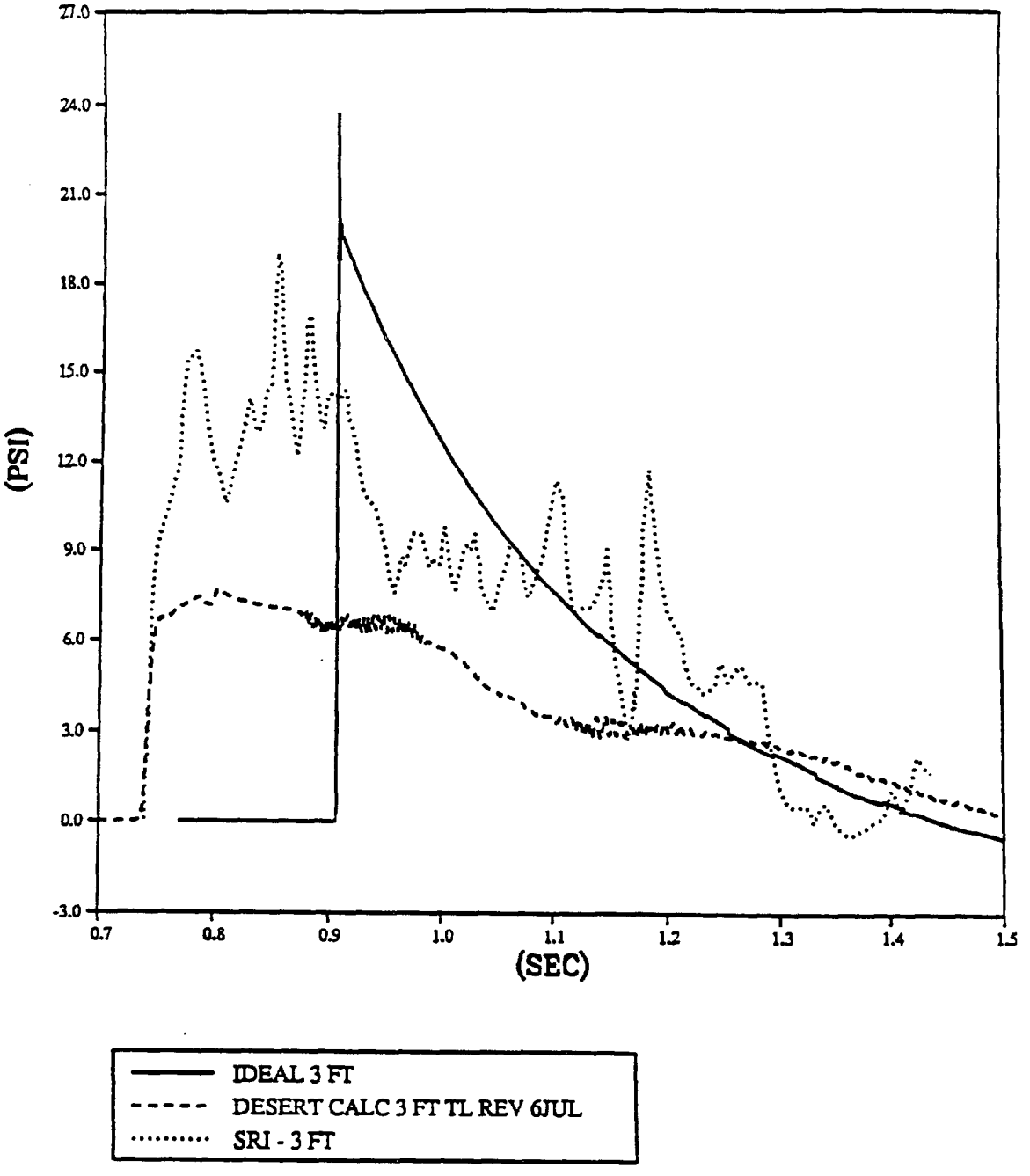

PRISCILLA
CALCULATION - DATA COMPARISONS
OVERPRESSURE AT 2500 FEET (762 M)

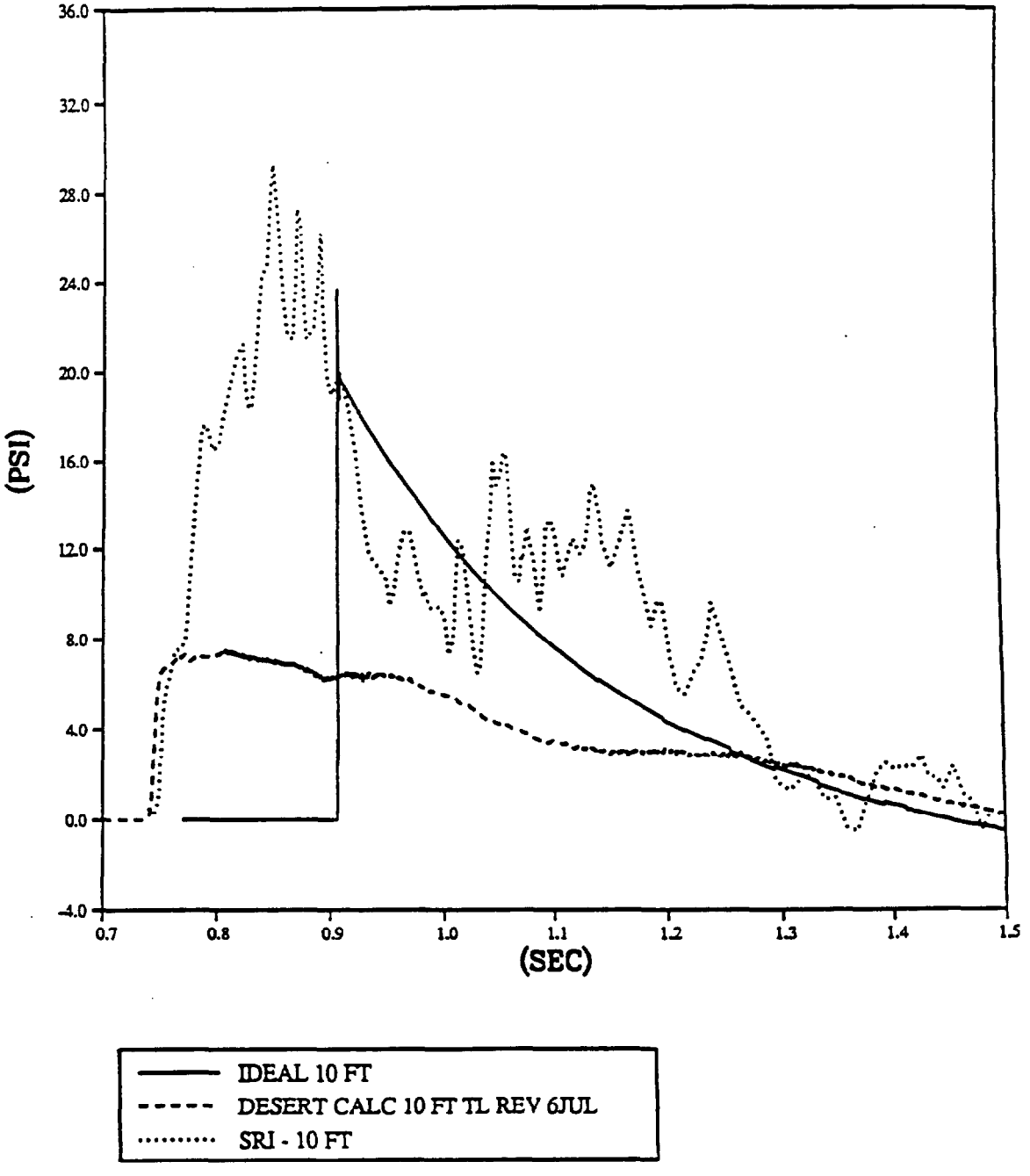

PRISCILLA
CALCULATION - DATA COMPARISONS
OVERPRESSURE AT 3000 FEET (914 M)

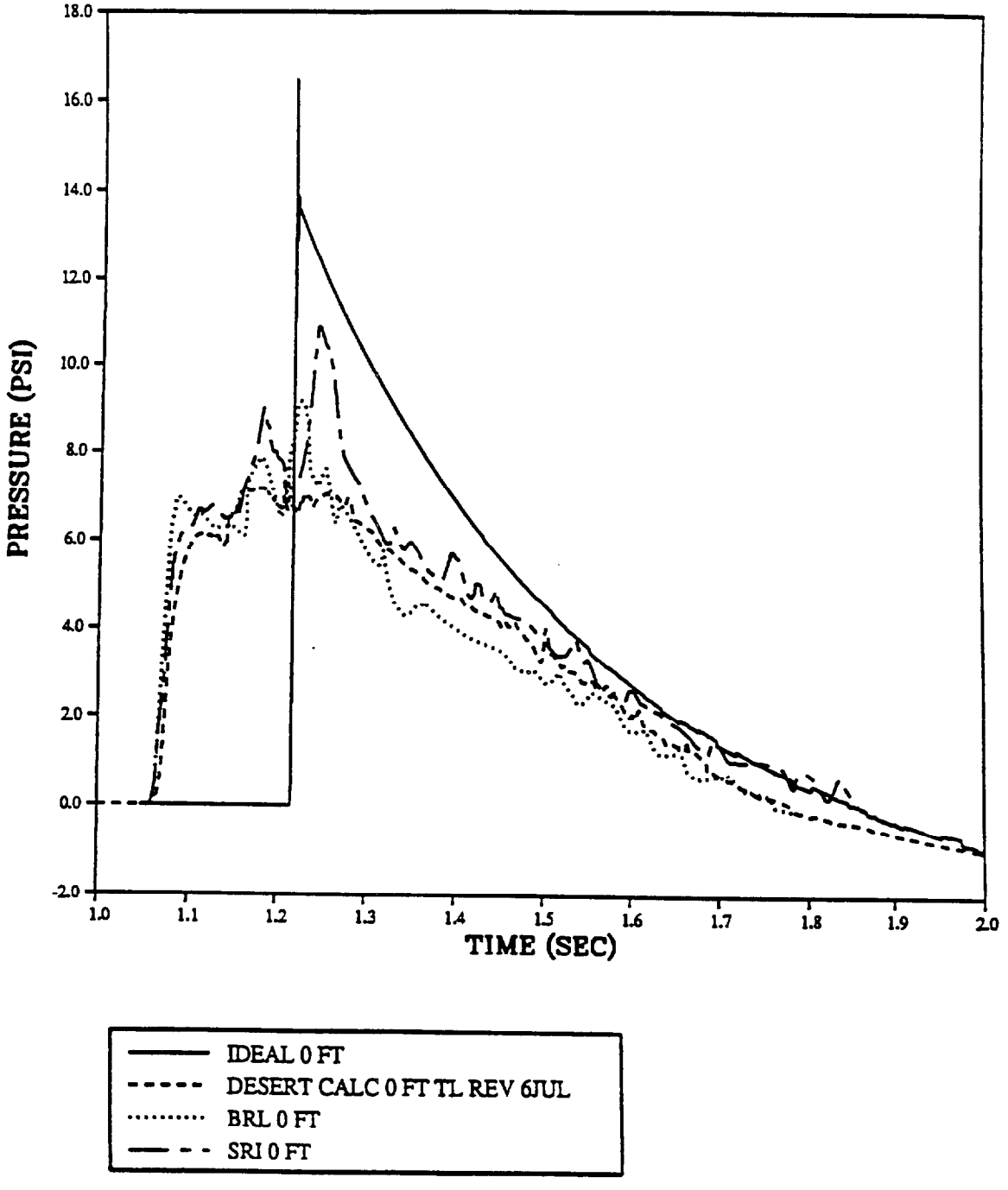

PRISCILLA
CALCULATION - DATA COMPARISONS
OVERPRESSURE AT 3000 FEET (914 M)

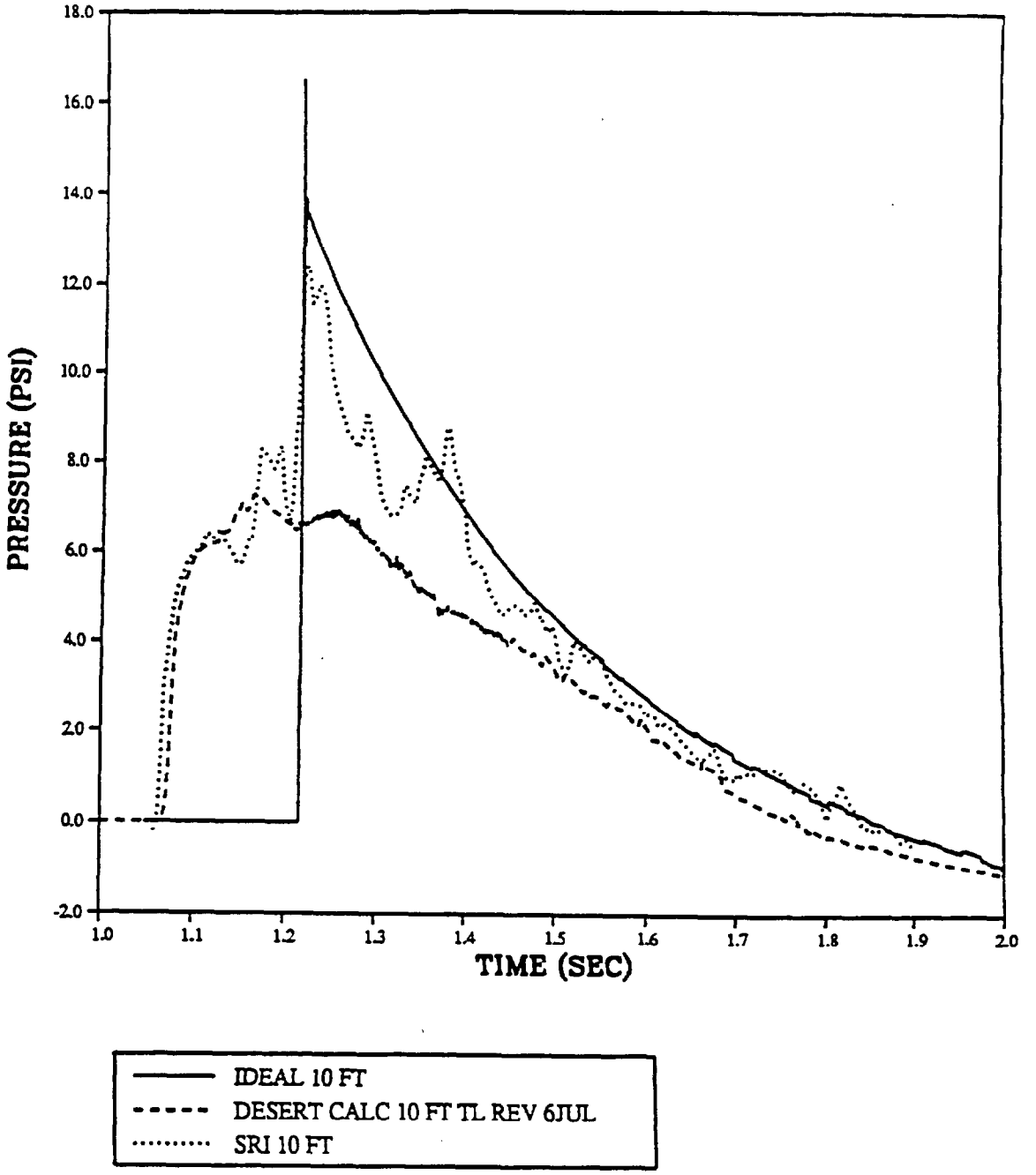

PRISCILLA
CALCULATION - DATA COMPARISONS
OVERPRESSURE AT 3500 FEET (1067 M)

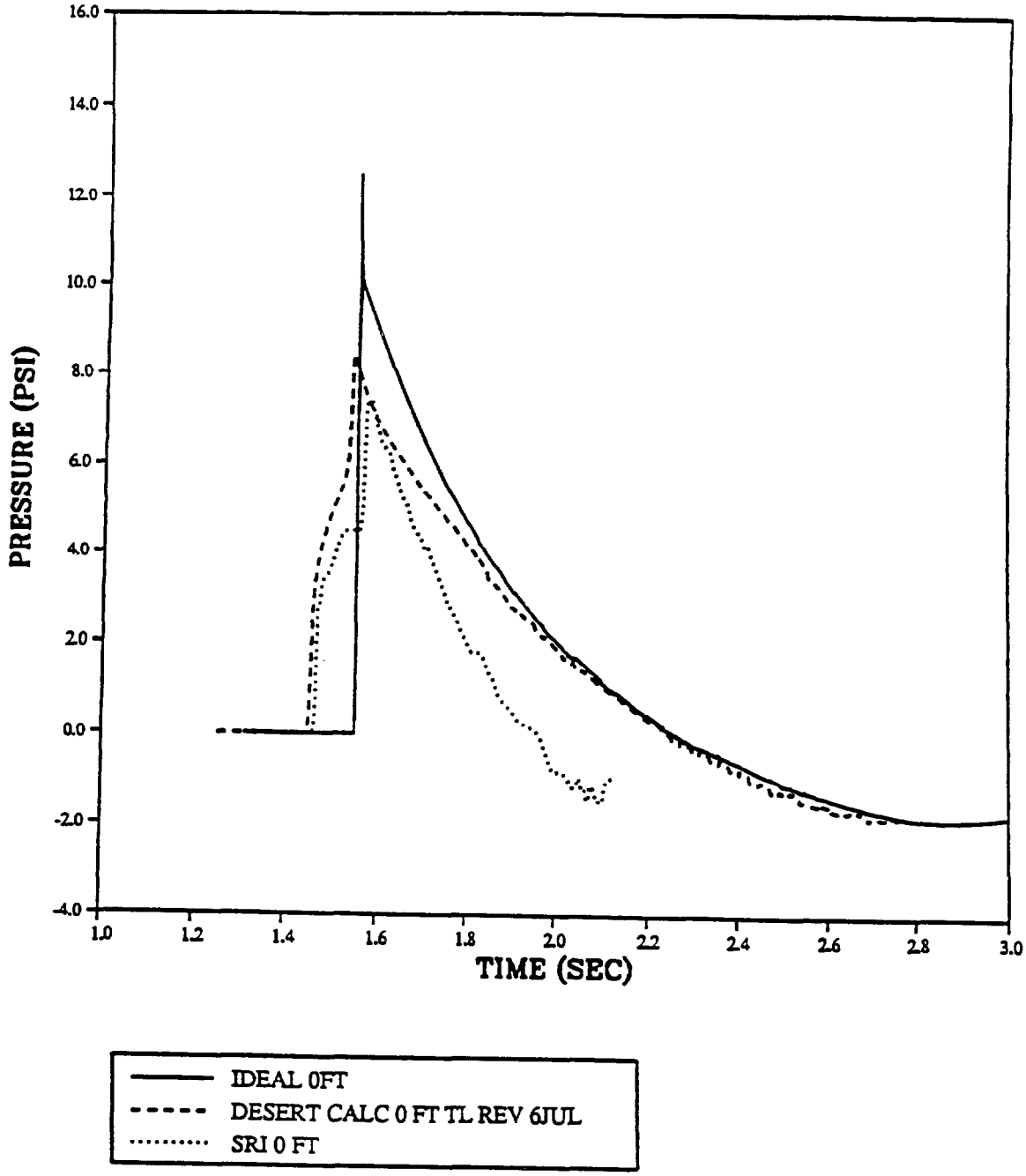

PRISCILLA
CALCULATION - DATA COMPARISONS
OVERPRESSURE AT 3500 FEET (1067 M)

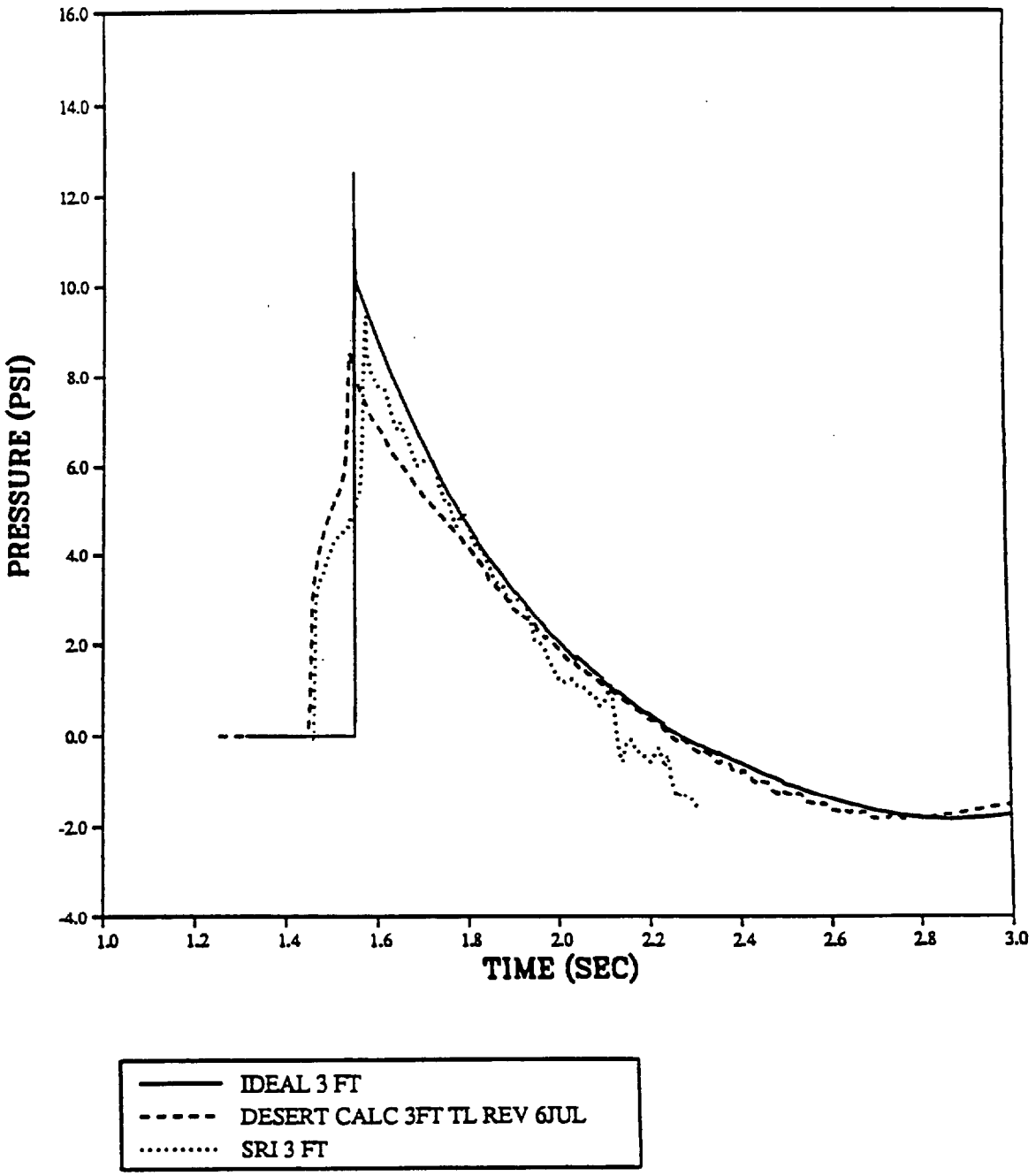

PRISCILLA
CALCULATION - DATA COMPARISONS
OVERPRESSURE AT 4000 FEET (1219 M)

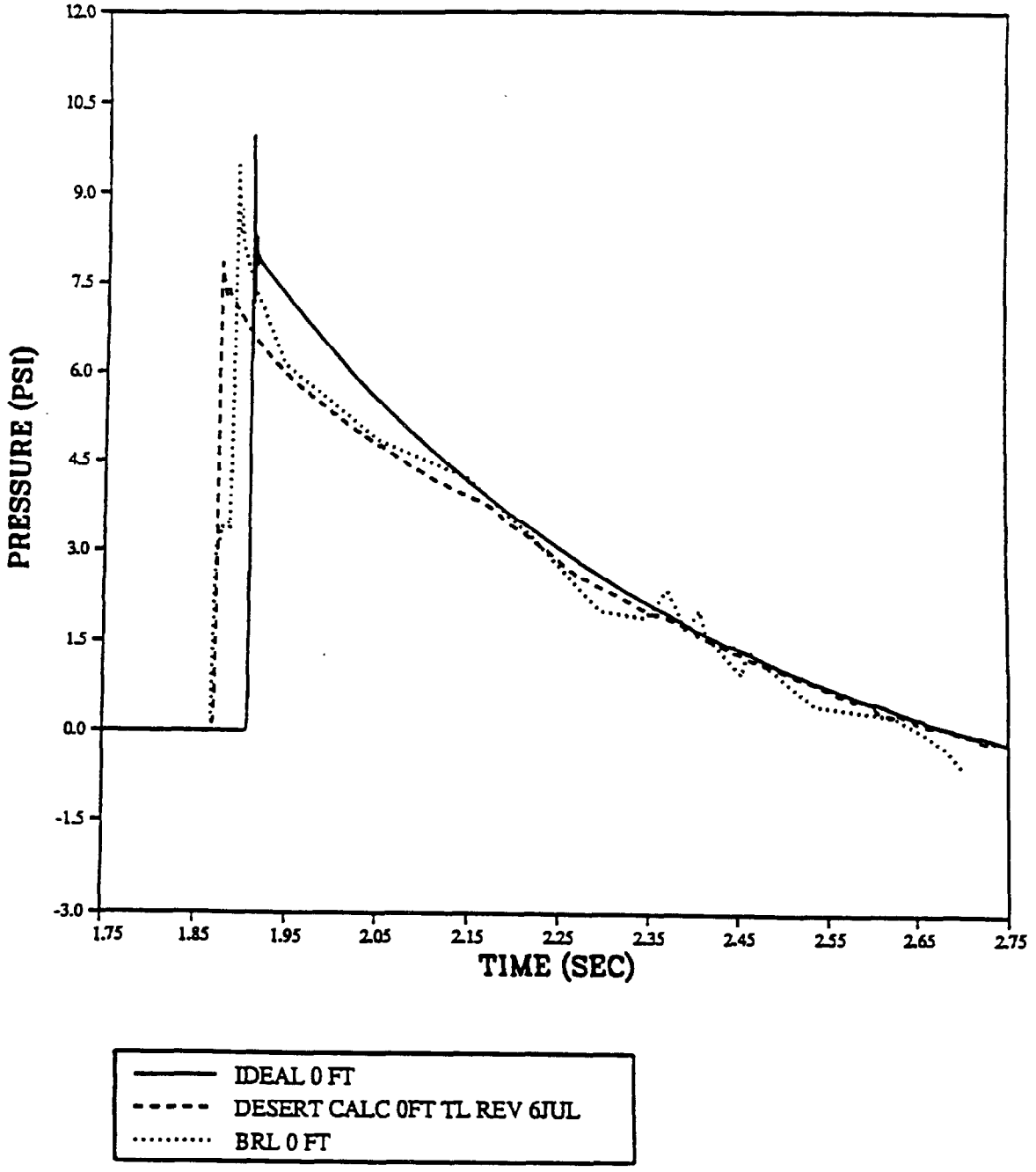

PRISCILLA
CALCULATION - DATA COMPARISONS
OVERPRESSURE AT 5000 FEET (1524 M)

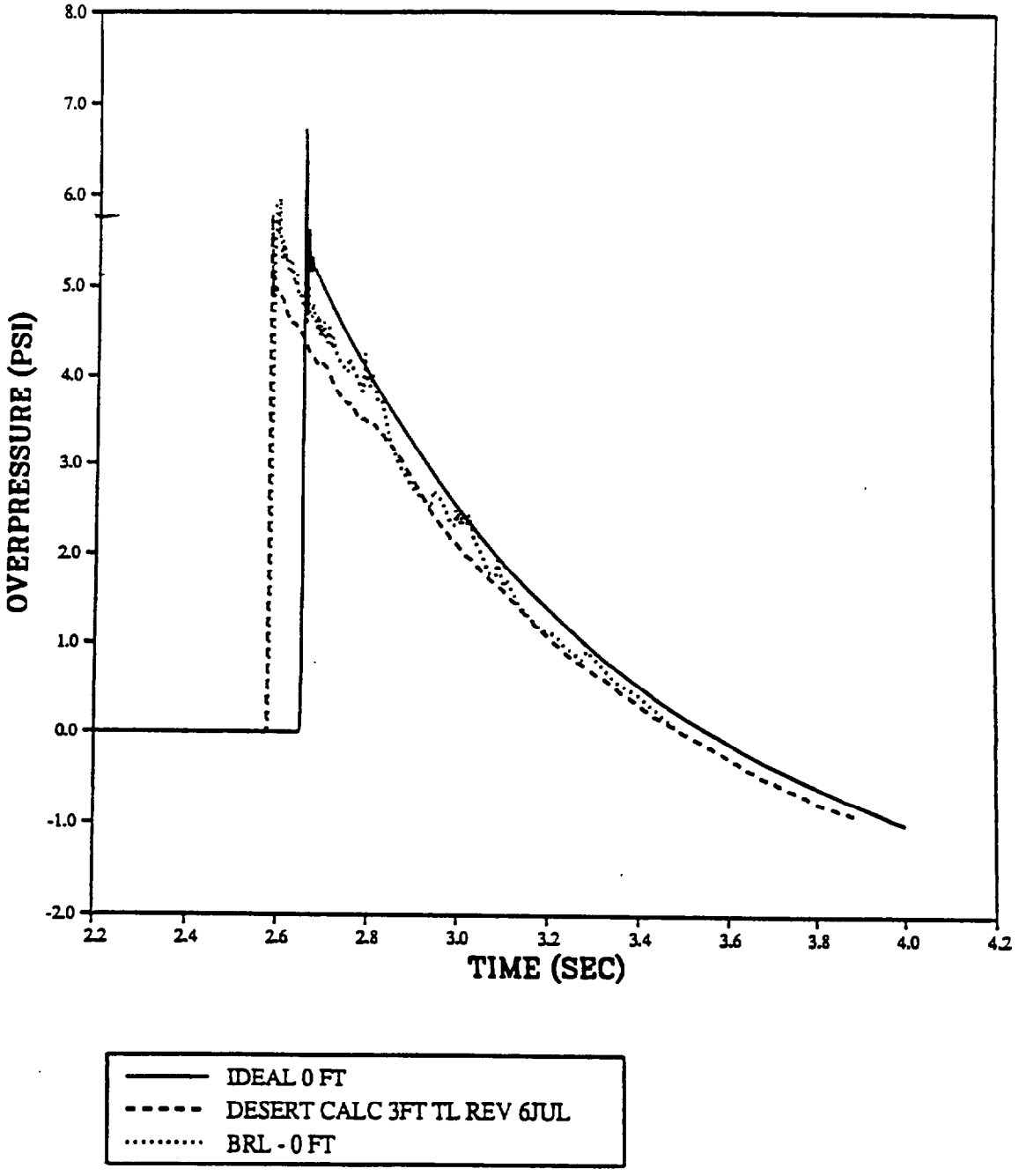

PRISCILLA
CALCULATION - DATA COMPARISONS
DYNAMIC PRESSURE AT 2000 FEET (607 M)

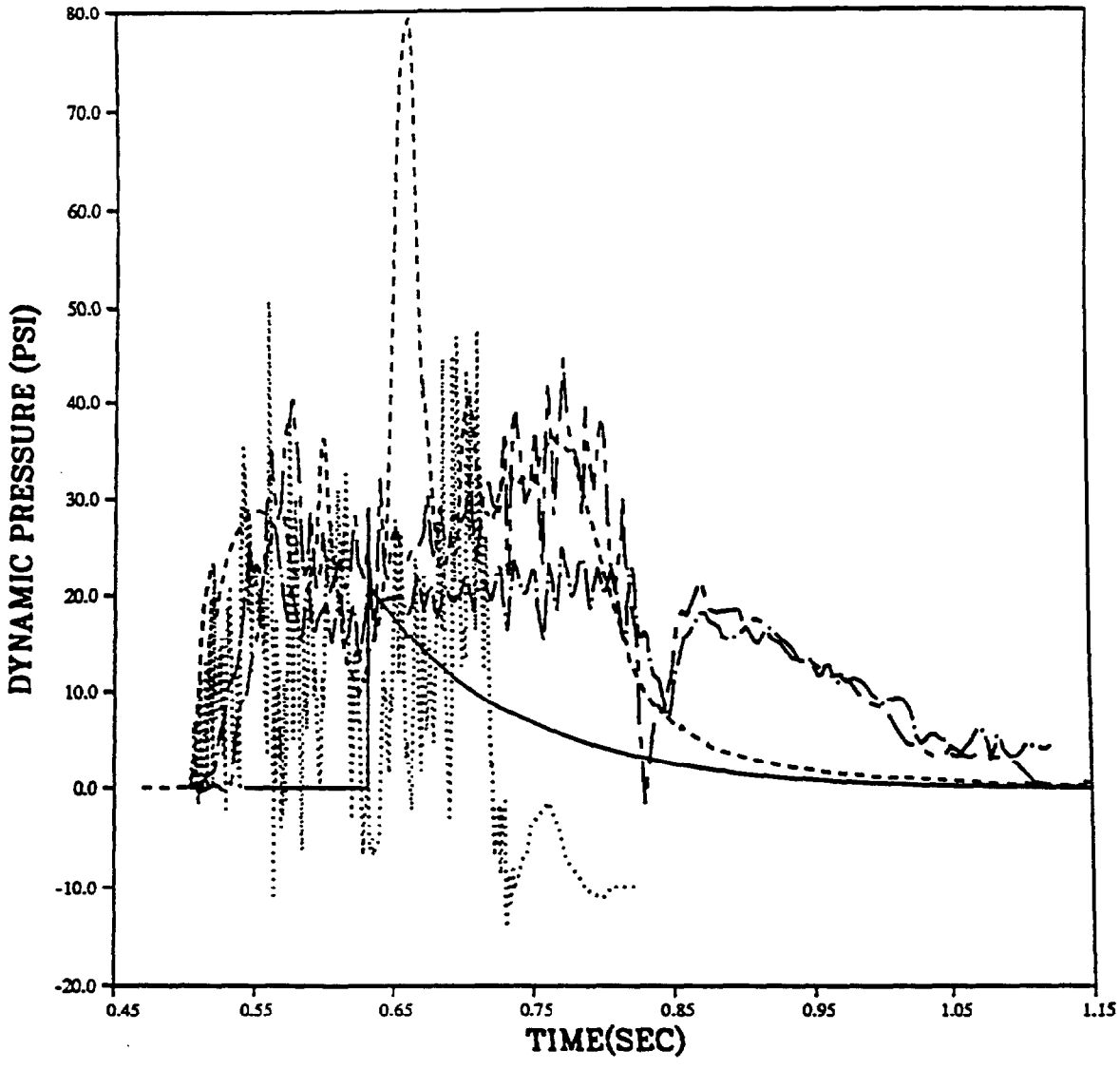

PRISCILLA
CALCULATION - DATA COMPARISONS
DYNAMIC PRESSURE AT 2000 FEET (607 M)

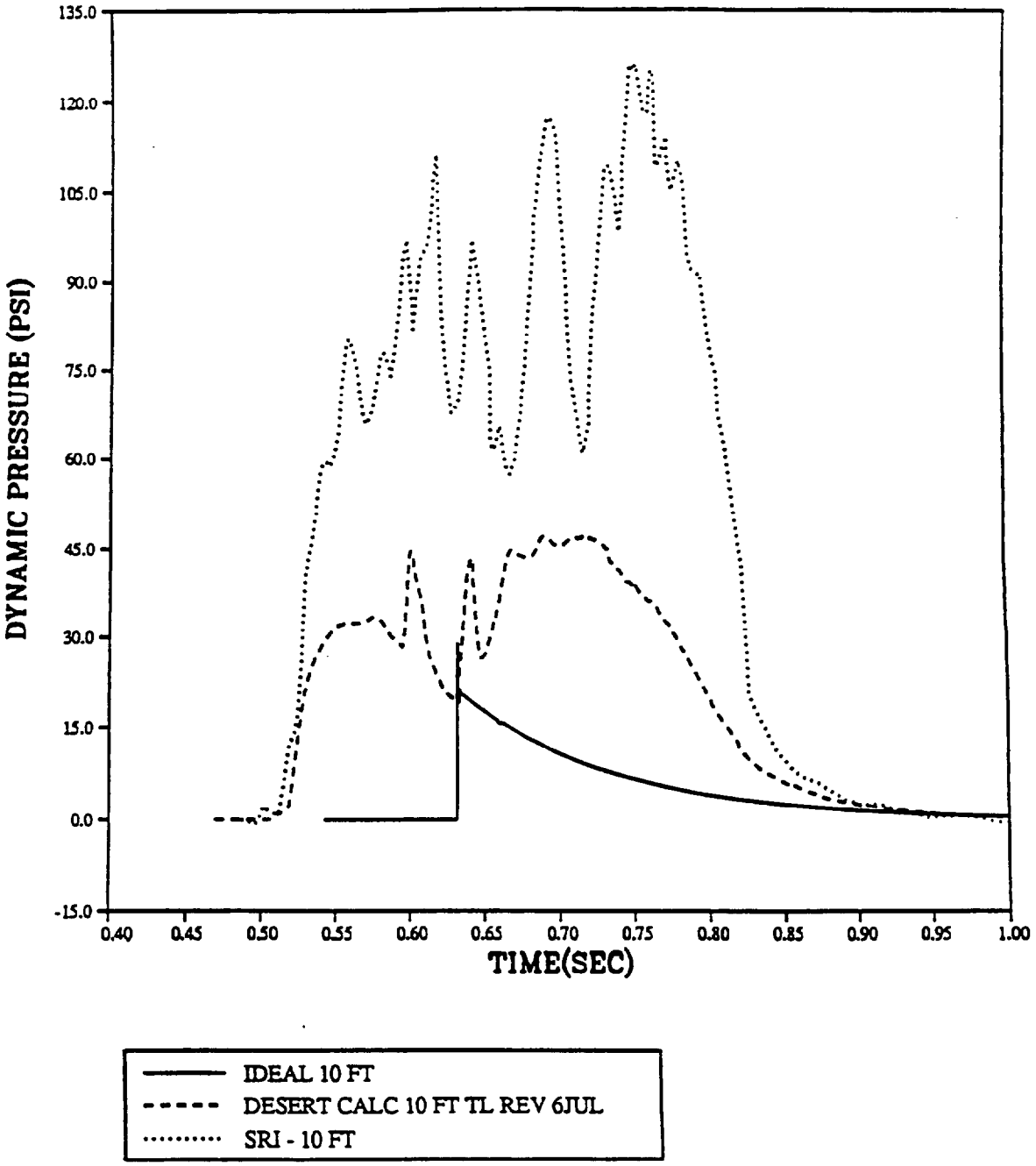

PRISCILLA
CALCULATION - DATA COMPARISONS
DYNAMIC PRESSURE AT 2500 FEET (762 M)

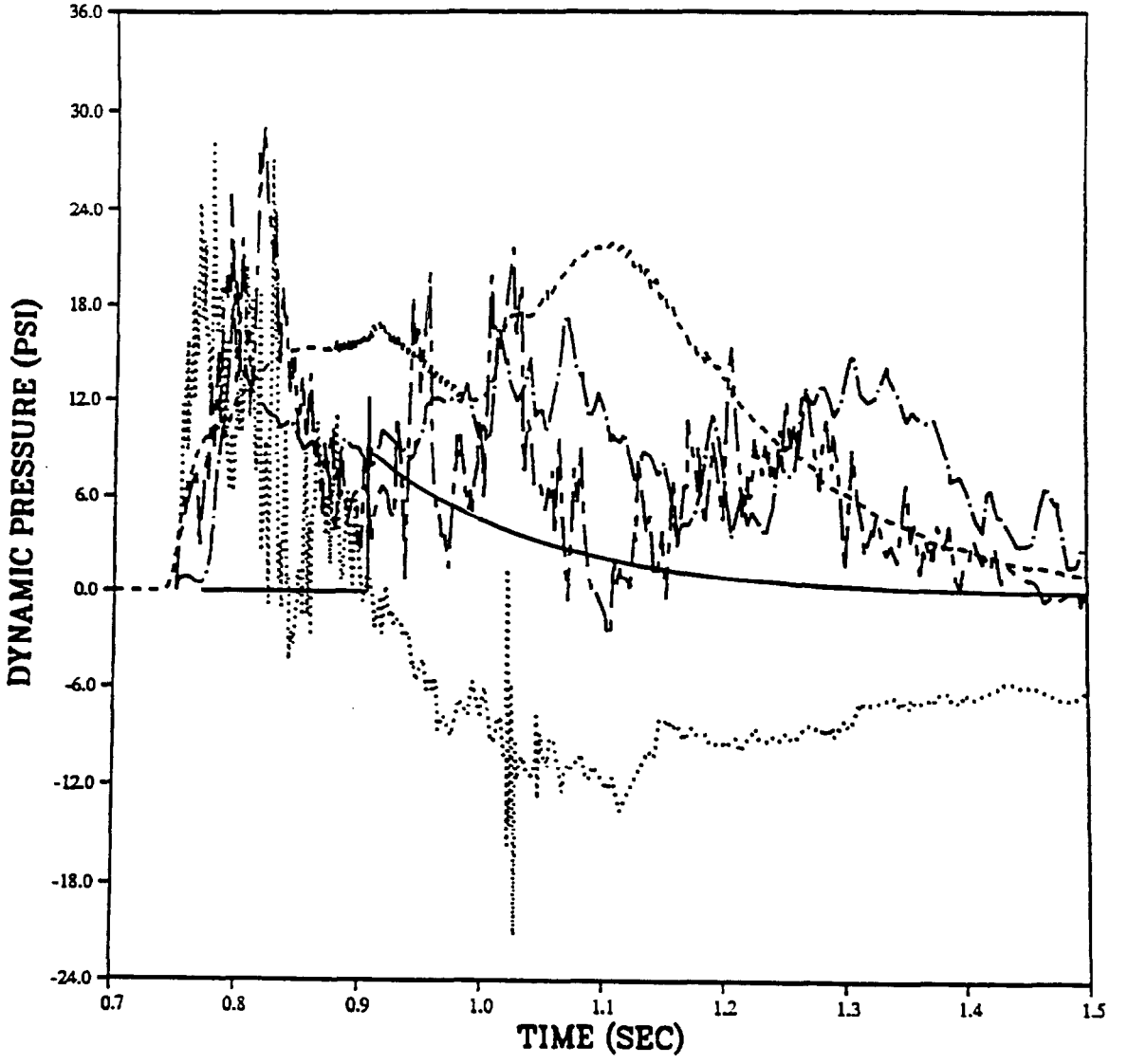

PRISCILLA
CALCULATION - DATA COMPARISONS
DYNAMIC PRESSURE AT 2500 FEET (762 M)

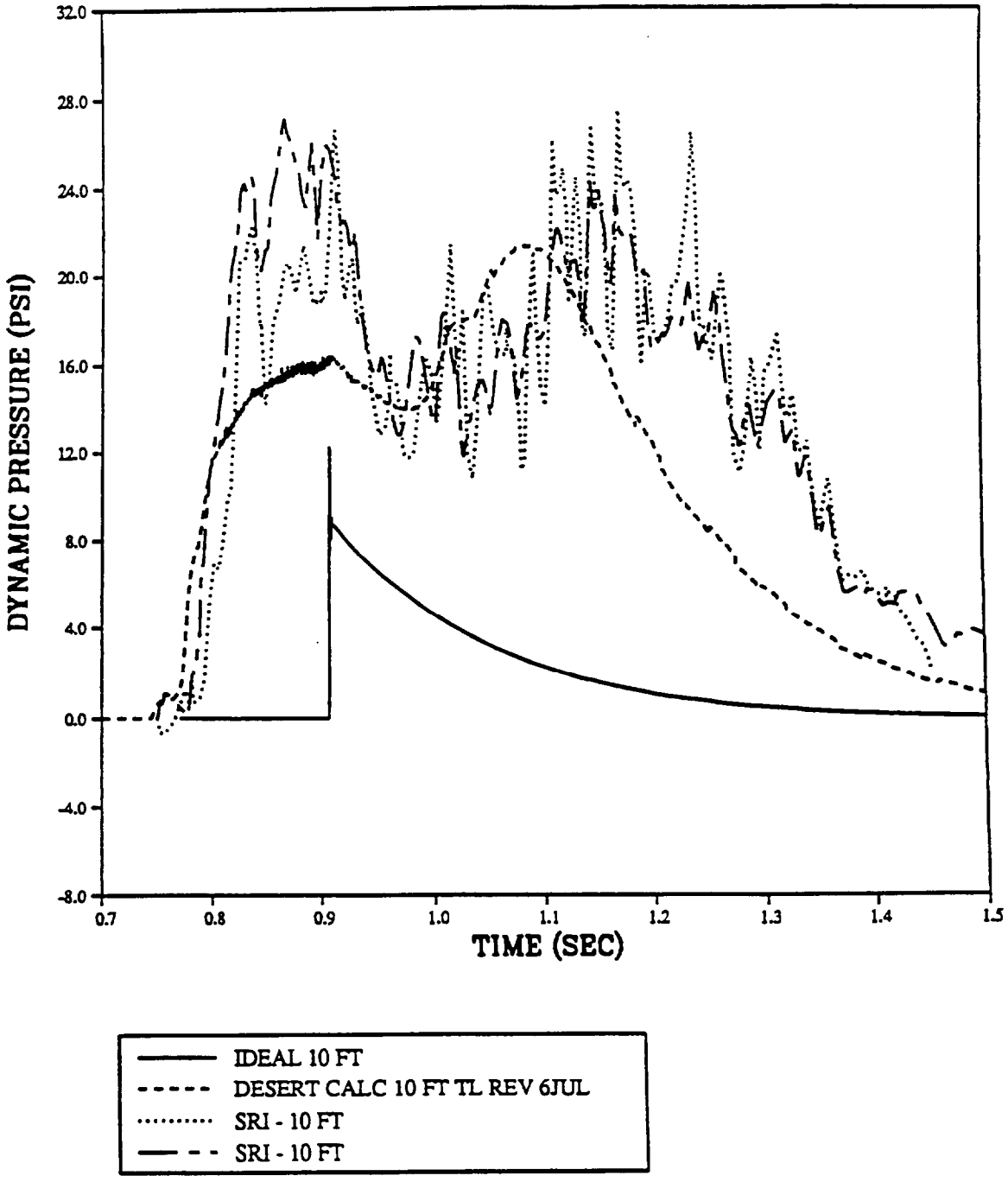

PRISCILLA
CALCULATION - DATA COMPARISONS
DYNAMIC PRESSURE AT 3000 FEET (762 M)

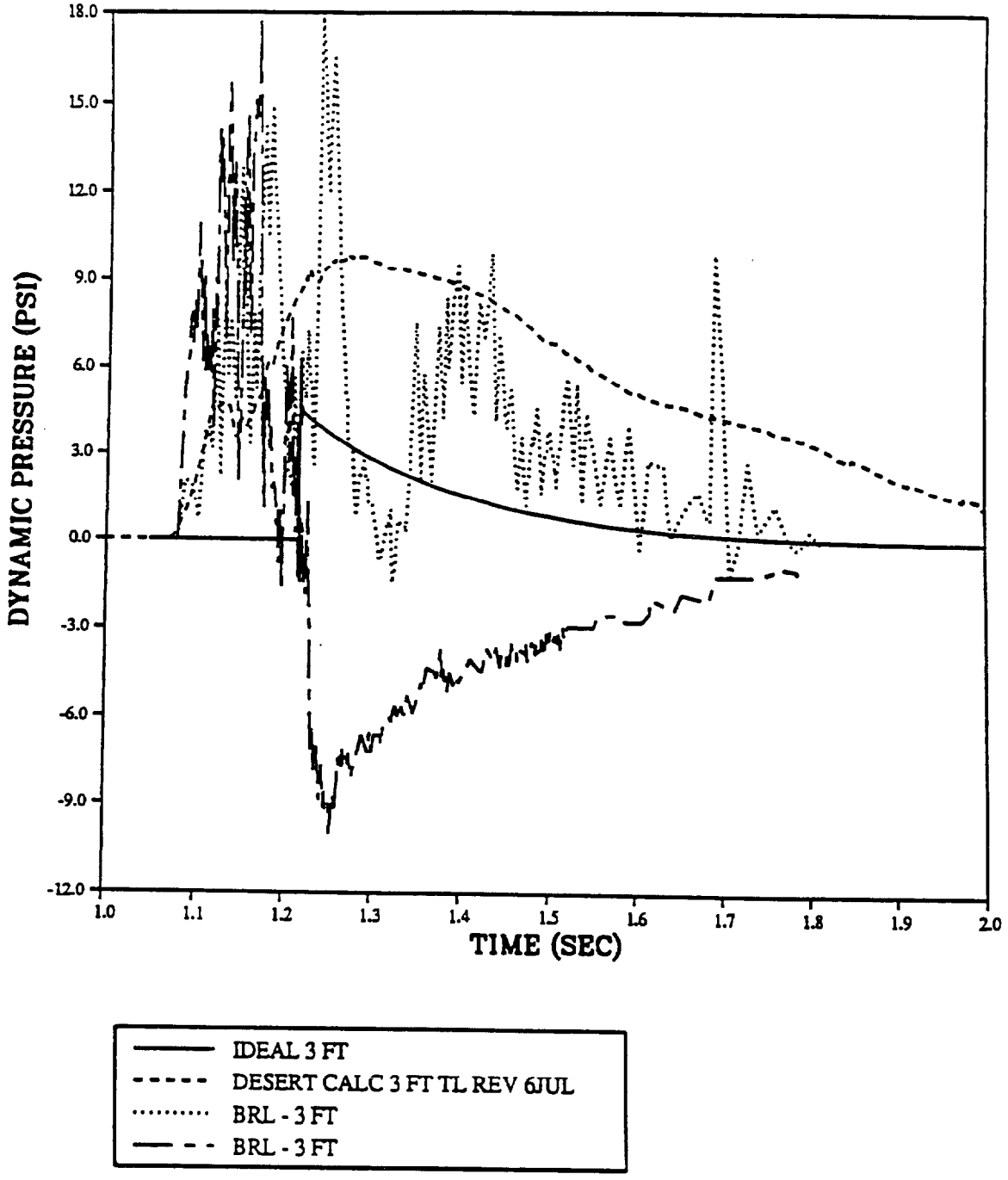

PRISCILLA
CALCULATION - DATA COMPARISONS
DYNAMIC PRESSURE AT 3000 FEET (762 M)

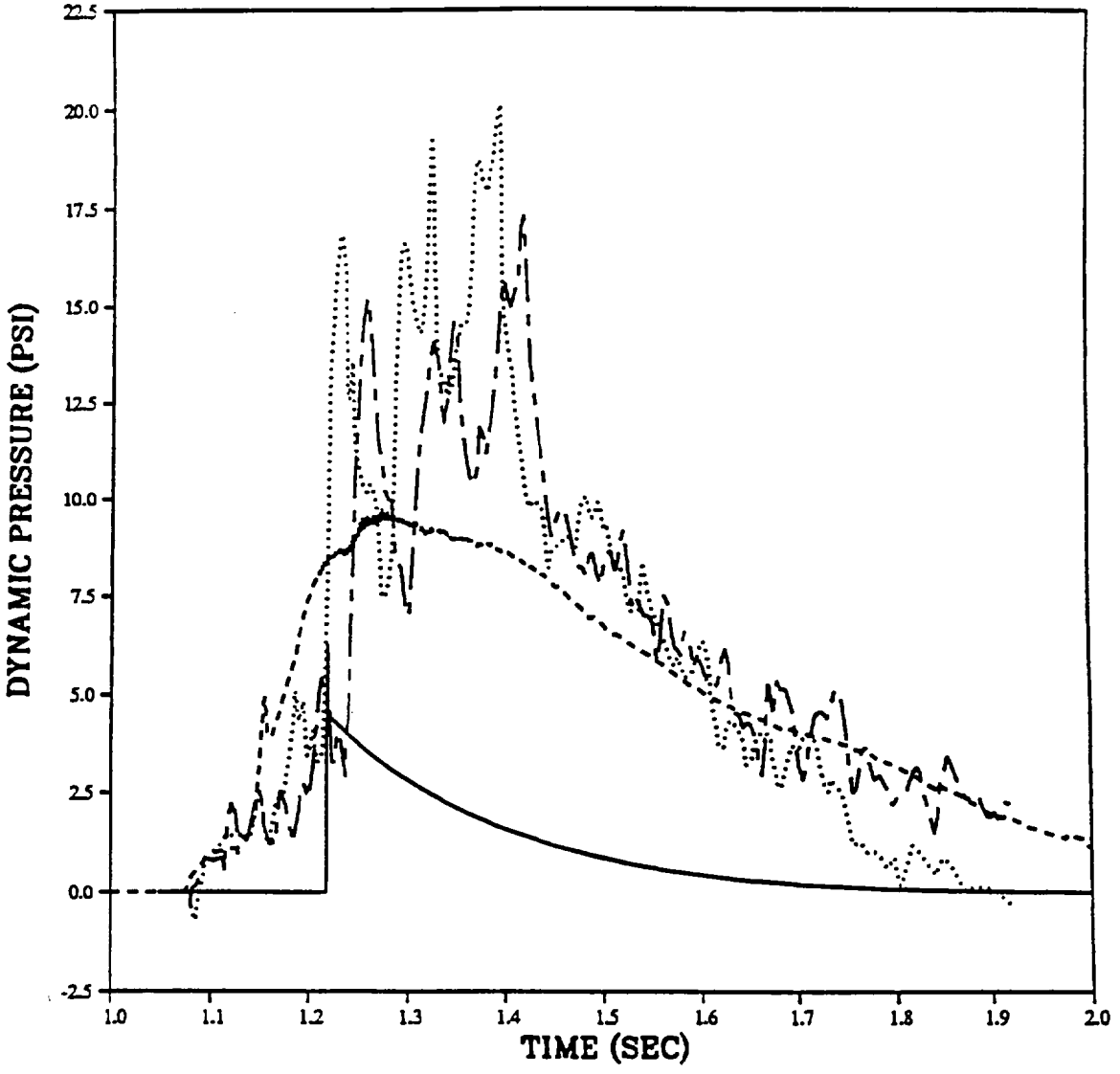

PRISCILLA
CALCULATION - DATA COMPARISONS
DYNAMIC PRESSURE AT 3500 FEET (1067 M)

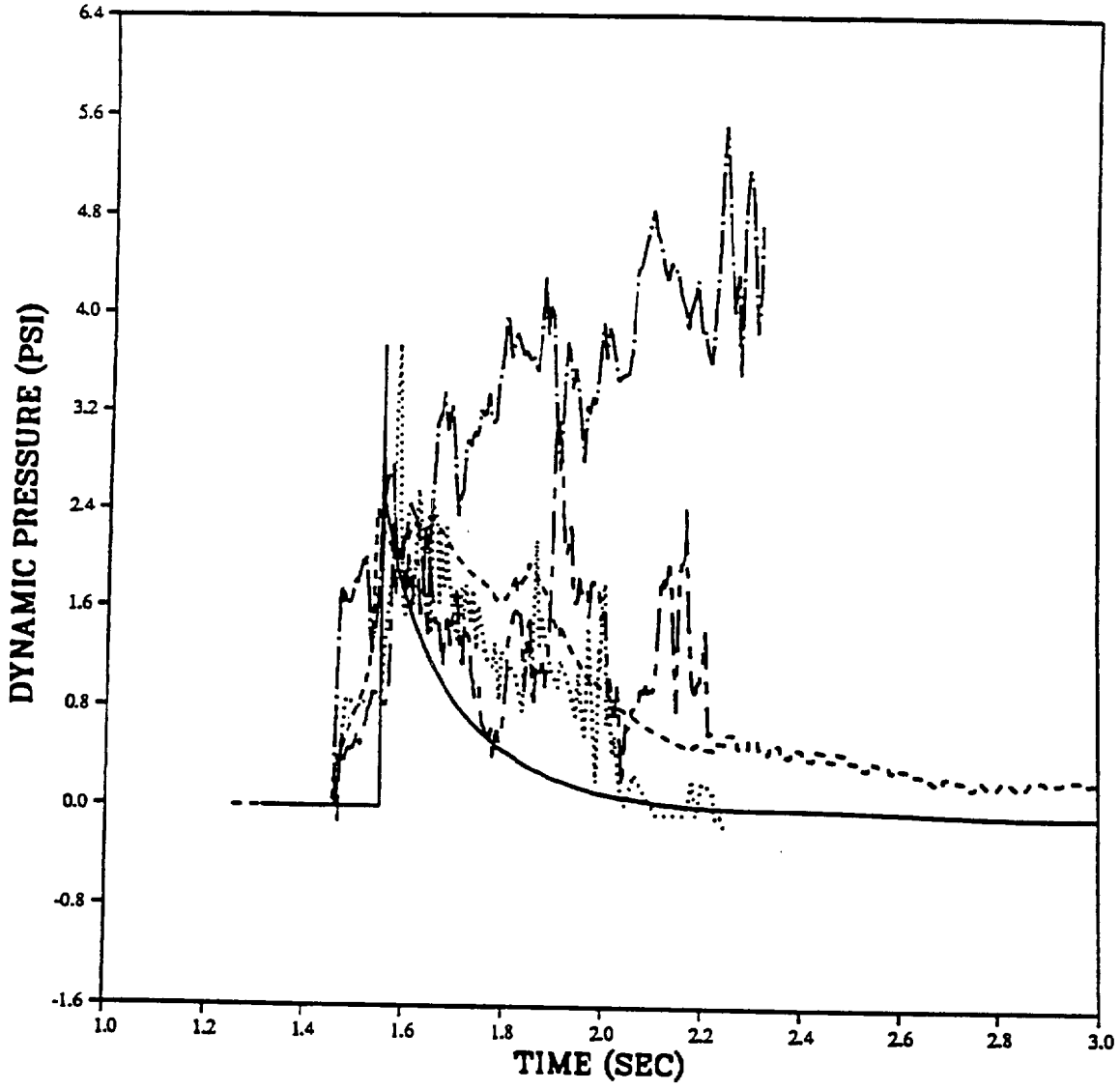

IDEAL 3FT
DESERT CALC 3FT TL REV 6JUL
BRL - 3 FT
SRI - 3 FT
SRI - 3 FT

PRISCILLA
CALCULATION - DATA COMPARISONS
DYNAMIC PRESSURE AT 3500 FEET (1067 M)

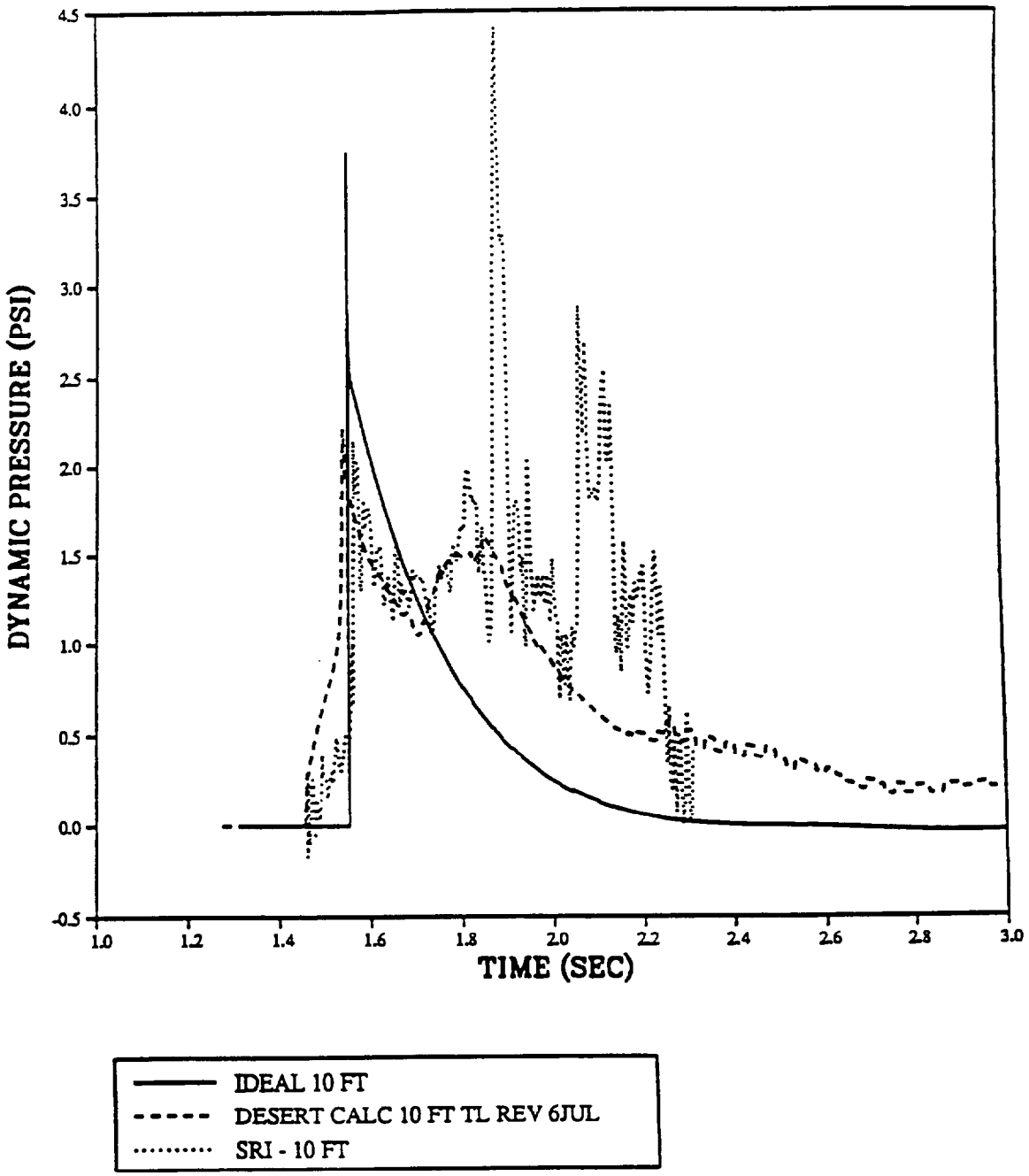

PRISCILLA
CALCULATION - DATA COMPARISONS
DYNAMIC PRESSURE AT 4000 FEET (1219 M)

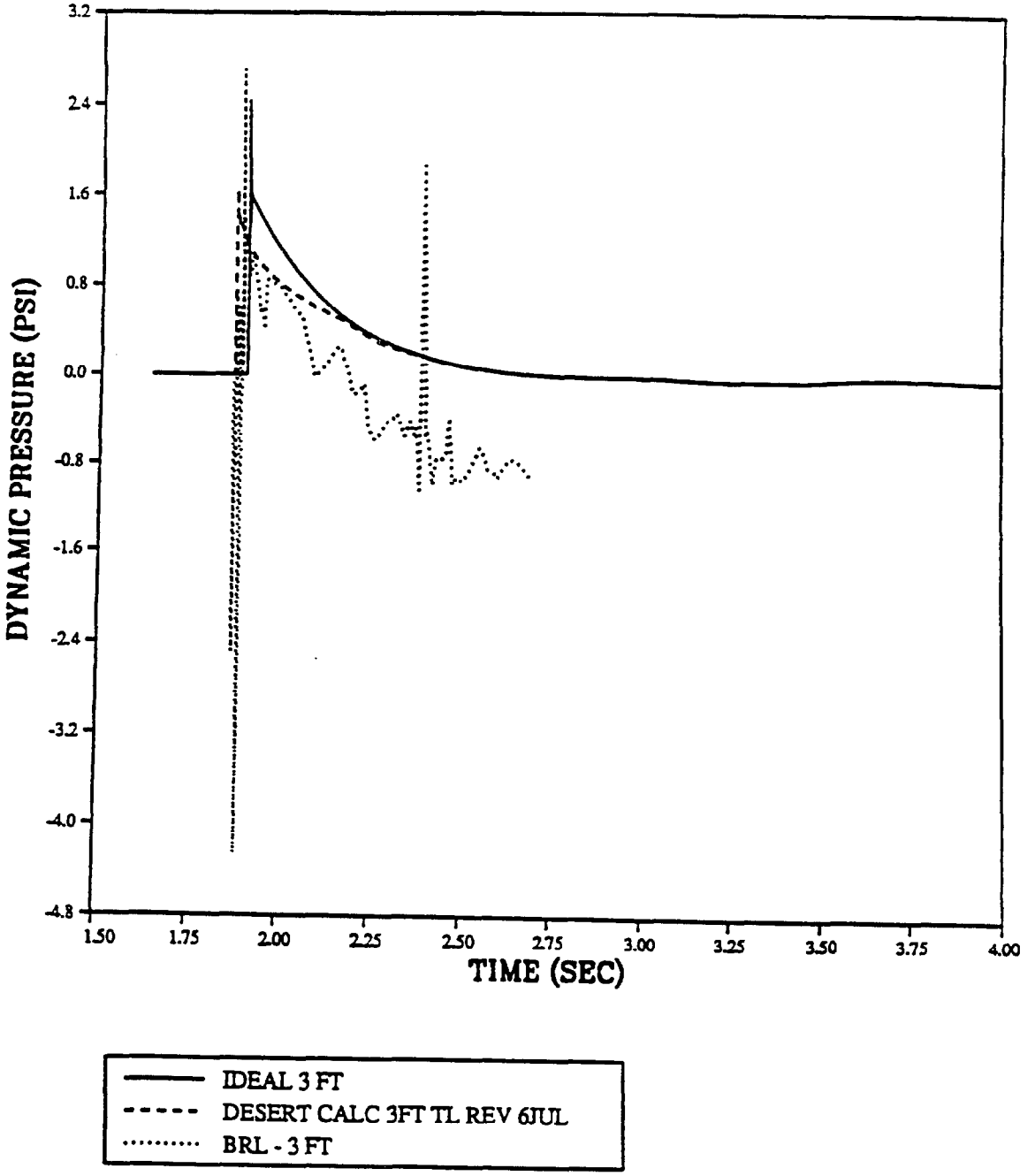

PRISCILLA
CALCULATION - DATA COMPARISONS
DYNAMIC PRESSURE AT 4500 FEET (1372 M)

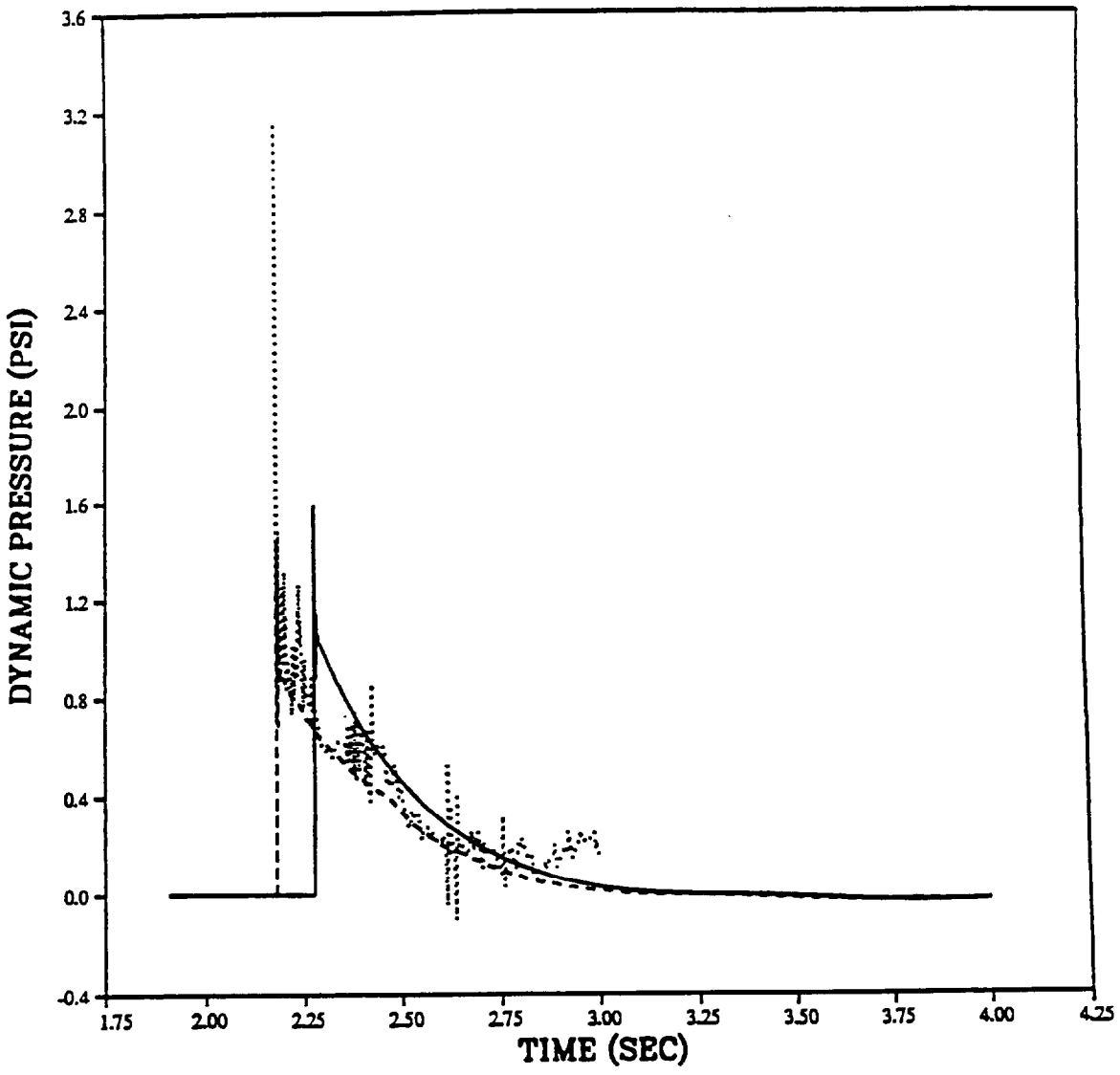

INTENTIONALLY LEFT BLANK.

APPENDIX C
HYDRODYNAMIC PARAMETERS AS A FUNCTION OF HEIGHT FOR SELECTED GROUND RANGES

This Appendix contains plots of important hydrodynamic parameters as a function of height above the surface at several ground ranges. The ground ranges were selected on the basis of predicted ideal overpressure levels. Results of calculated ideal and precursor parameters are displayed on each plot. Because of the problem with 32-bit truncation causing the precursor stations to move prior to shock arrival, most of the precursor results include two curves; one on either side of the ideal range.

PRISCILLA DESERT
OVERPRESSURE AT 2100 FEET
VERTICAL PROFILE

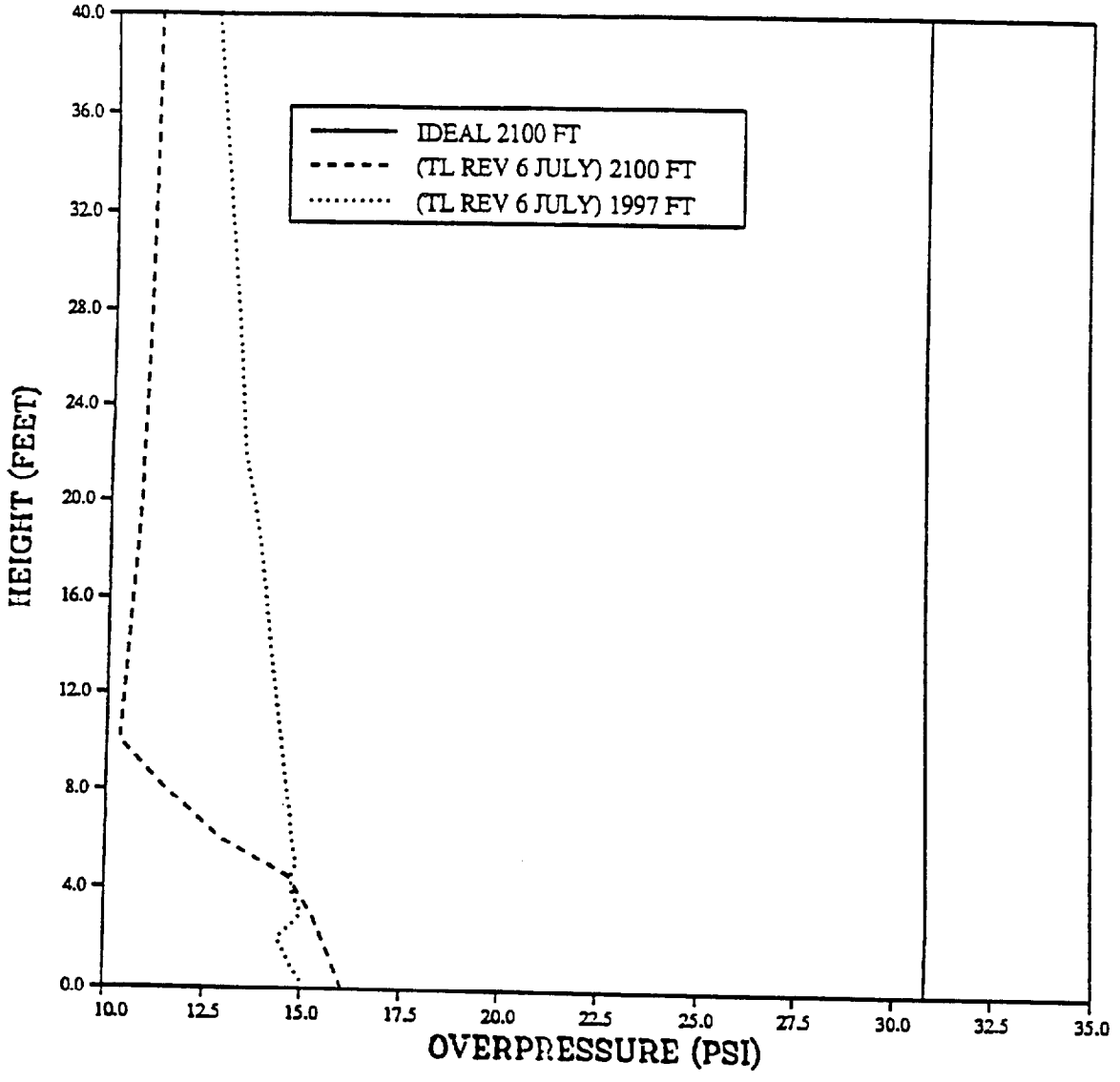

PRISCILLA DESERT
OVERPRESSURE AT 2300 FEET
VERTICAL PROFILE

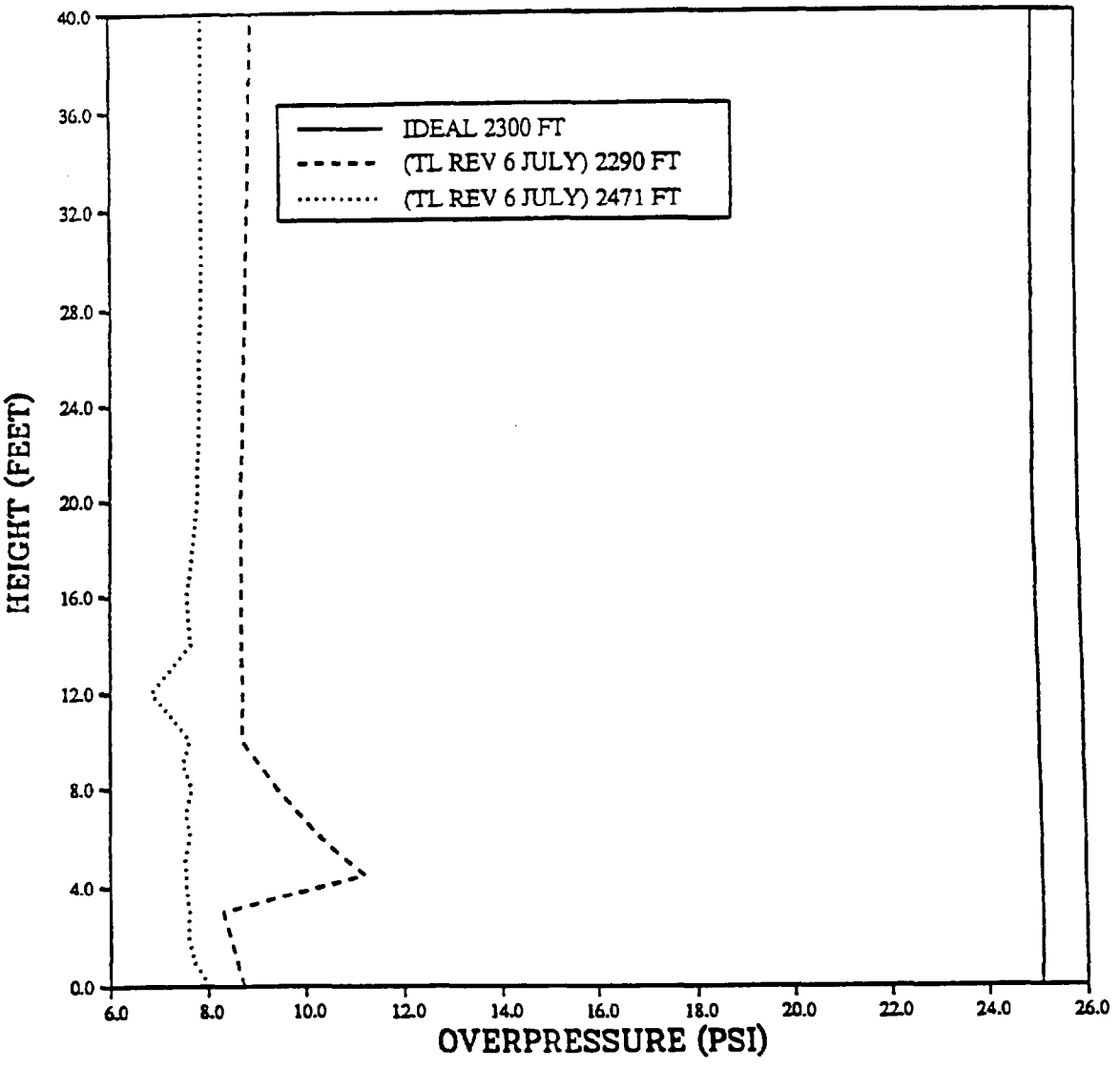

PRISCILLA DESERT
OVERPRESSURE AT 2550 FEET
VERTICAL PROFILE

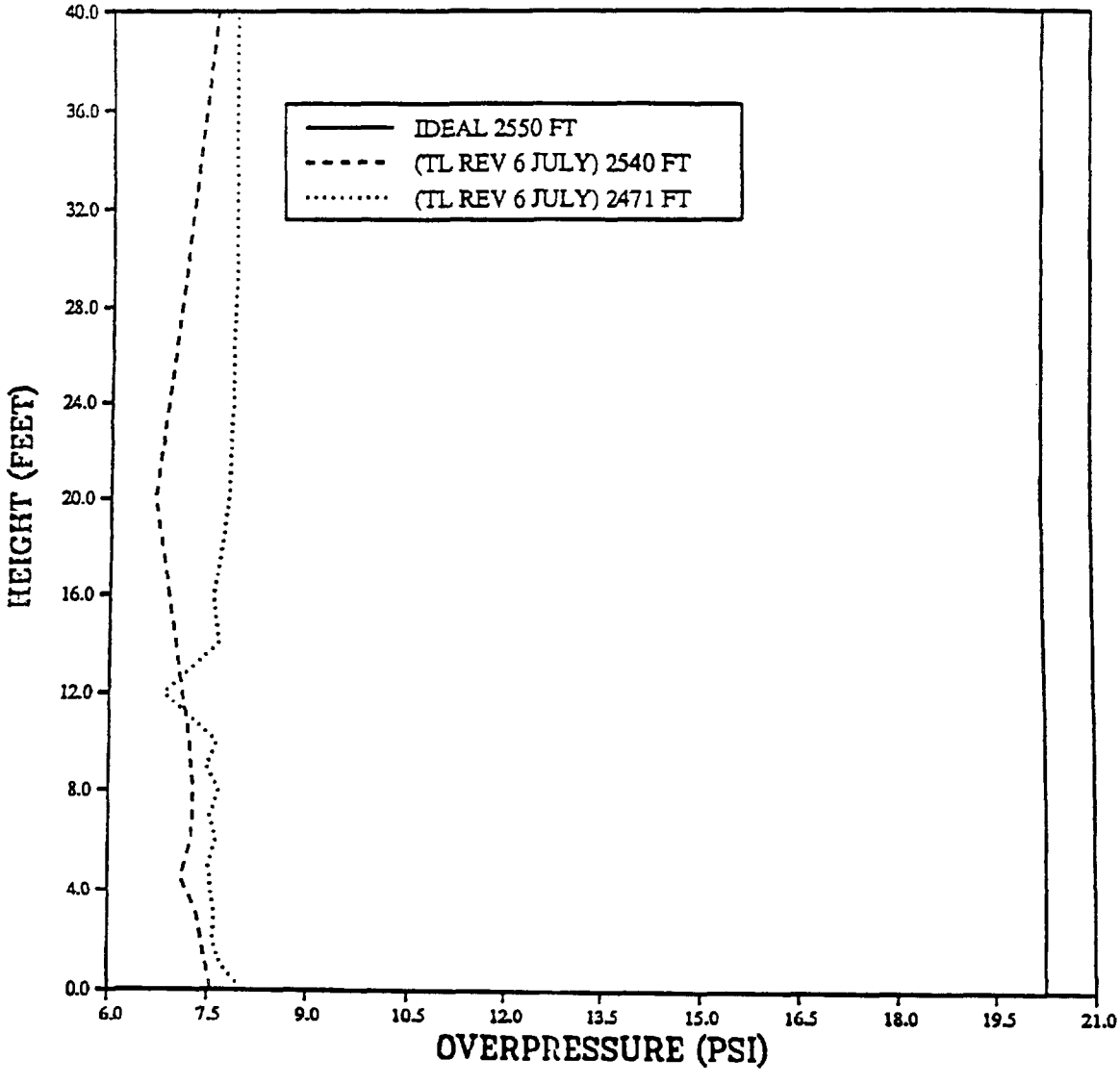

PRISCILLA DESERT
OVERPRESSURE AT 2950 FEET
VERTICAL PROFILE

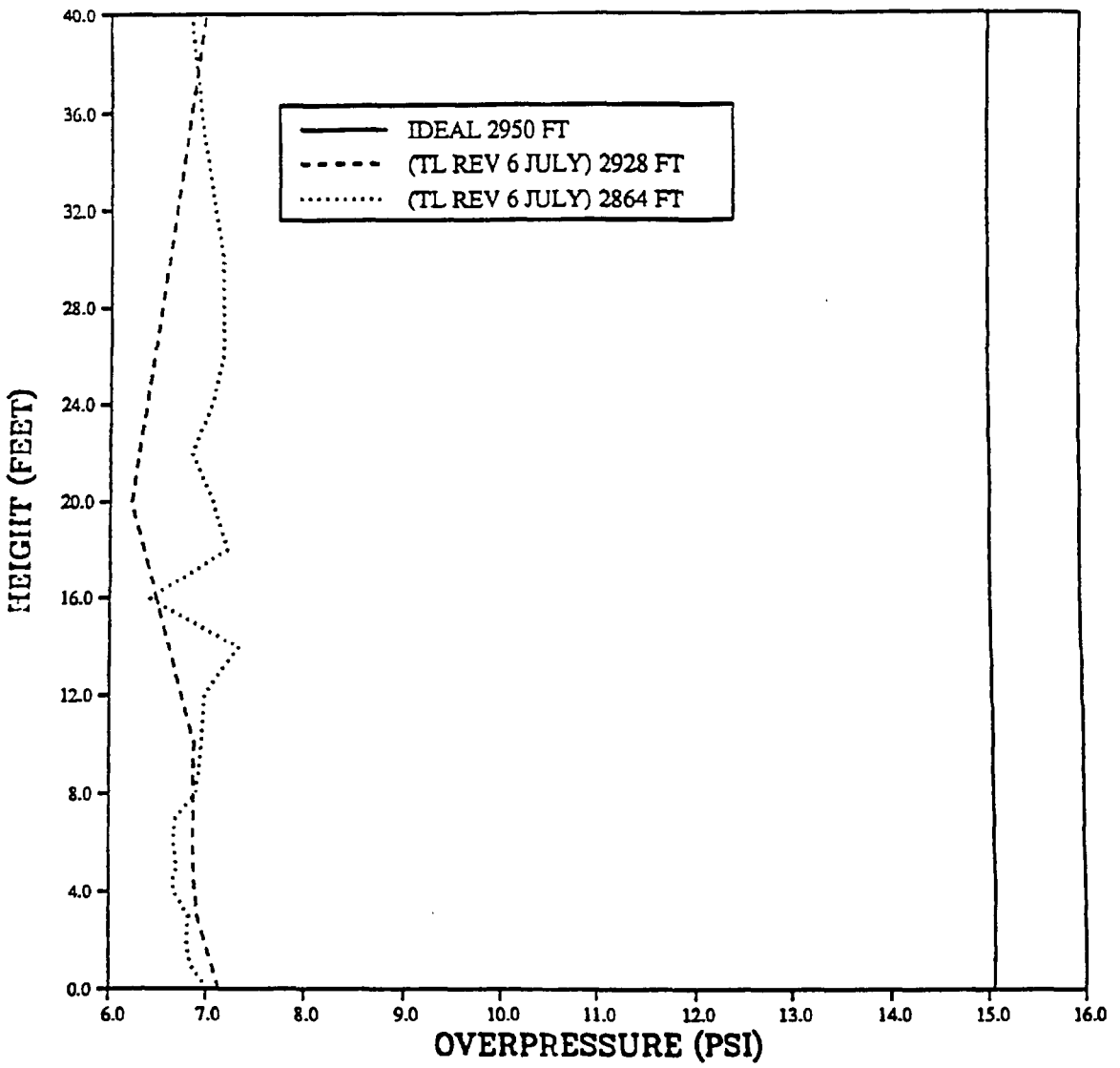

PRISCILLA DESERT
OVERPRESSURE AT 3250 FEET
VERTICAL PROFILE

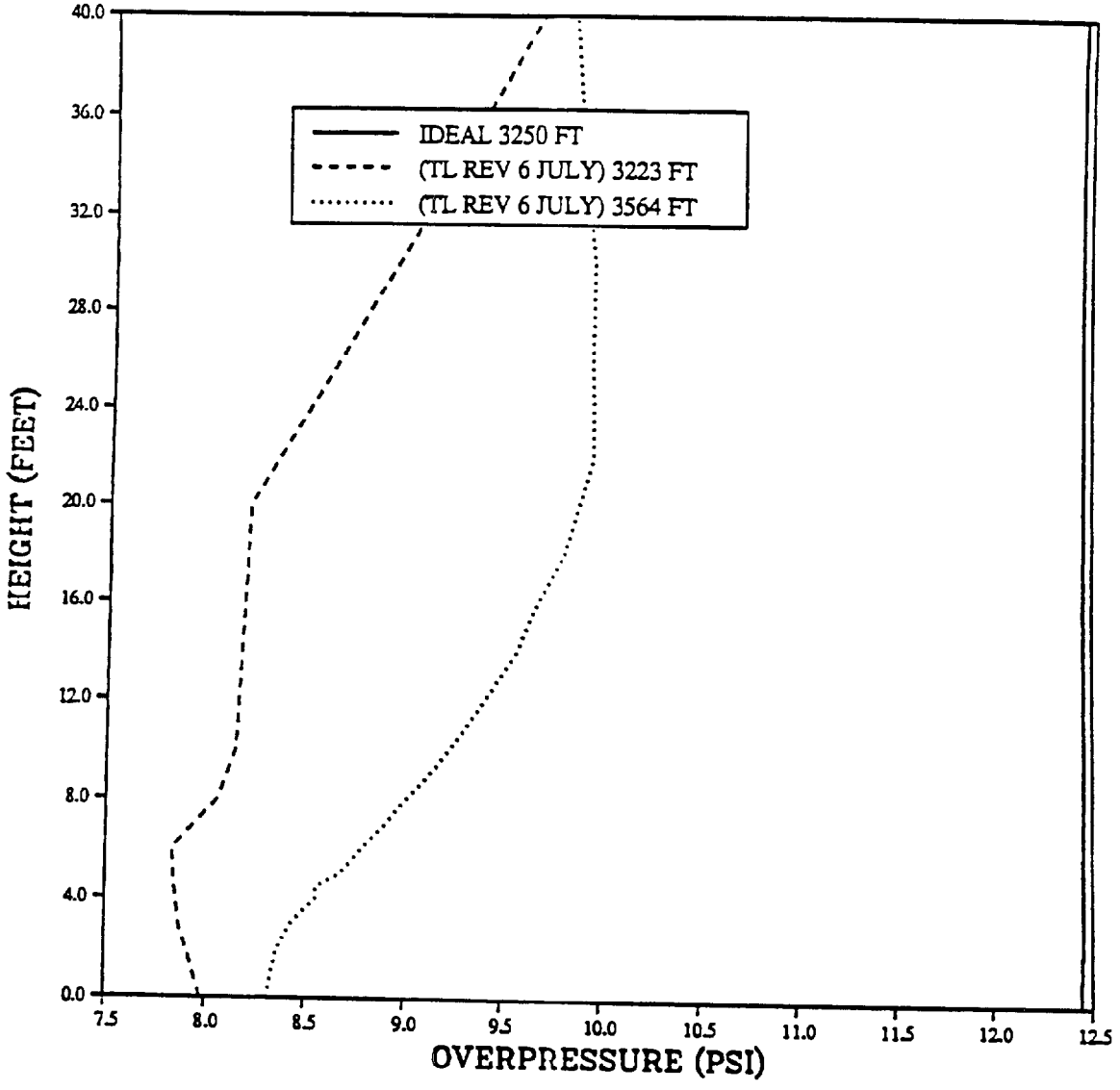

PRISCILLA DESERT
OVERPRESSURE AT 3650 FEET
VERTICAL PROFILE

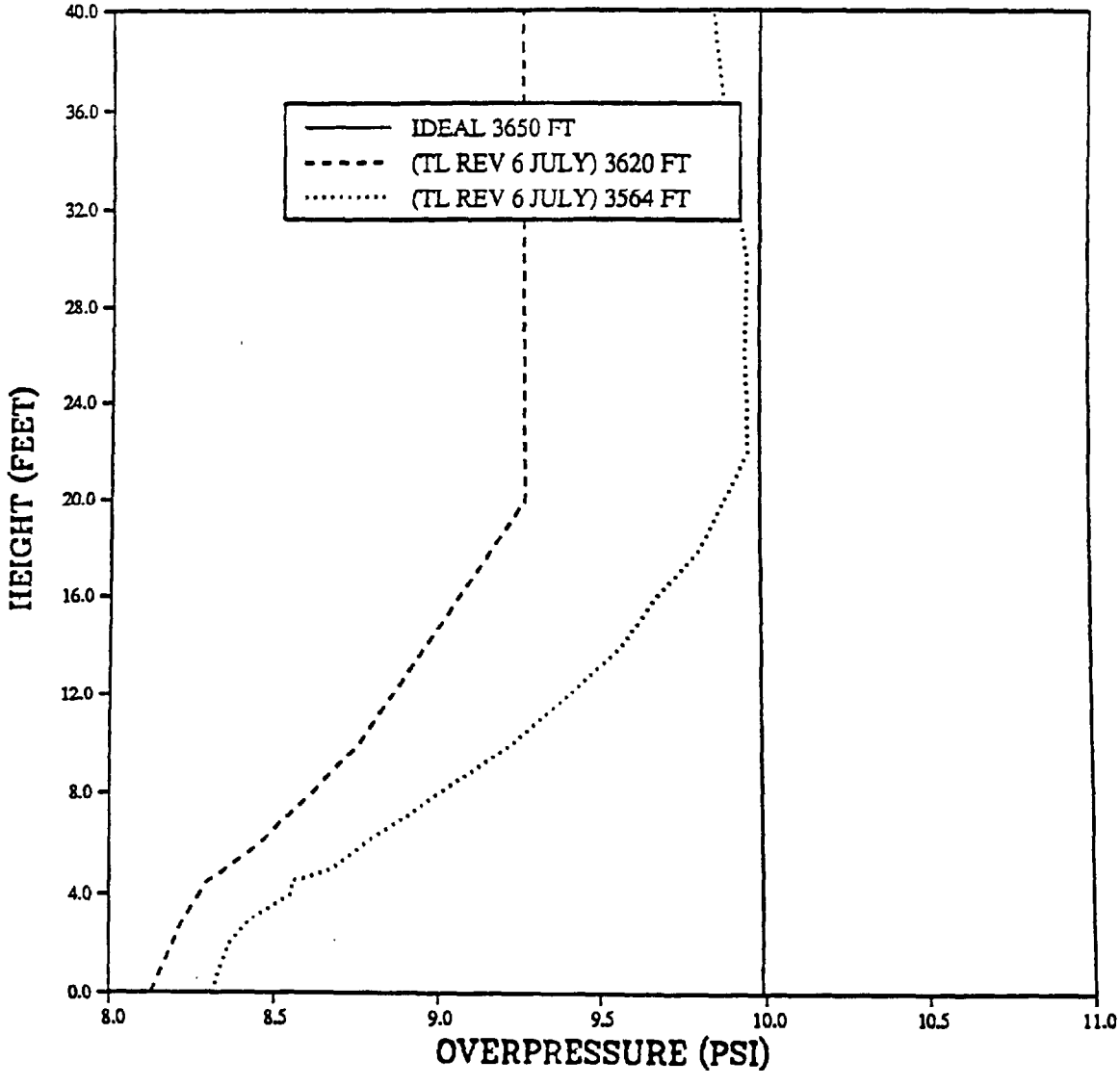

PRISCILLA DESERT
OVERPRESSURE AT 4100 FEET
VERTICAL PROFILE

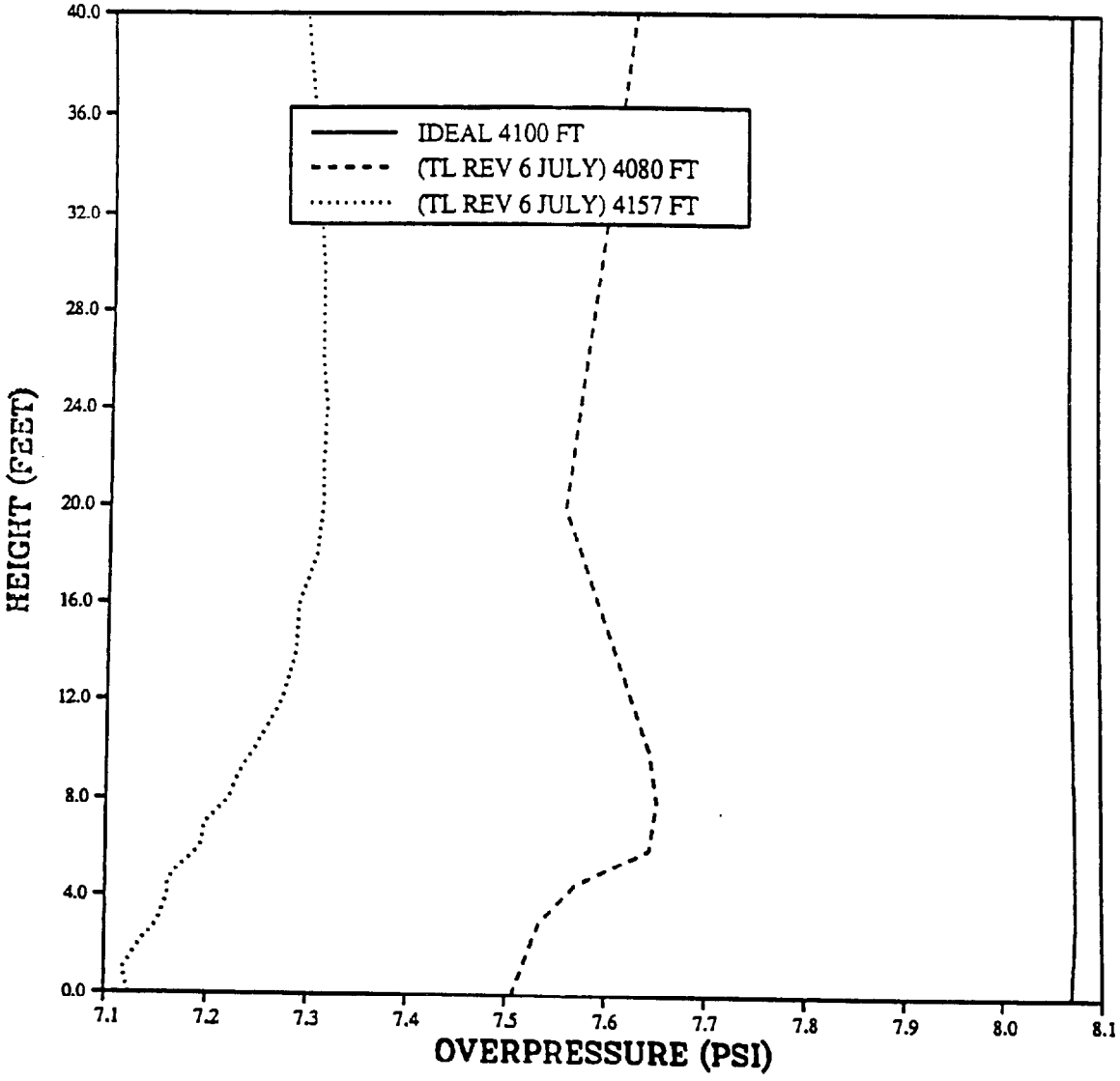

PRISCILLA DESERT
OVERPRESSURE AT 4900 FEET
VERTICAL PROFILE

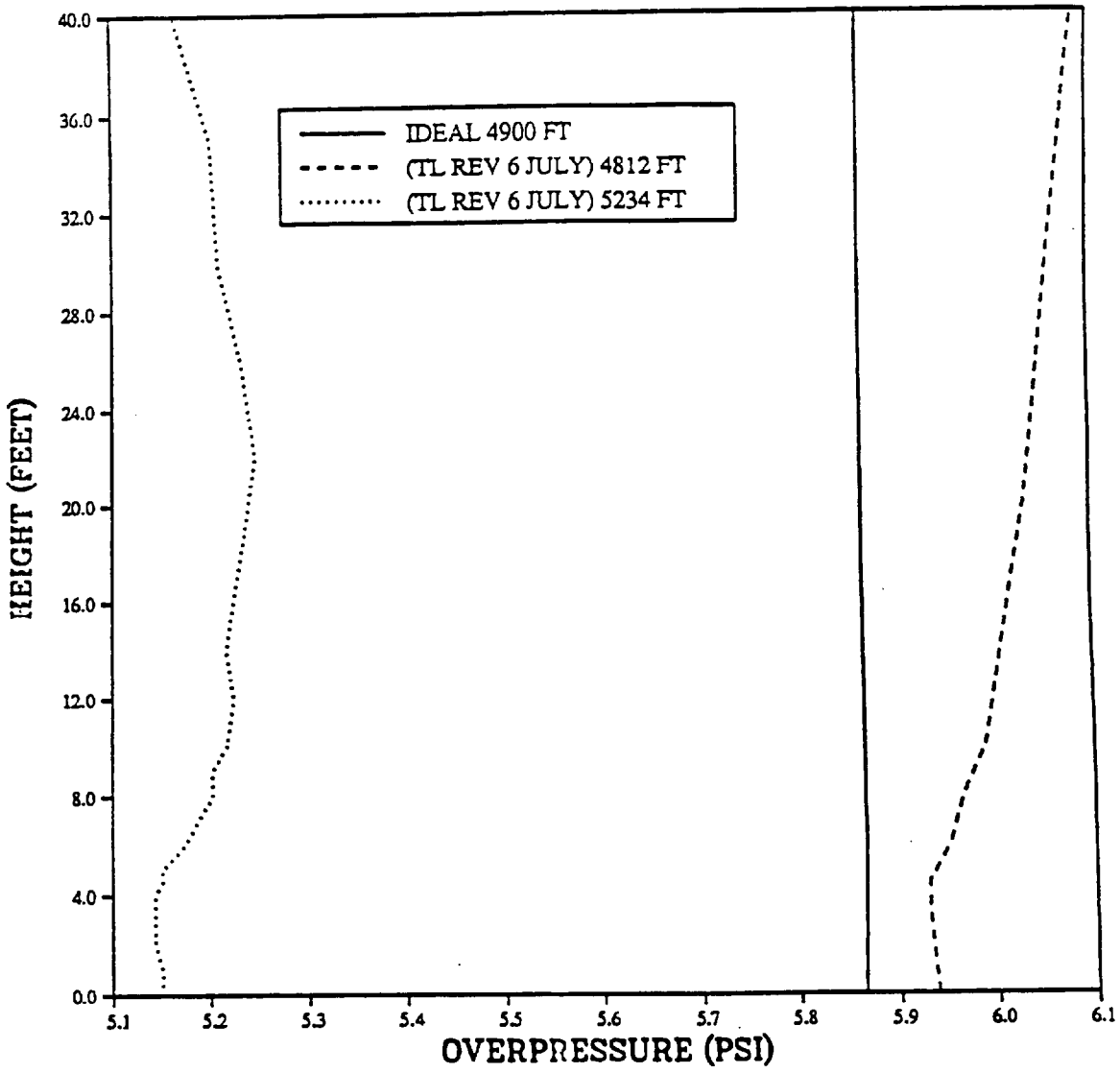

PRISCILLA DESERT
OVERPRESSURE AT 5350 FEET
VERTICAL PROFILE

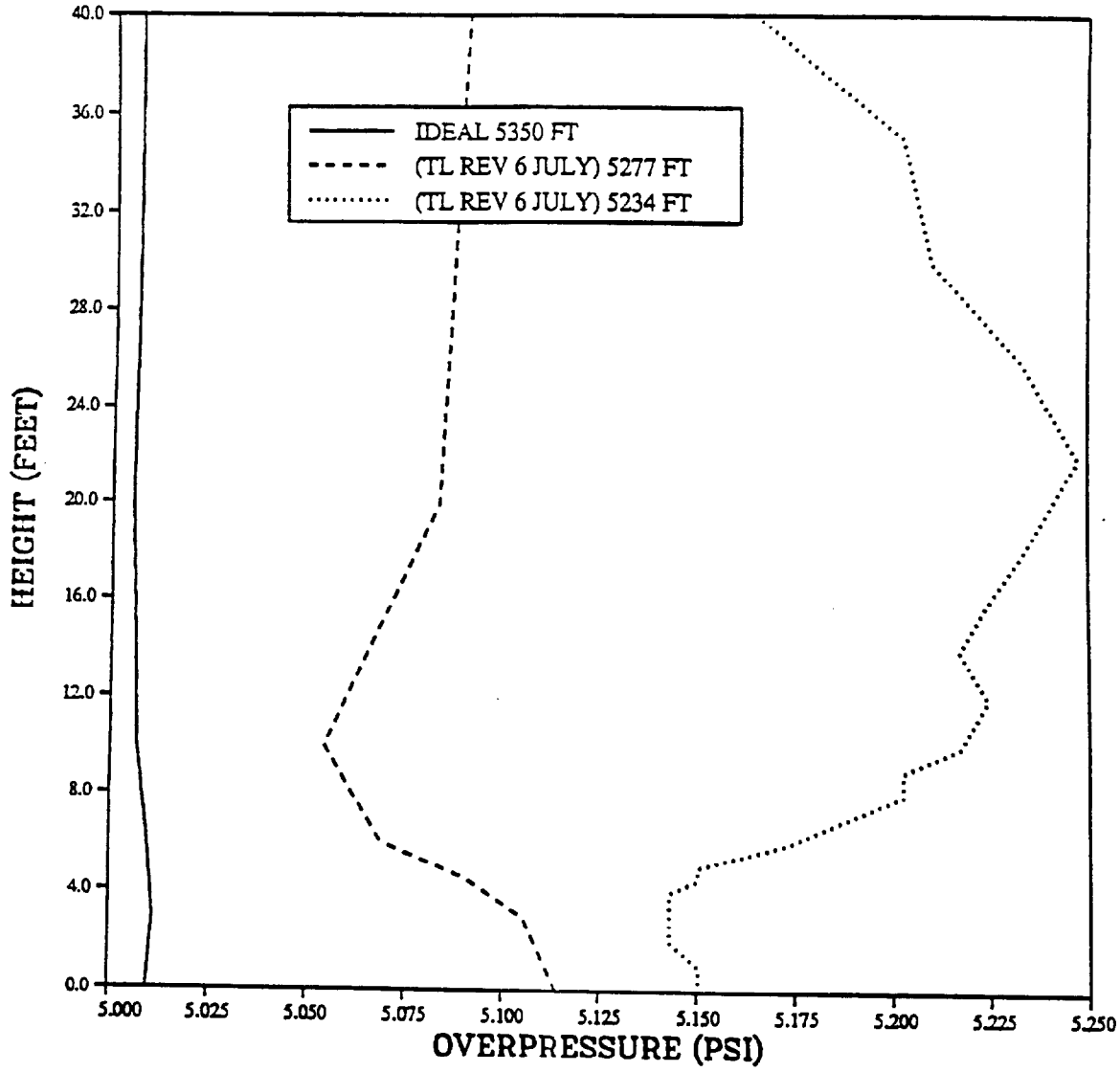

PRISCILLA DESERT
OVERPRESSURE IMPULSE
VERTICAL PROFILE AT 2100 FEET

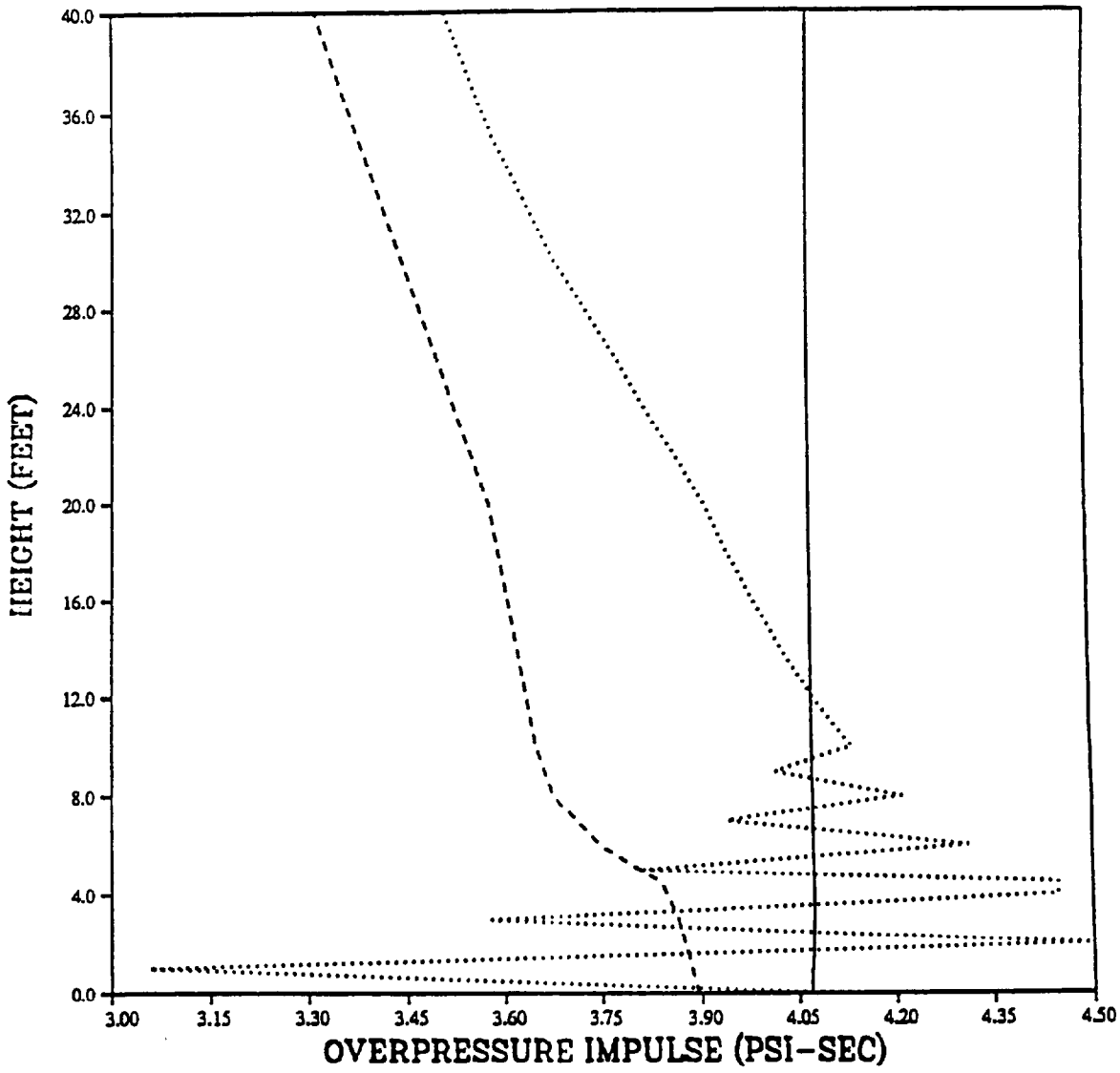

PRISCILLA DESERT
OVERPRESSURE IMPULSE
VERTICAL PROFILE AT 2300 FEET

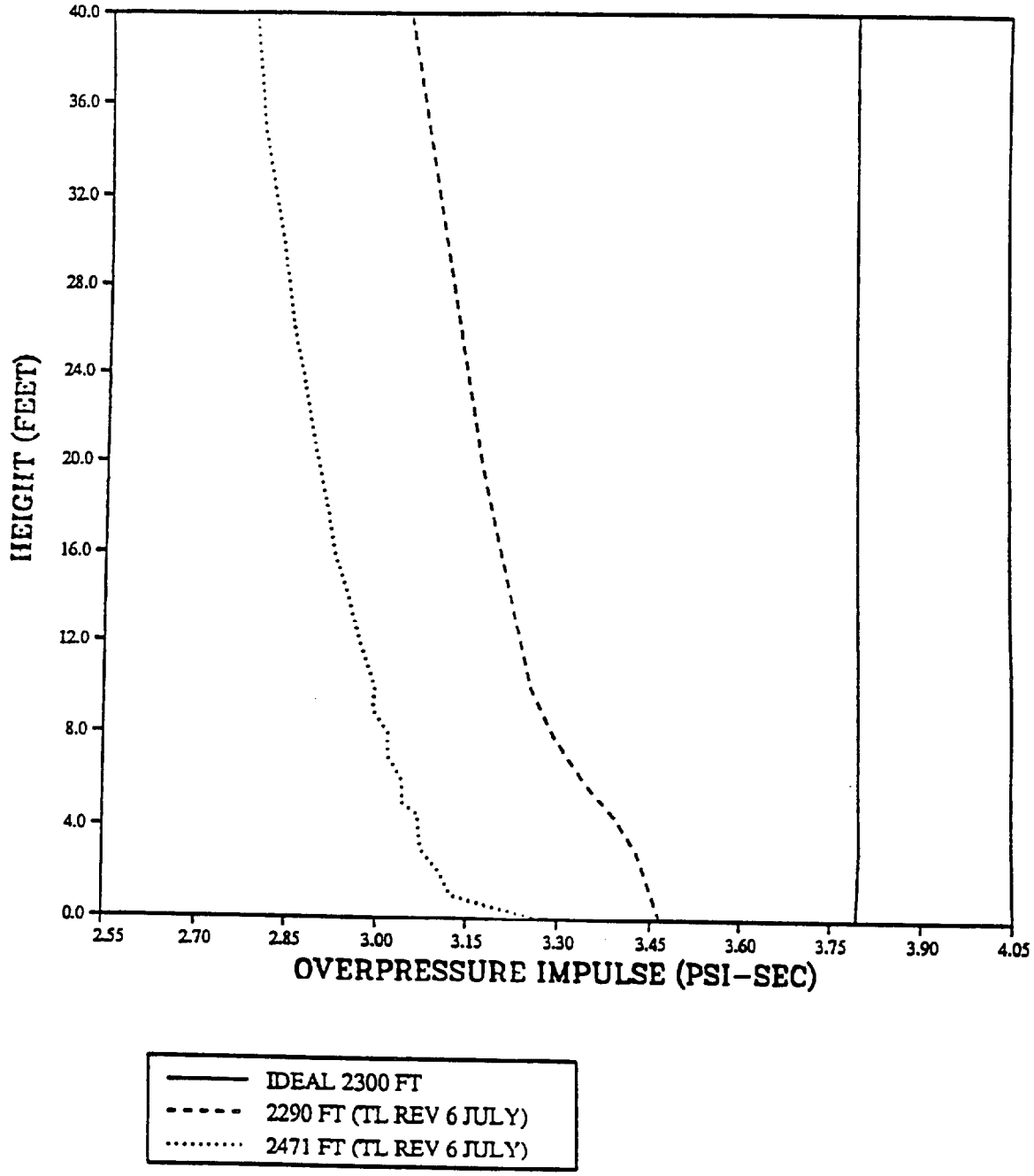

PRISCILLA DESERT
OVERPRESSURE IMPULSE
VERTICAL PROFILE AT 2550 FEET

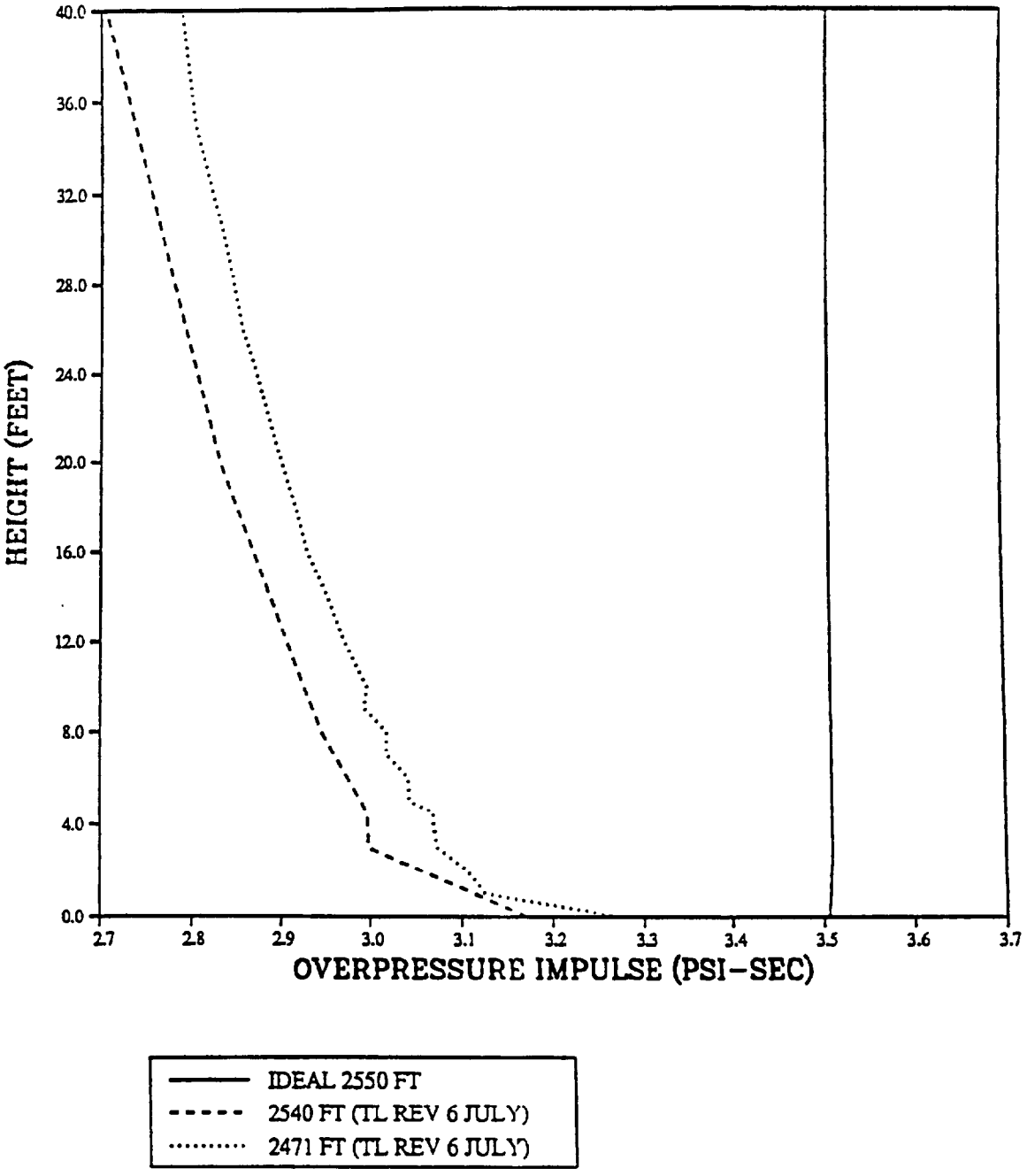

PRISCILLA DESERT
OVERPRESSURE IMPULSE
VERTICAL PROFILE AT 2950 FEET

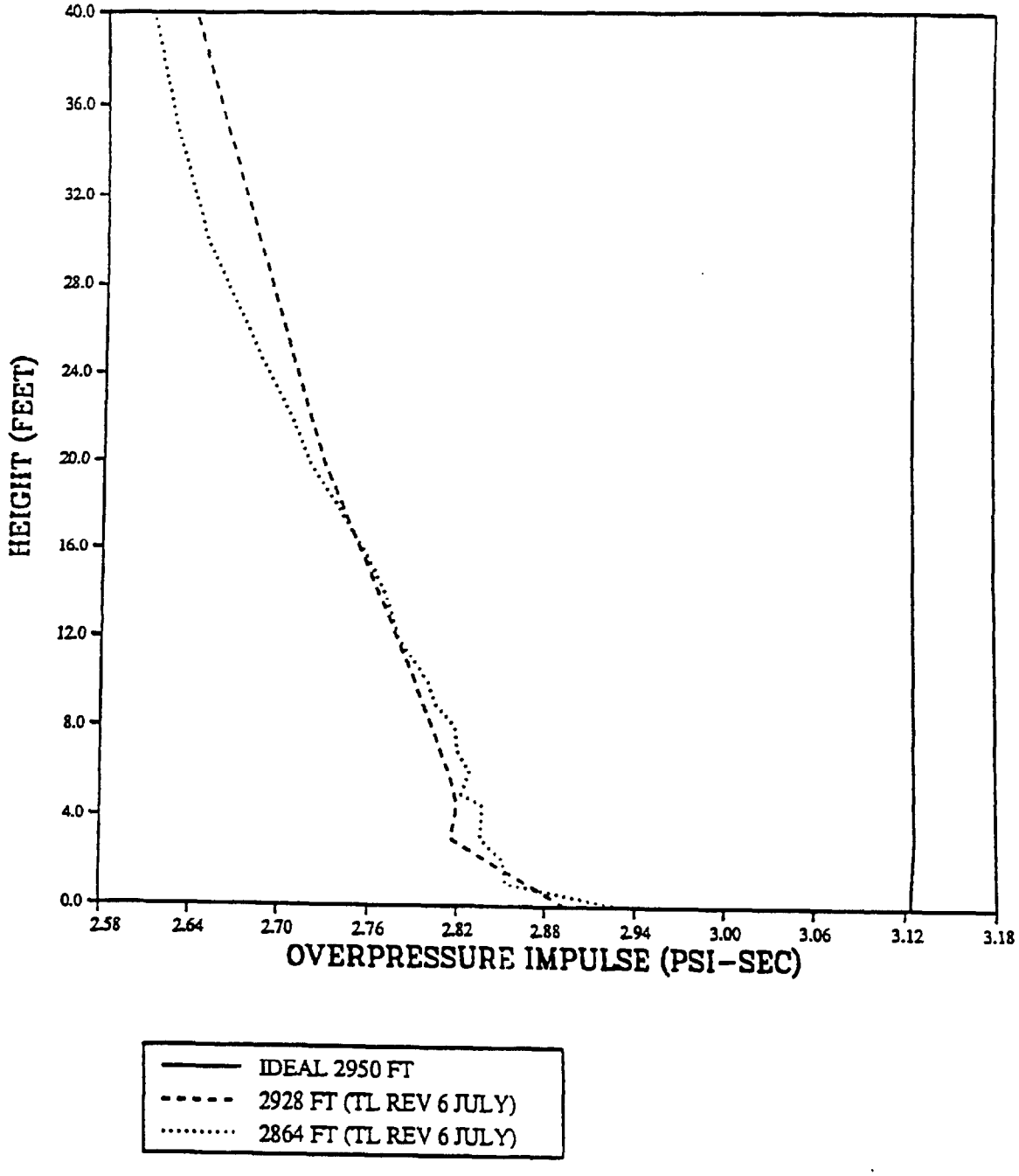

PRISCILLA DESERT
OVERPRESSURE IMPULSE
VERTICAL PROFILE AT 3250 FEET

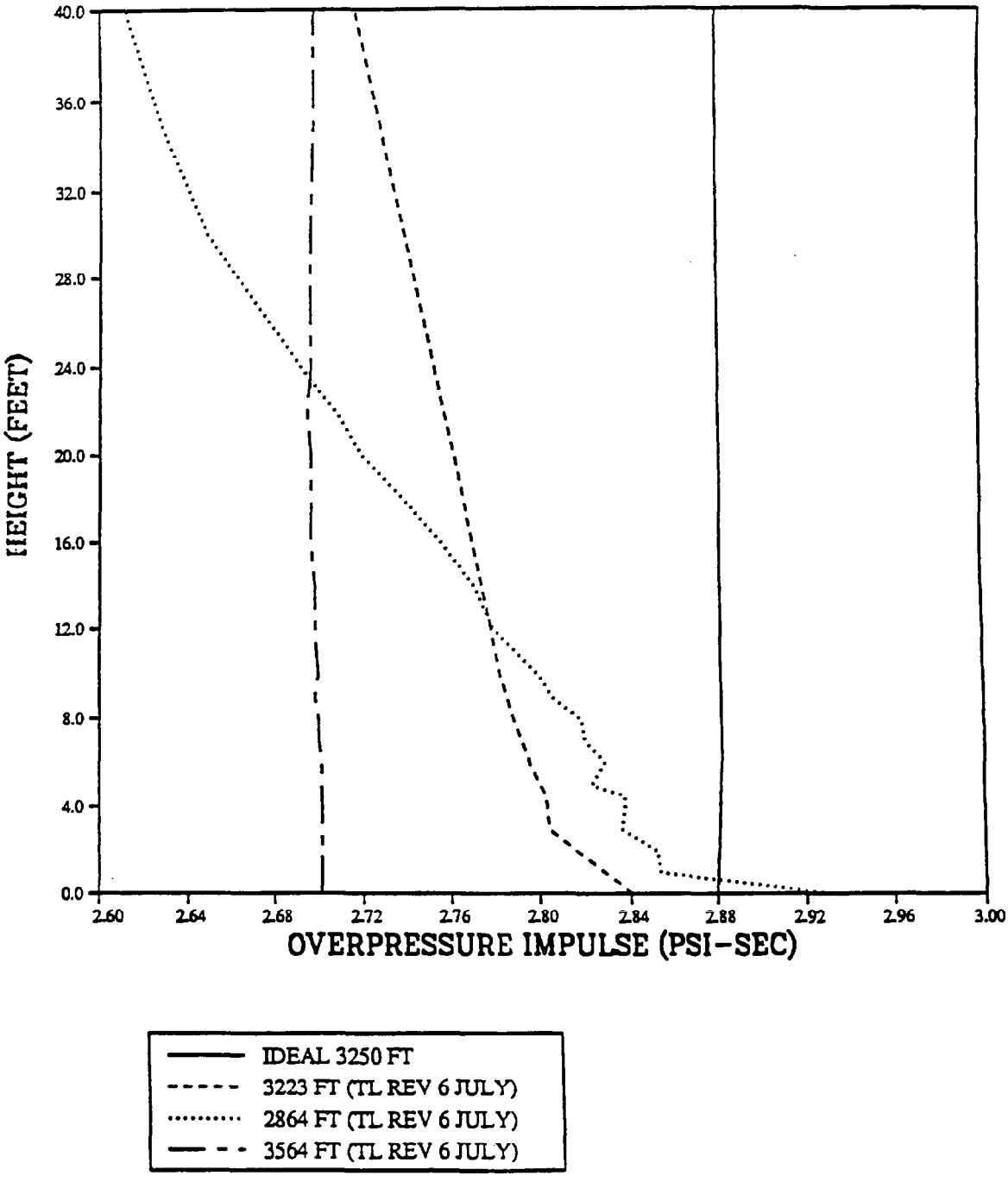

PRISCILLA DESERT
OVERPRESSURE IMPULSE
VERTICAL PROFILE AT 3650 FEET

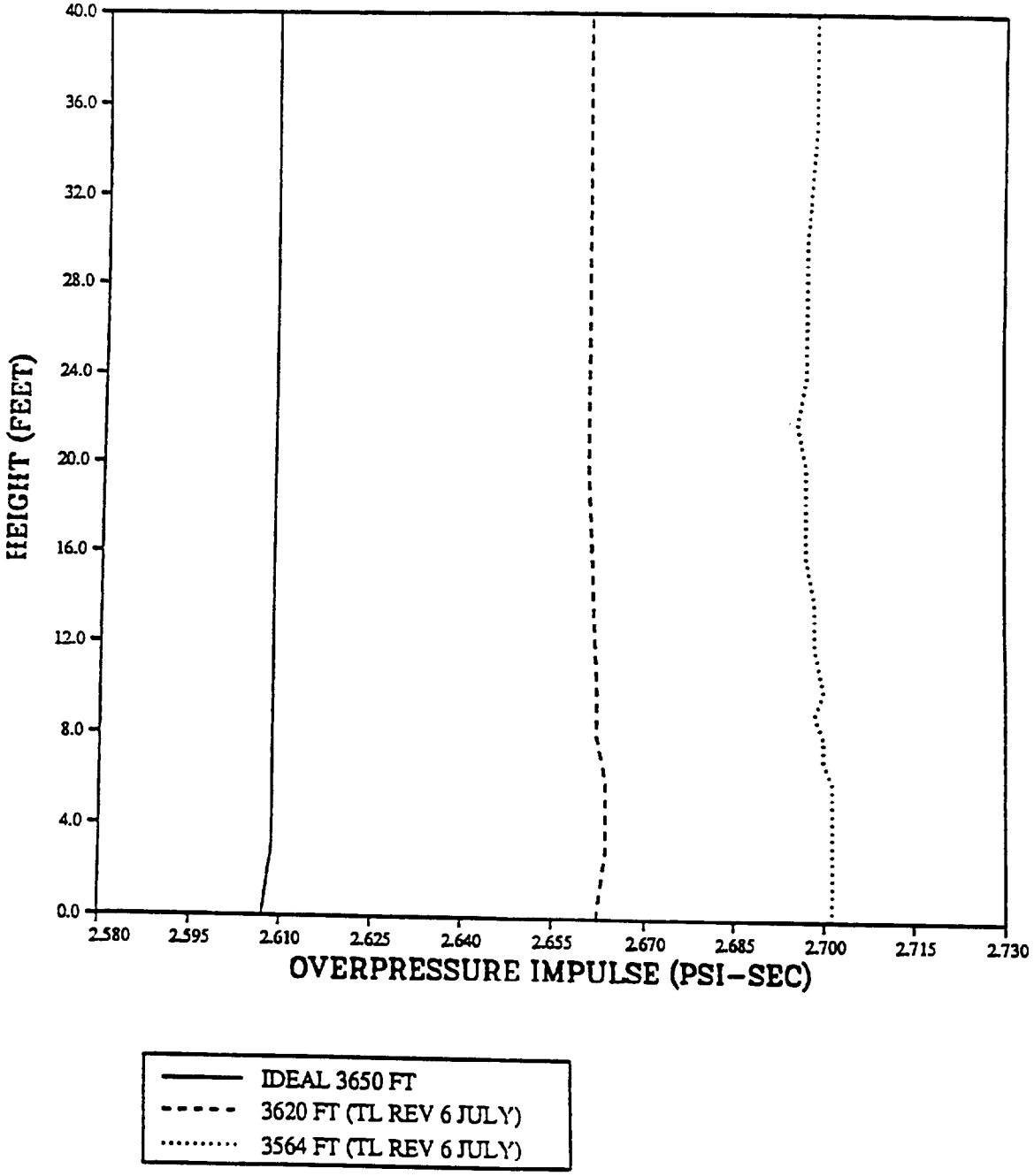

PRISCILLA DESERT
OVERPRESSURE IMPULSE
VERTICAL PROFILE AT 4100 FEET

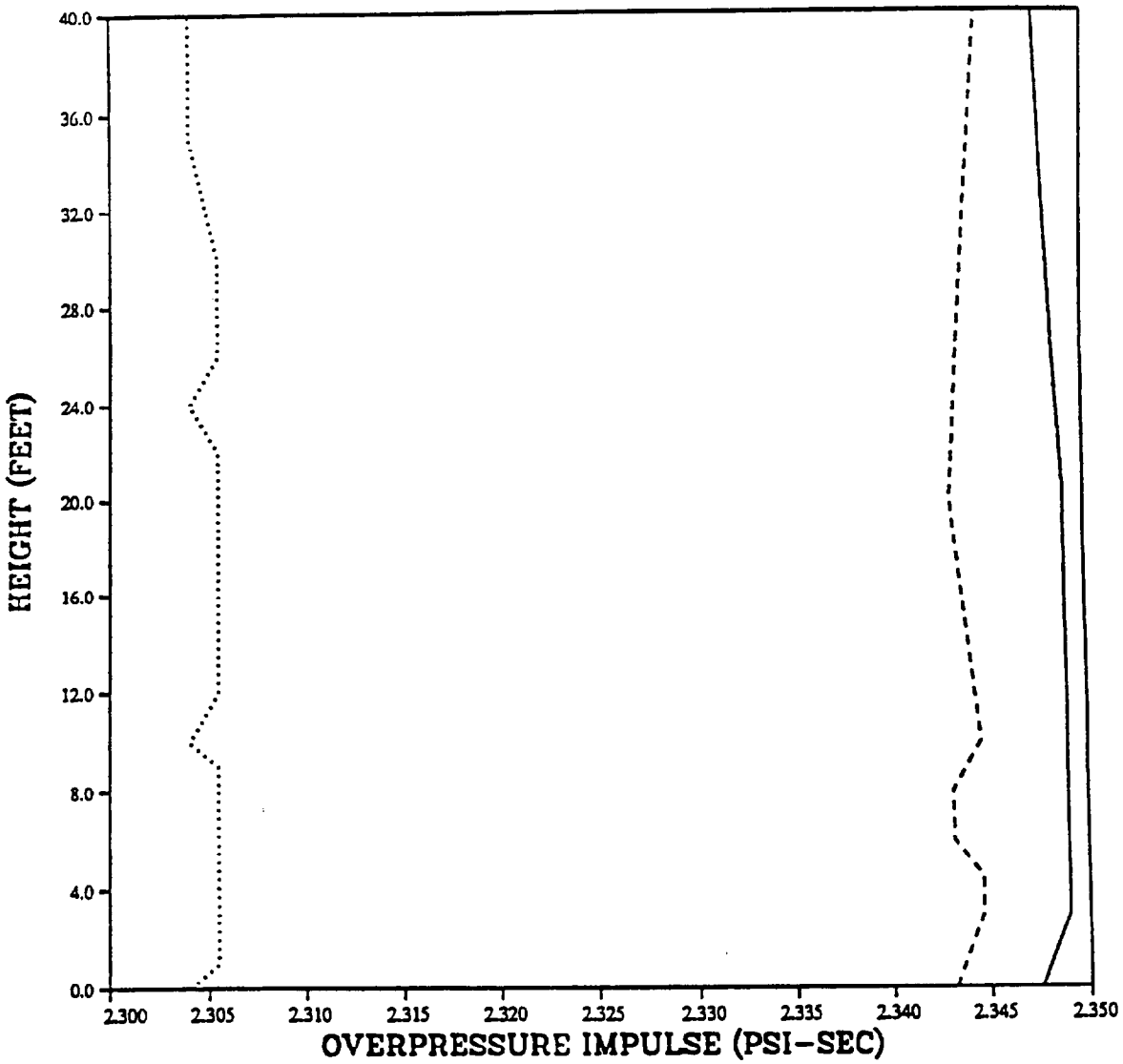

PRISCILLA DESERT
OVERPRESSURE IMPULSE
VERTICAL PROFILE AT 4900 FEET

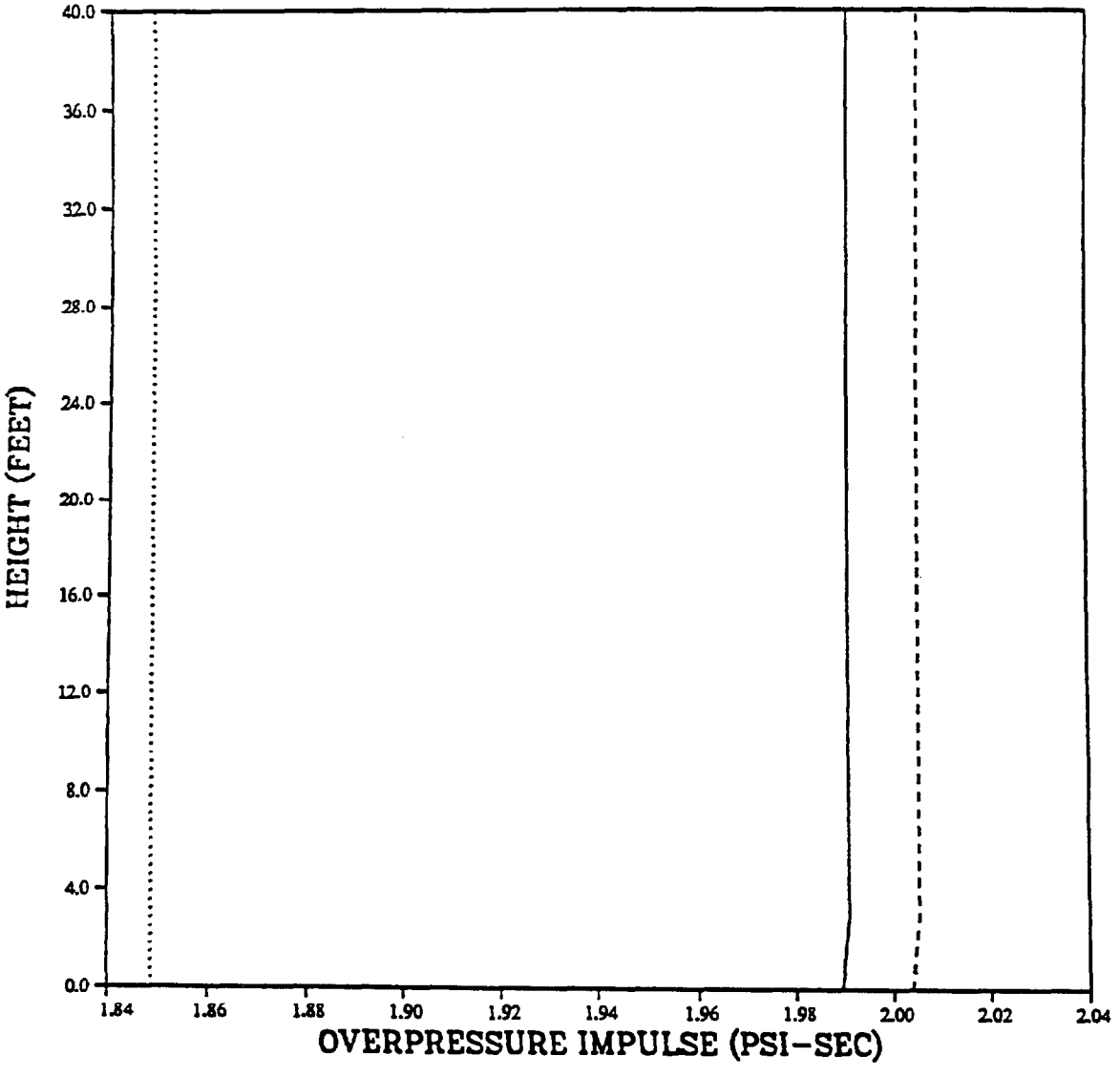

PRISCILLA DESERT
OVERPRESSURE IMPULSE
VERTICAL PROFILE AT 5350 FEET

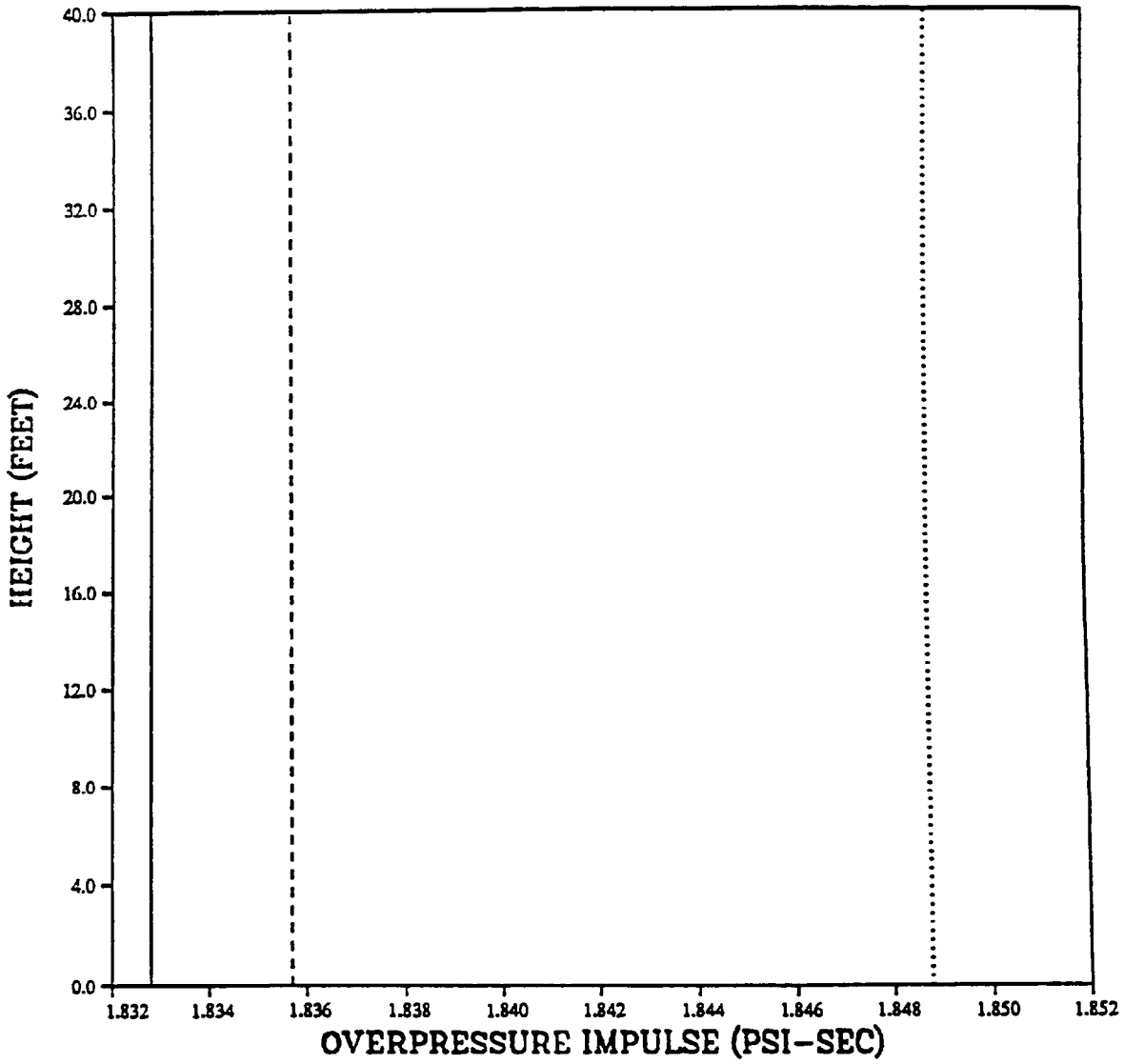

PRISCILLA
ARRIVAL TIME
VERTICAL PROFILE AT 2100 FEET

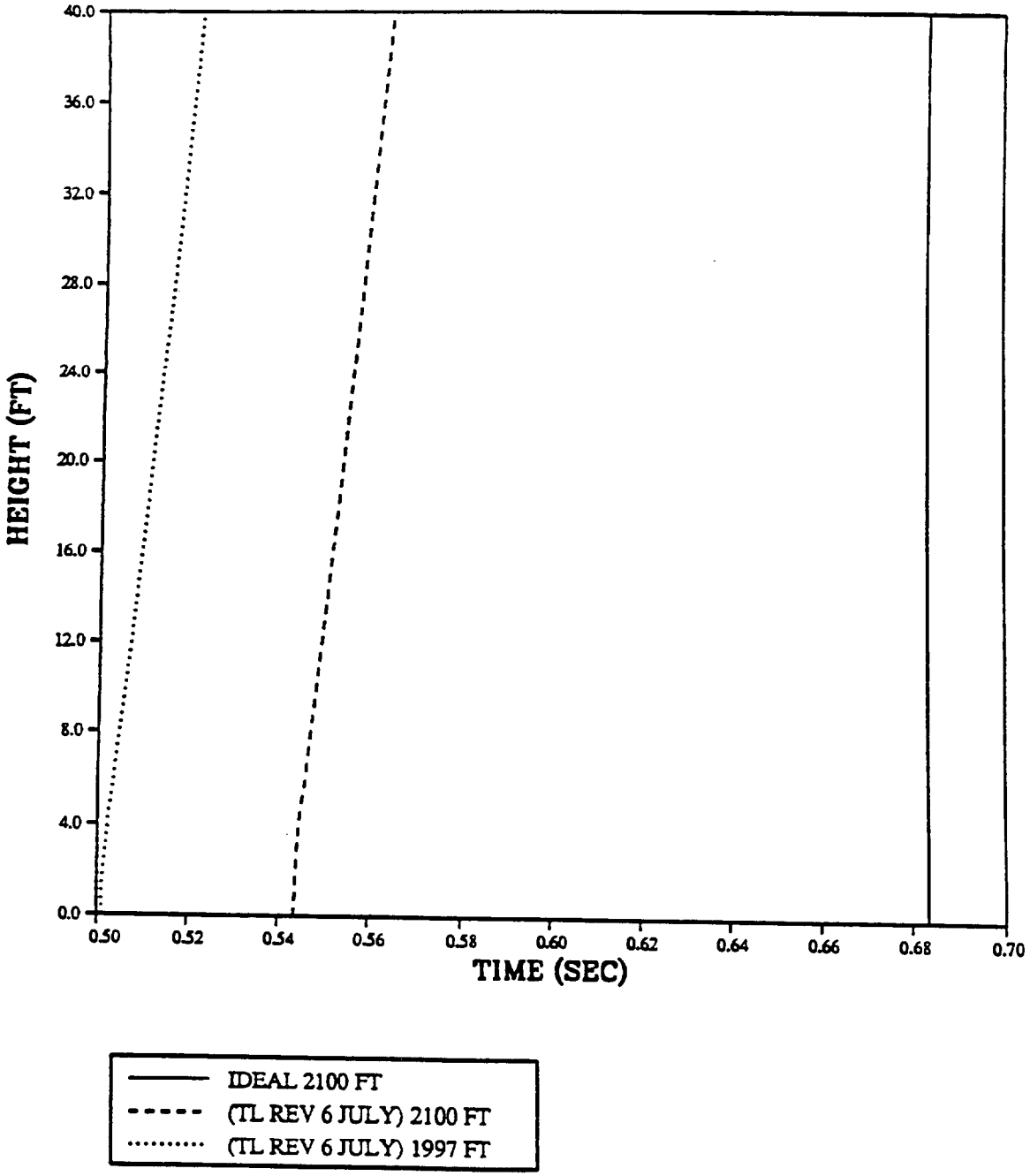

PRISCILLA
ARRIVAL TIME
VERTICAL PROFILE AT 2300 FEET

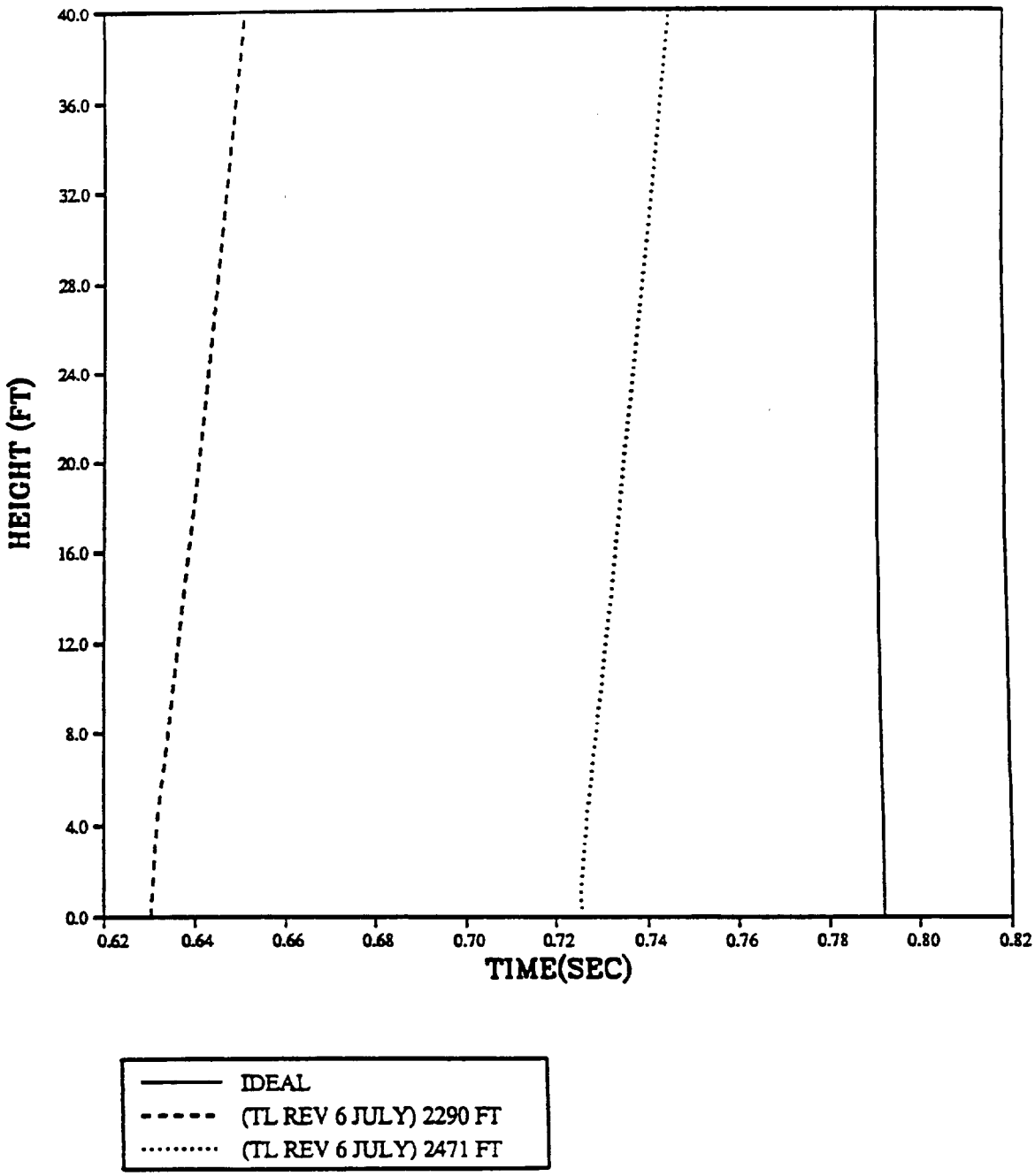

PRISCILLA
ARRIVAL TIME
VERTICAL PROFILE AT 2550 FEET

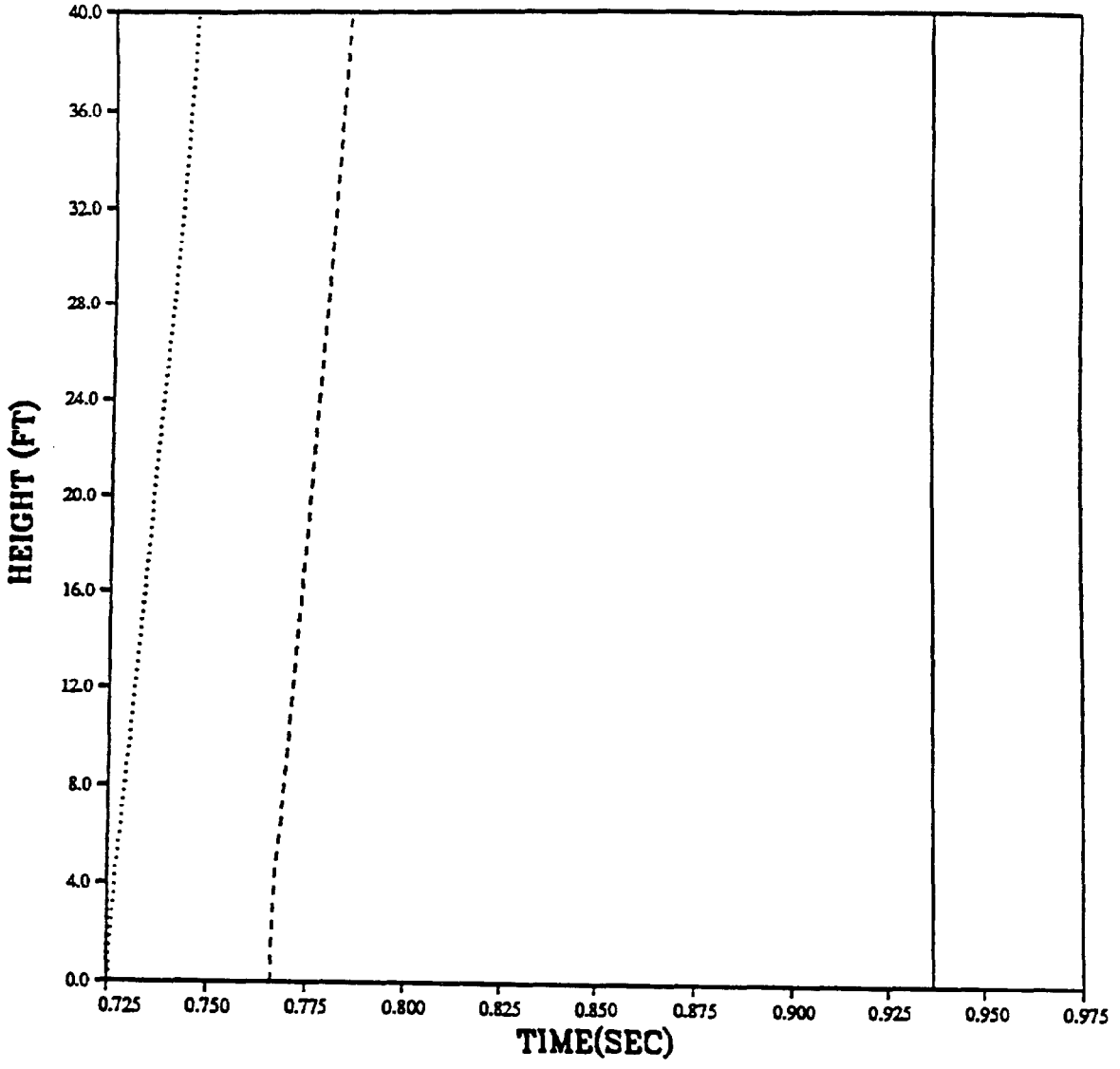

PRISCILLA
ARRIVAL TIME
VERTICAL PROFILE AT 2950 FEET

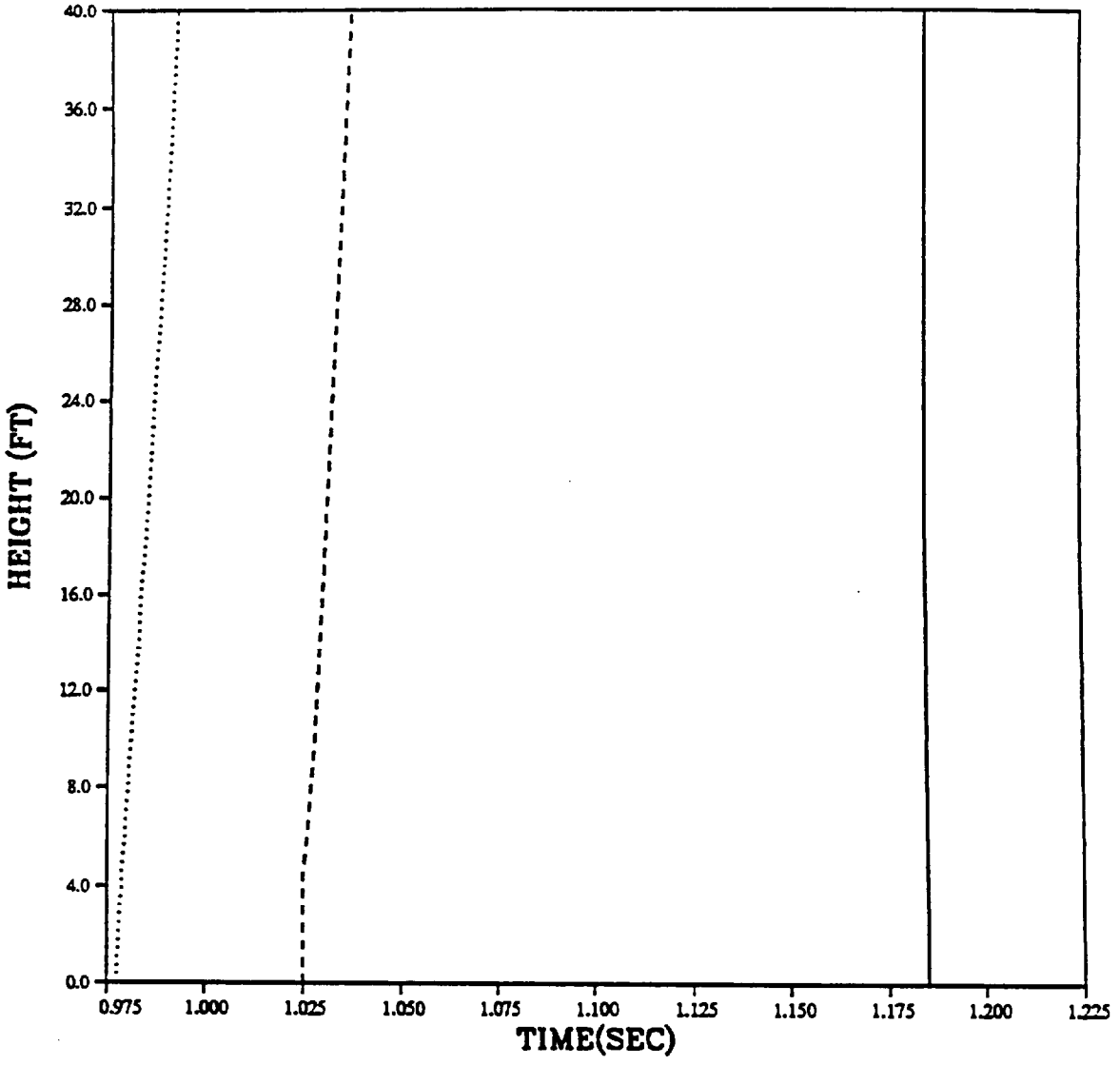

PRISCILLA
ARRIVAL TIME
VERTICAL PROFILE AT 3250 FEET

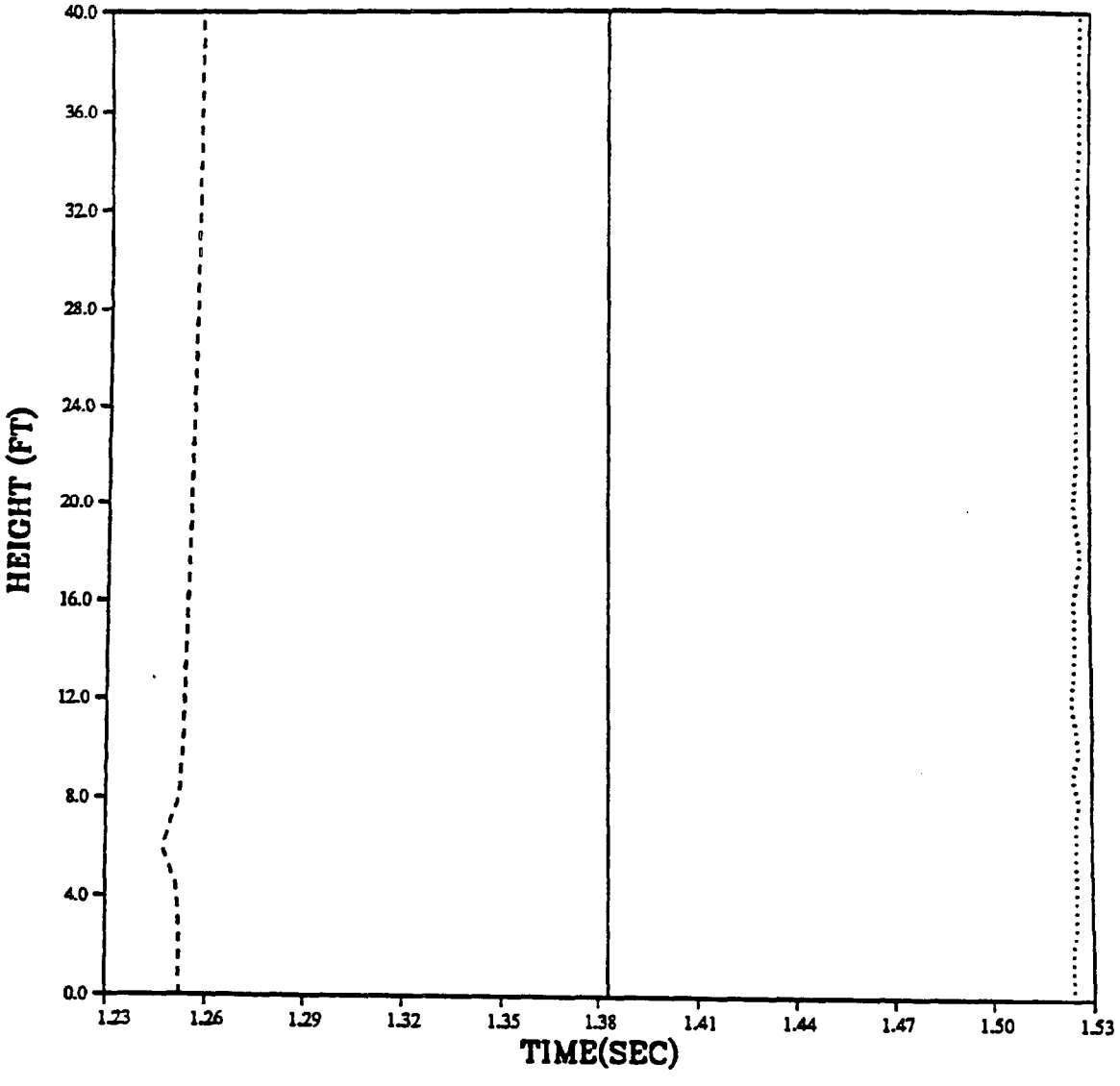

PRISCILLA
ARRIVAL TIME
VERTICAL PROFILE AT 3650 FEET

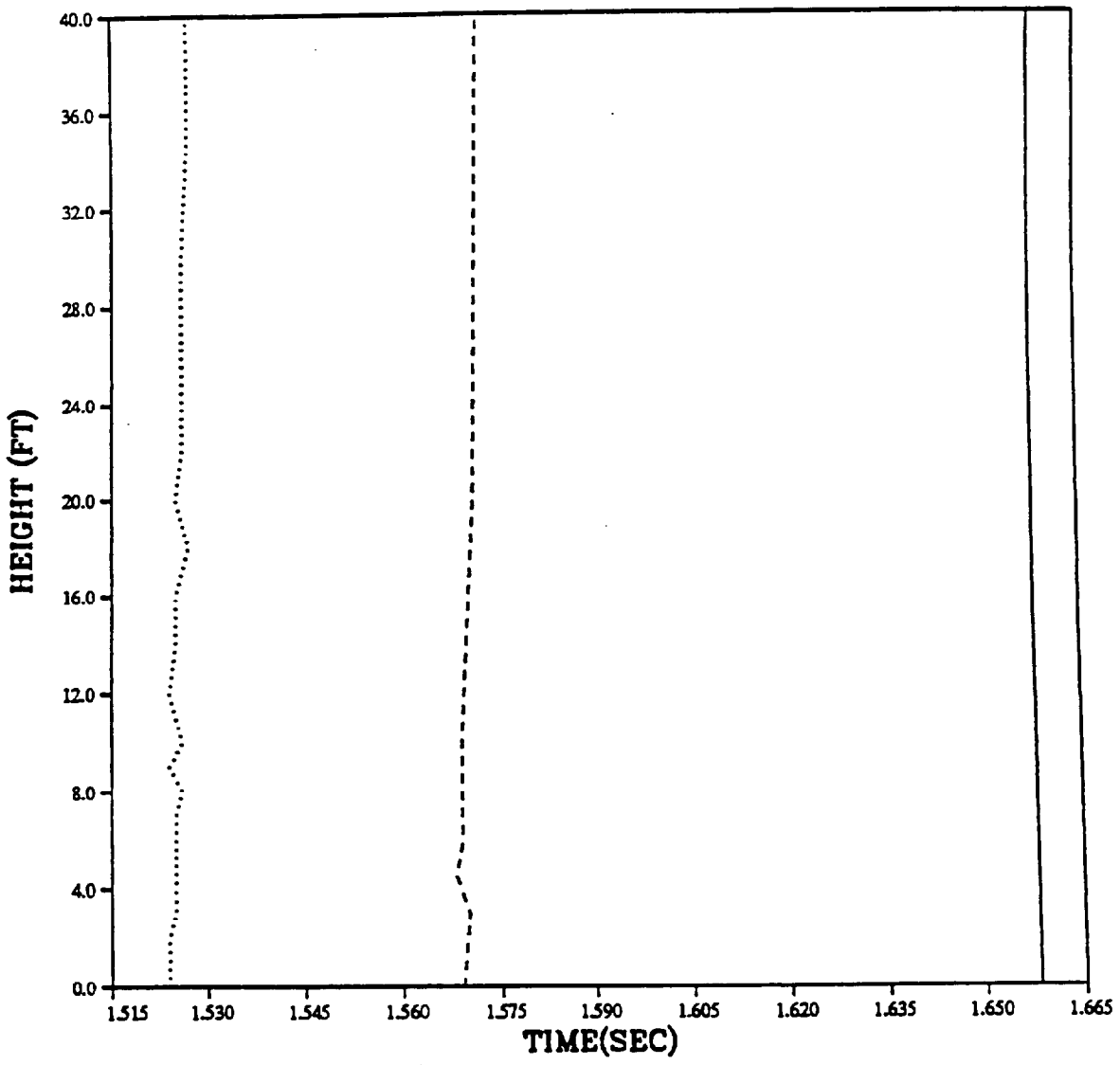

PRISCILLA
ARRIVAL TIME
VERTICAL PROFILE AT 4100 FEET

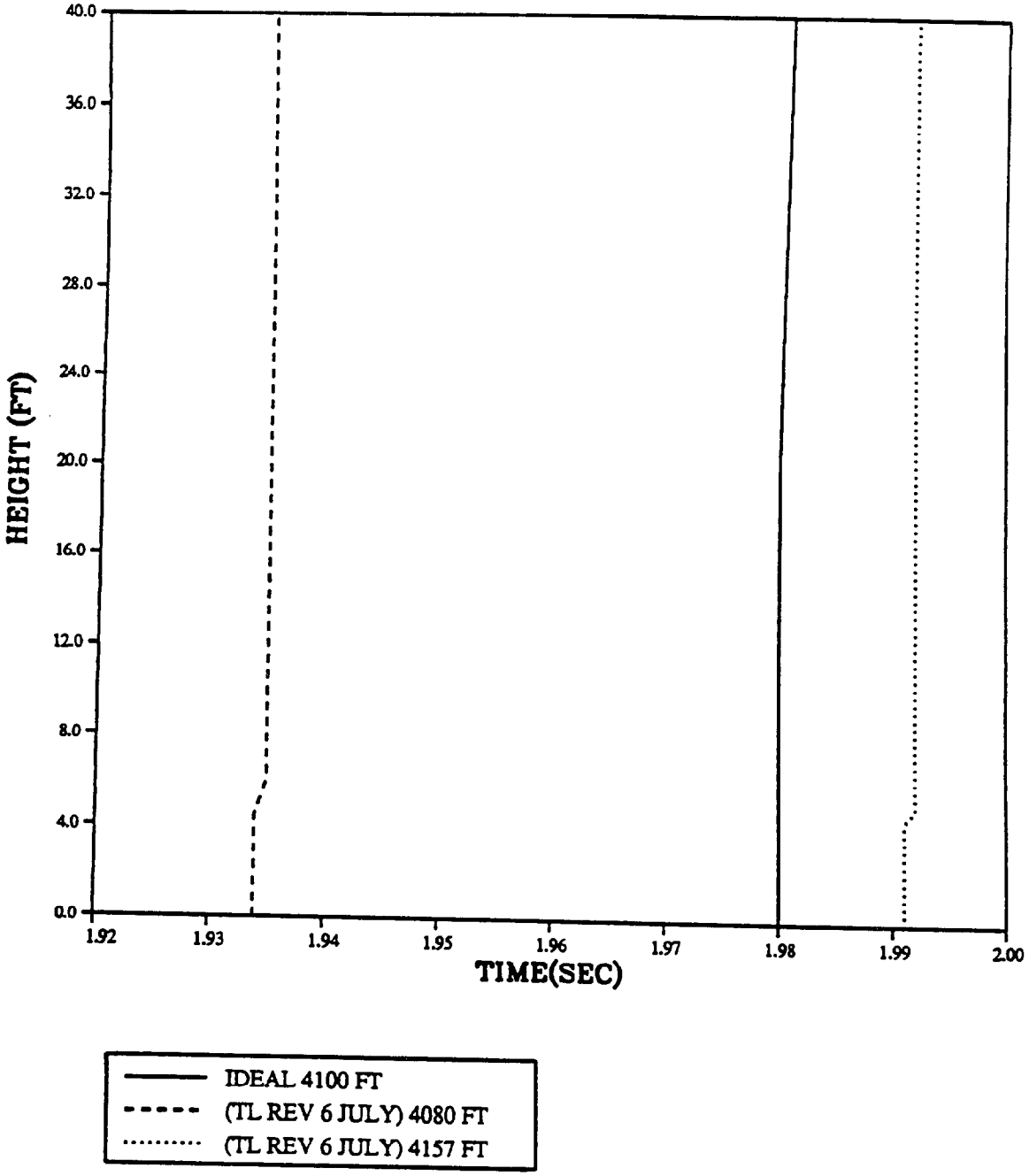

PRISCILLA
ARRIVAL TIME
VERTICAL PROFILE AT 4900 FEET

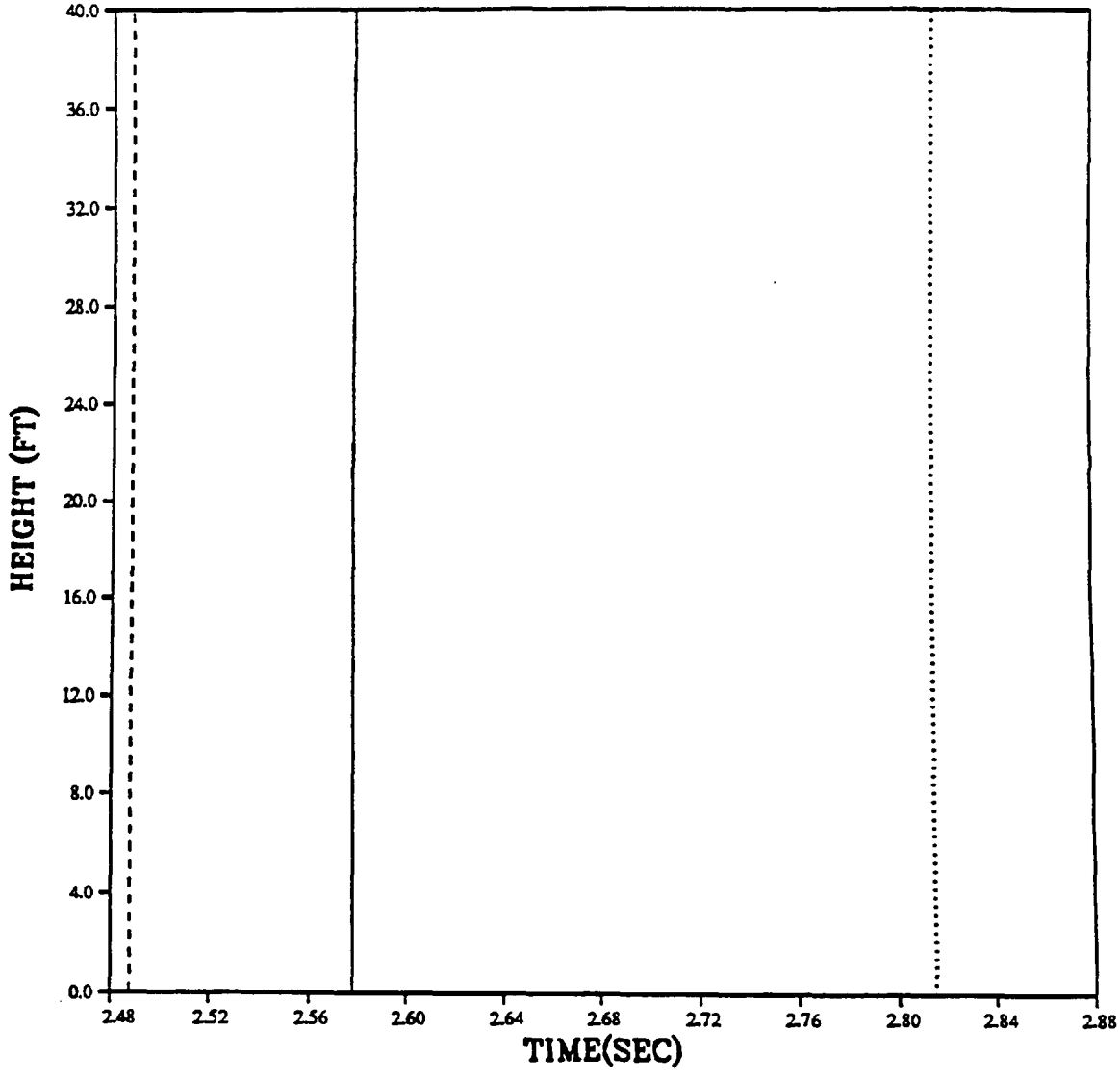

PRISCILLA
ARRIVAL TIME
VERTICAL PROFILE AT 5350 FEET

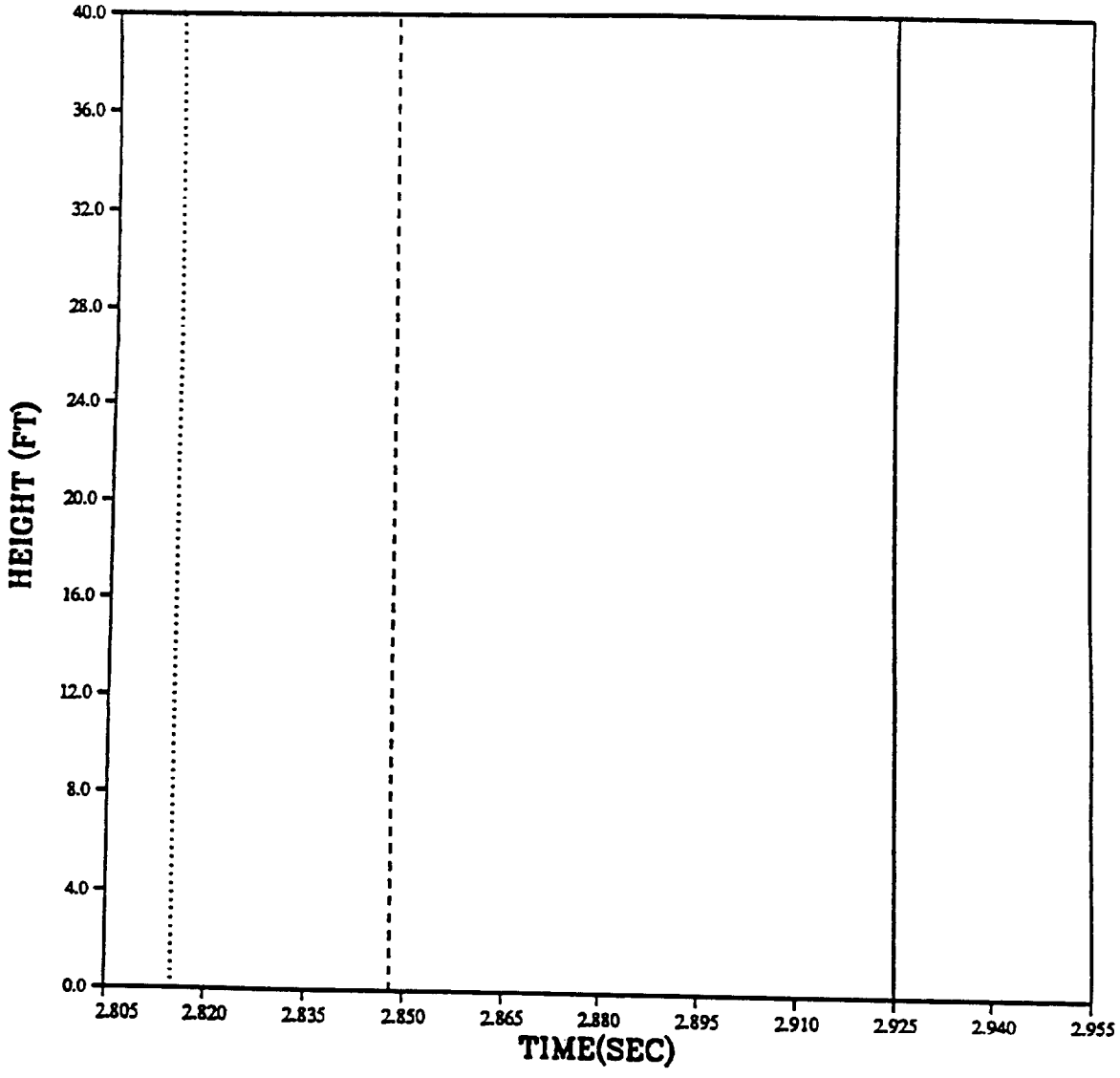

PRISCILLA DESERT
HORIZONTAL DYNAMIC PRESSURE PEAKS
VERTICAL PROFILE AT 2100 FEET

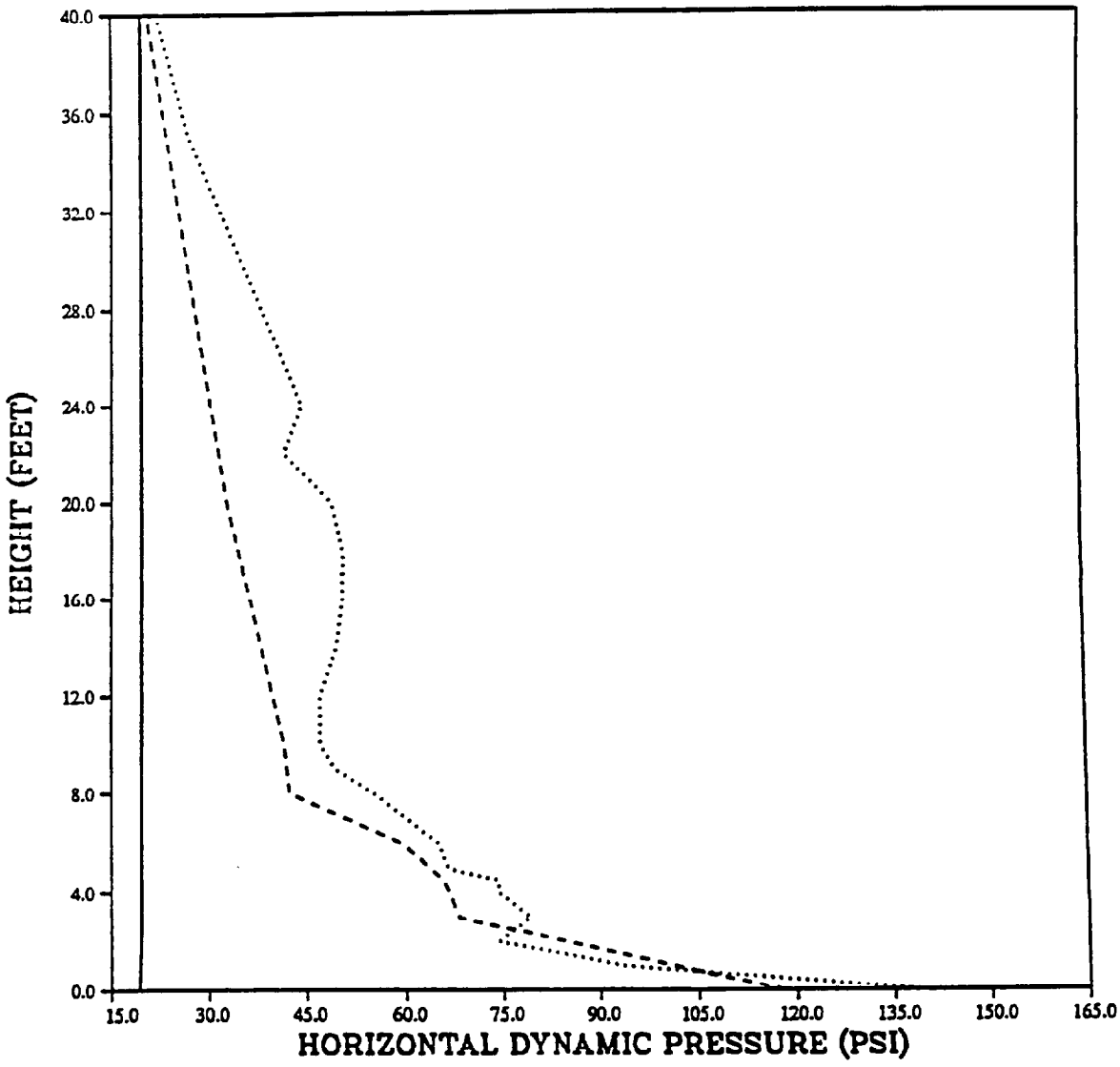

PRISCILLA DESERT
HORIZONTAL DYNAMIC PRESSURE PEAKS
VERTICAL PROFILE AT 2300 FEET

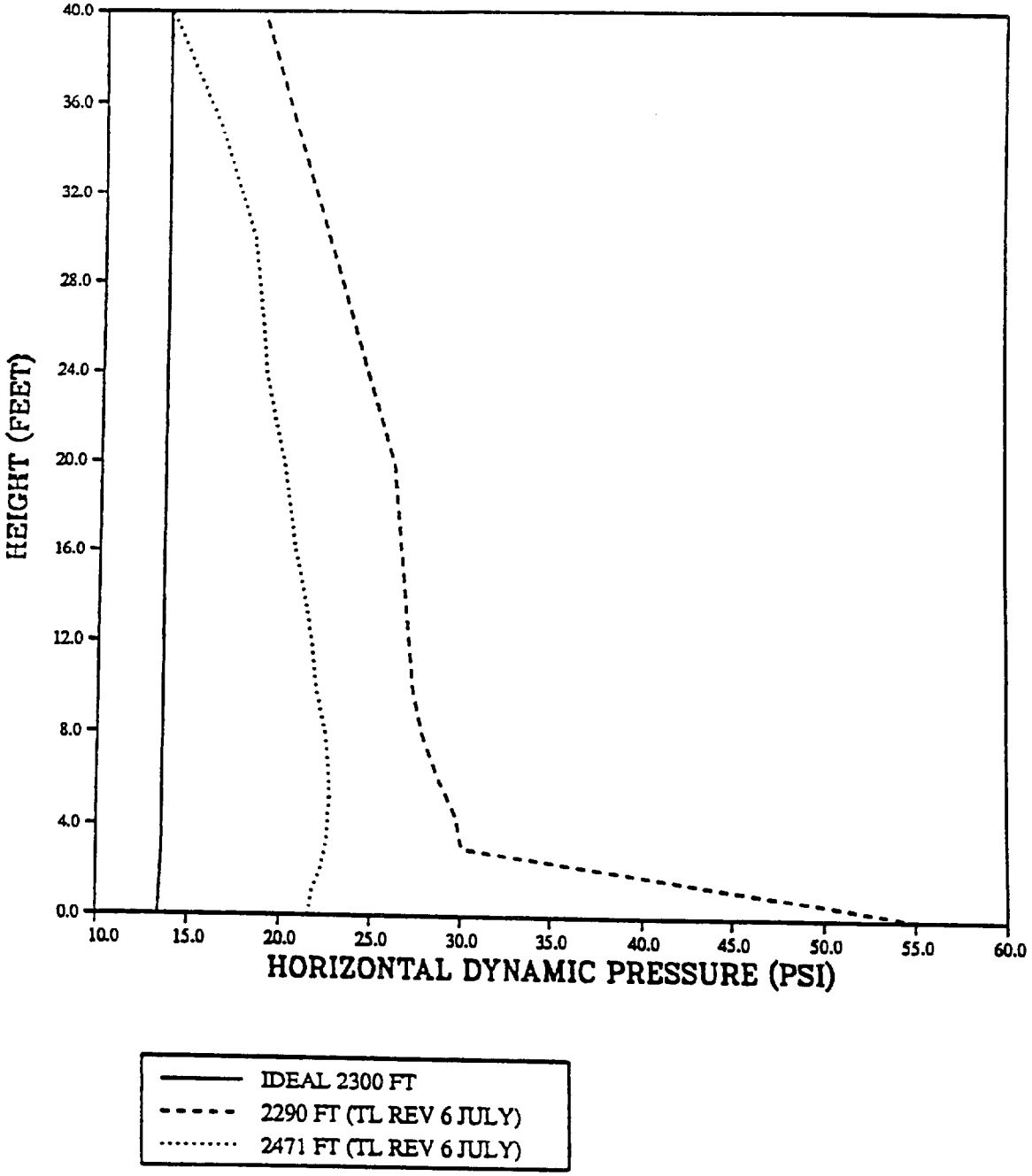

PRISCILLA DESERT
HORIZONTAL DYNAMIC PRESSURE PEAKS
VERTICAL PROFILE AT 2550 FEET

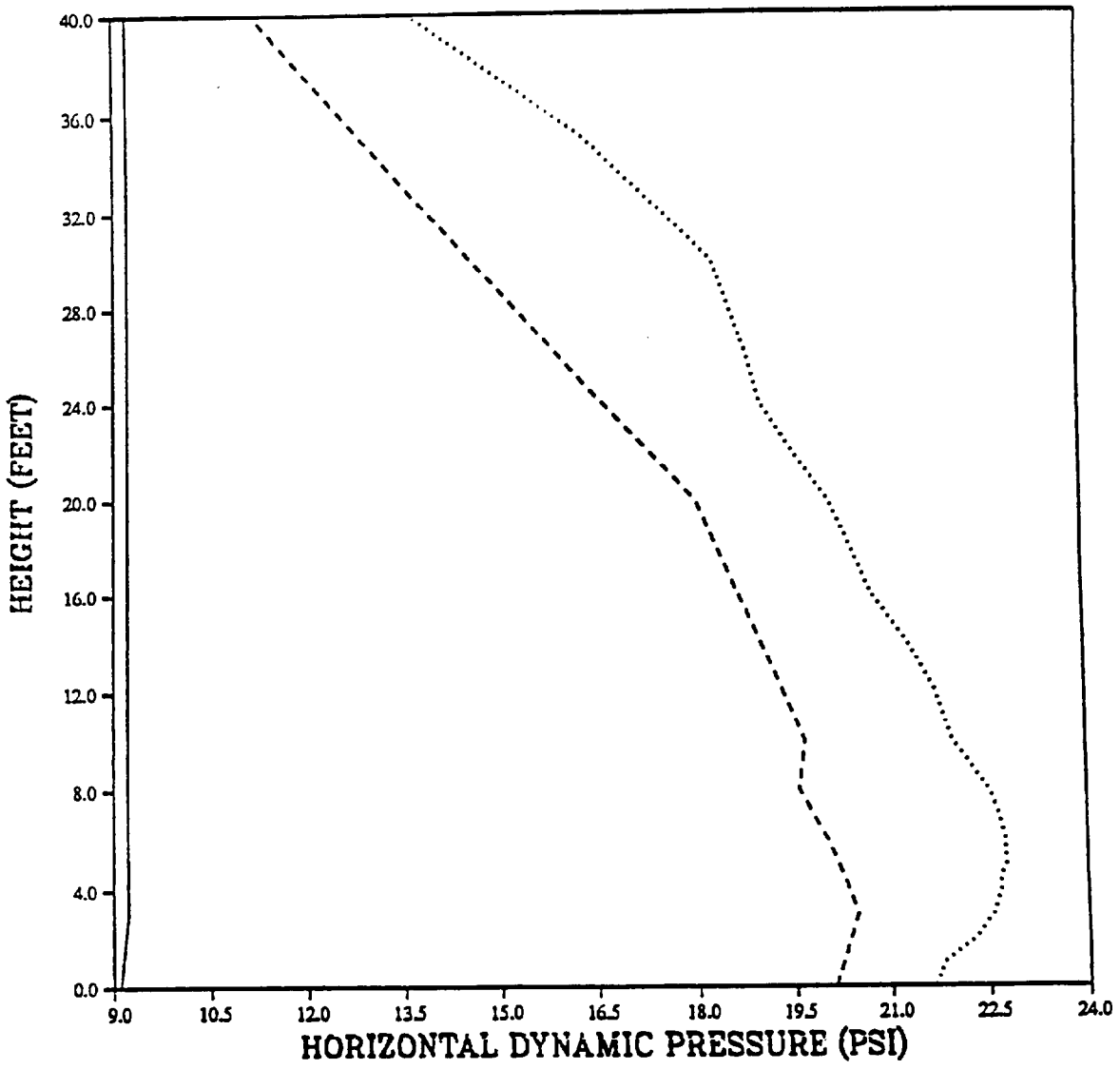

PRISCILLA DESERT
HORIZONTAL DYNAMIC PRESSURE PEAKS
VERTICAL PROFILE AT 2950 FEET

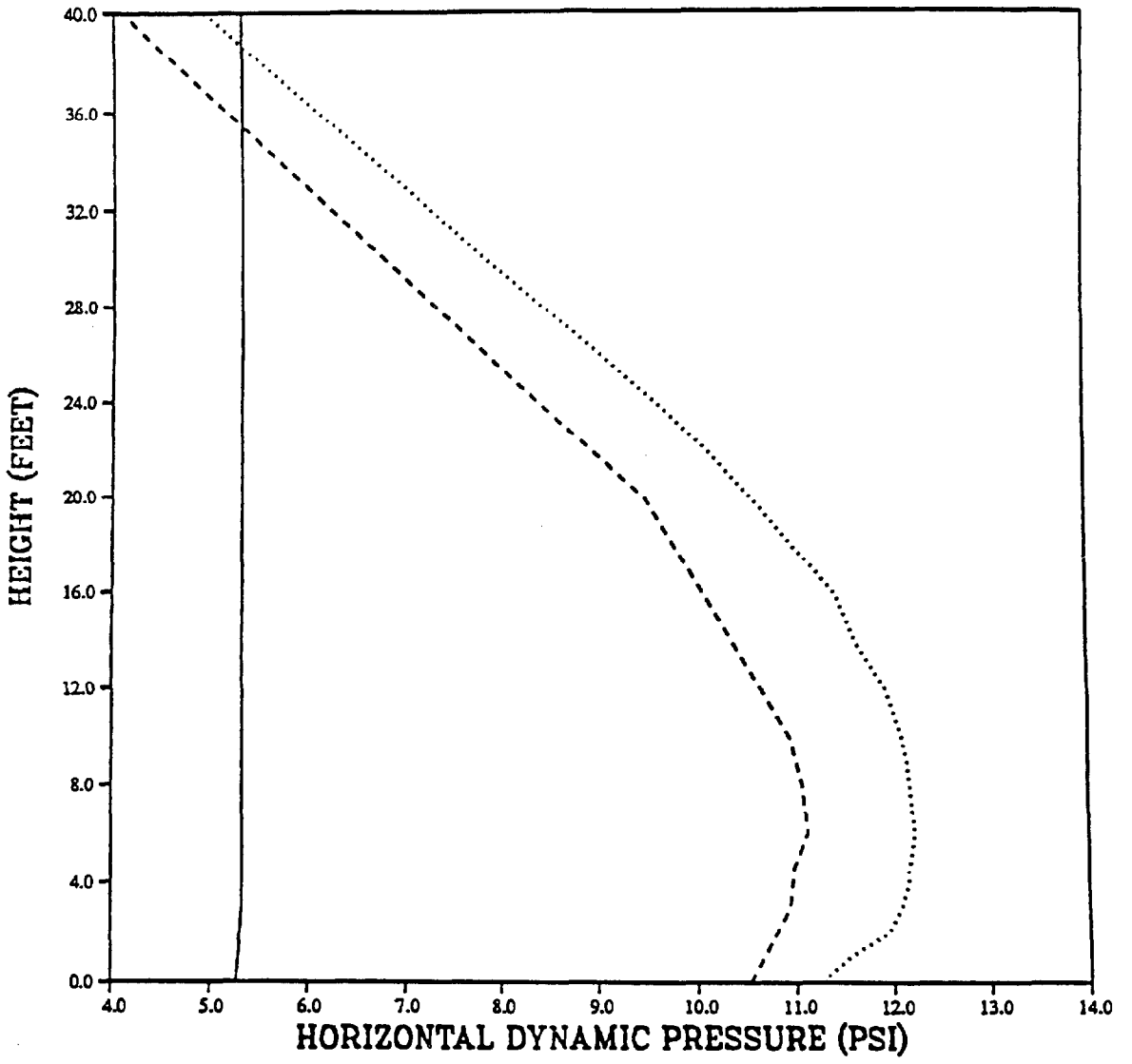

IDEAL 2950 FT
2928 FT (TL REV 6 JULY)
2864 FT (TL REV 6 JULY)

PRISCILLA DESERT
HORIZONTAL DYNAMIC PRESSURE PEAKS
VERTICAL PROFILE AT 3250 FEET

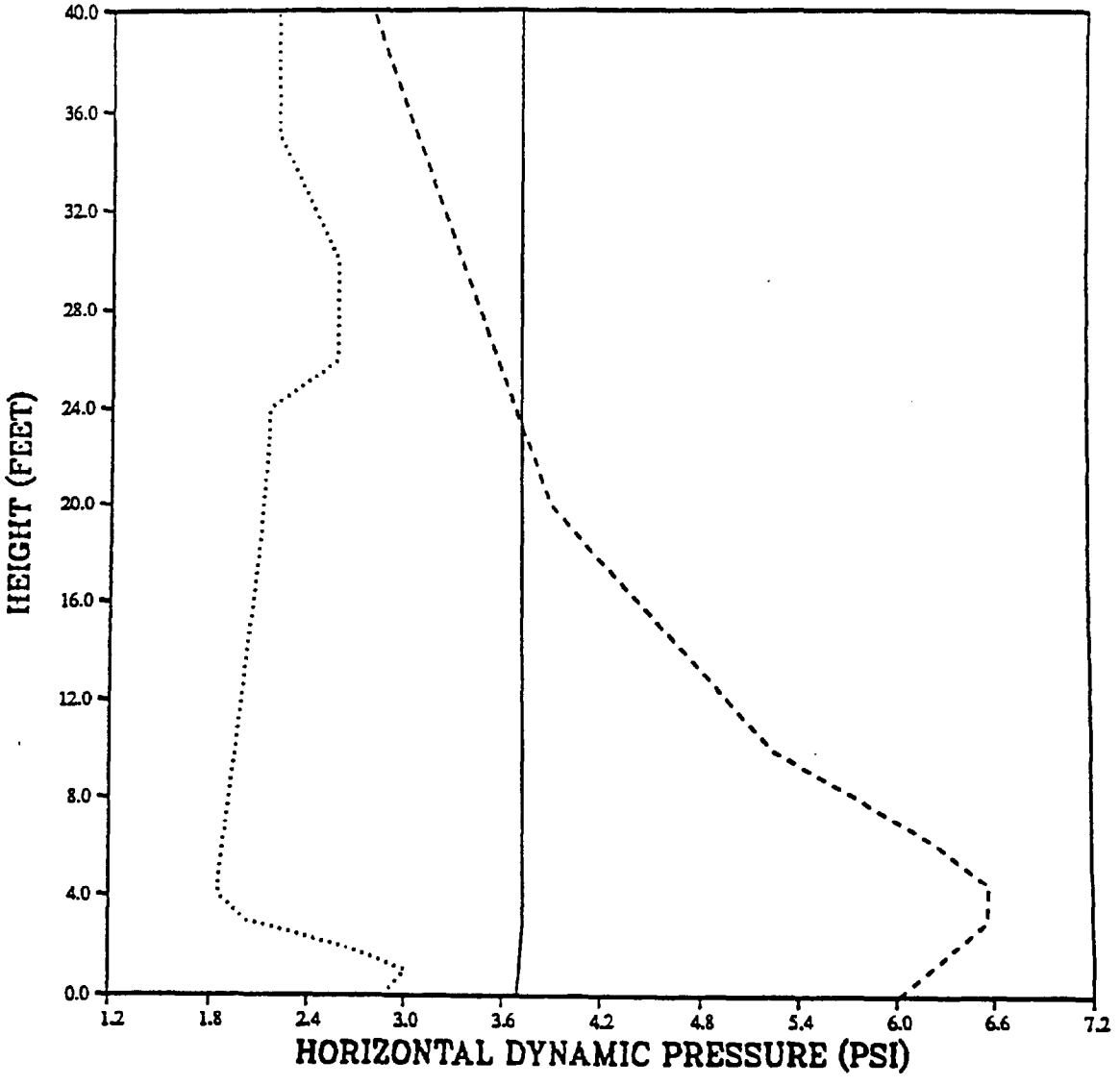

PRISCILLA DESERT
HORIZONTAL DYNAMIC PRESSURE PEAKS
VERTICAL PROFILE AT 3650 FEET

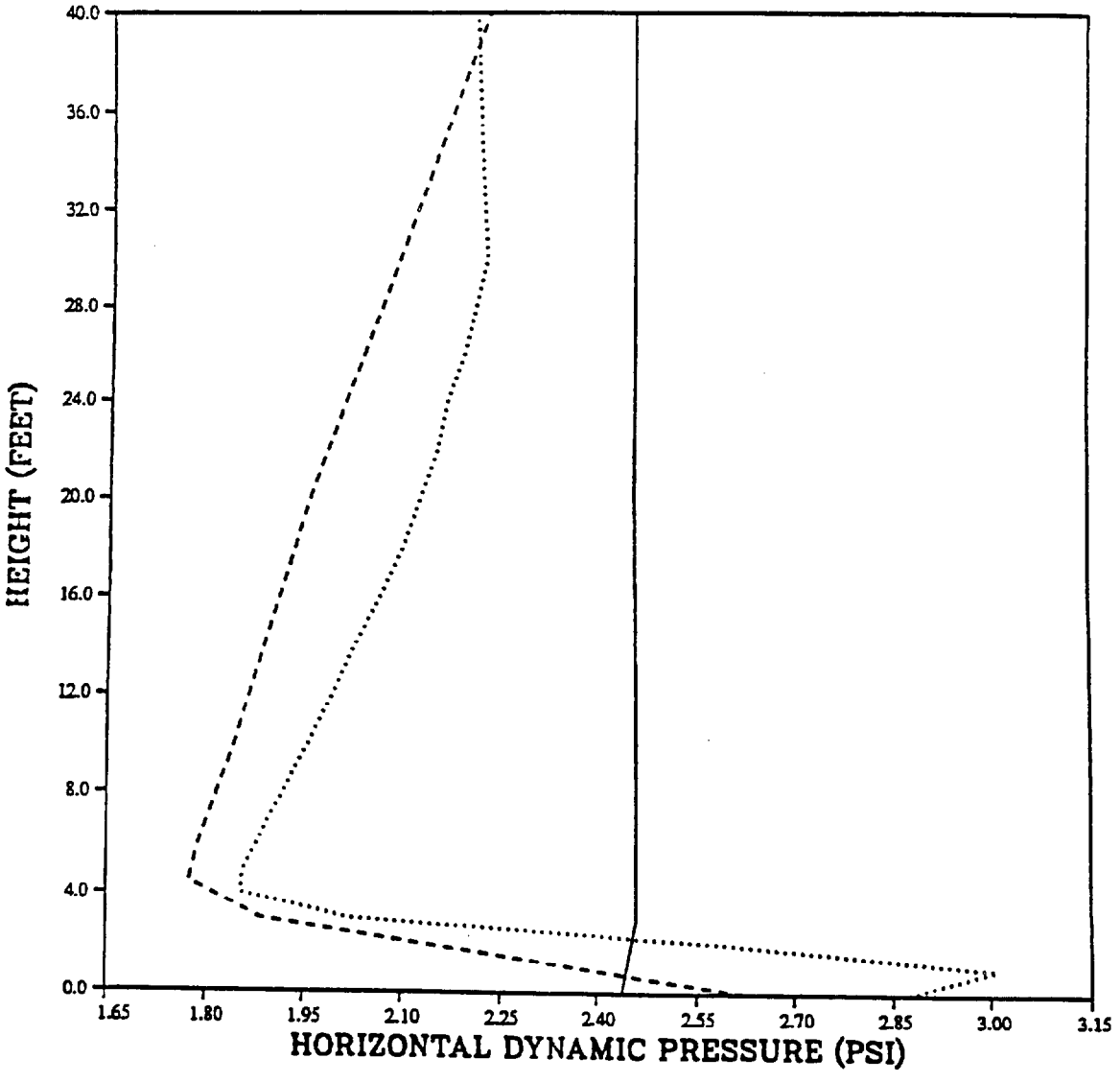

PRISCILLA DESERT
HORIZONTAL DYNAMIC PRESSURE PEAKS
VERTICAL PROFILE AT 4100 FEET

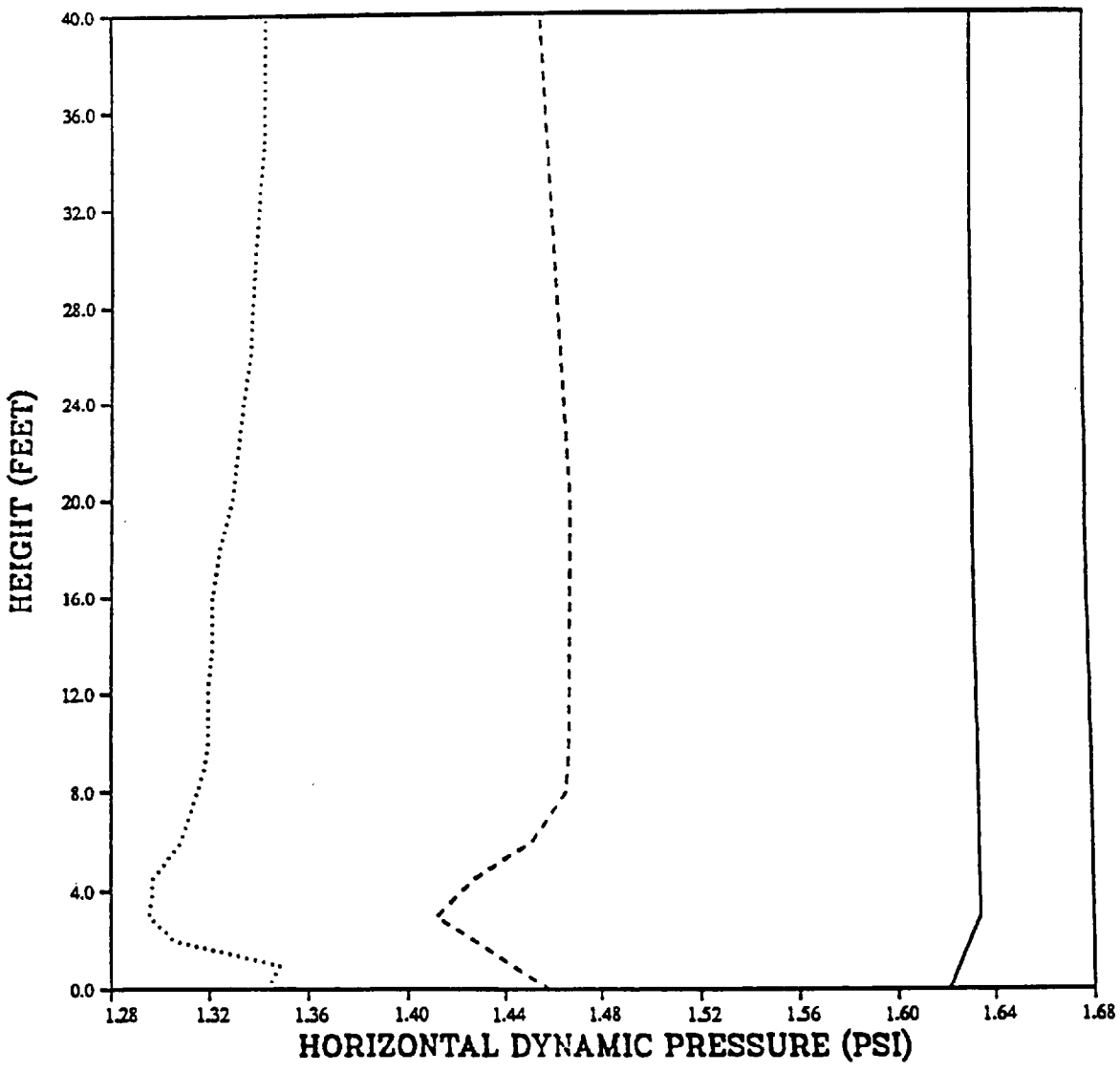

PRISCILLA DESERT
HORIZONTAL DYNAMIC PRESSURE PEAKS
VERTICAL PROFILE AT 4900 FEET

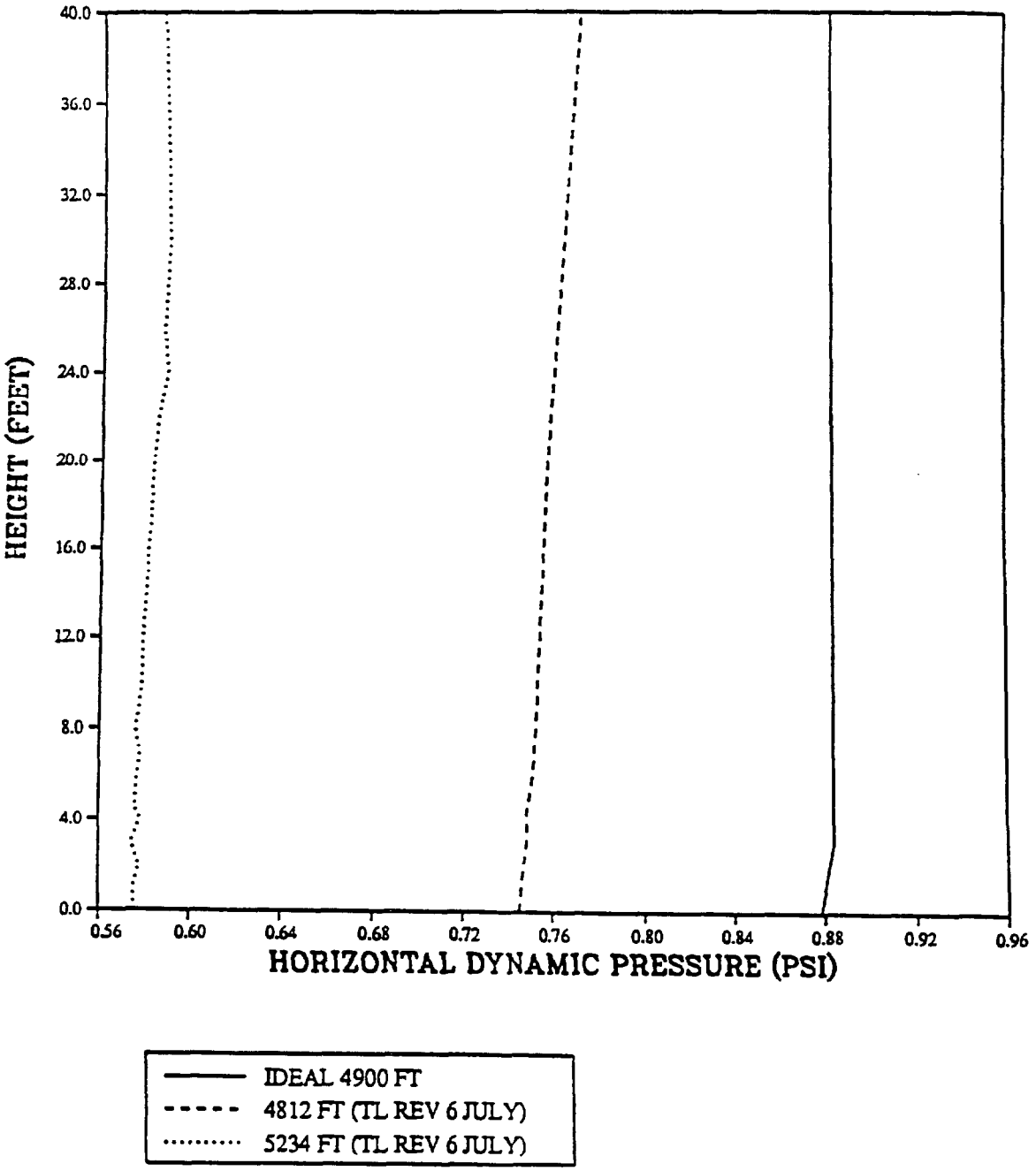

PRISCILLA DESERT
HORIZONTAL DYNAMIC PRESSURE PEAKS
VERTICAL PROFILE AT 5350 FEET

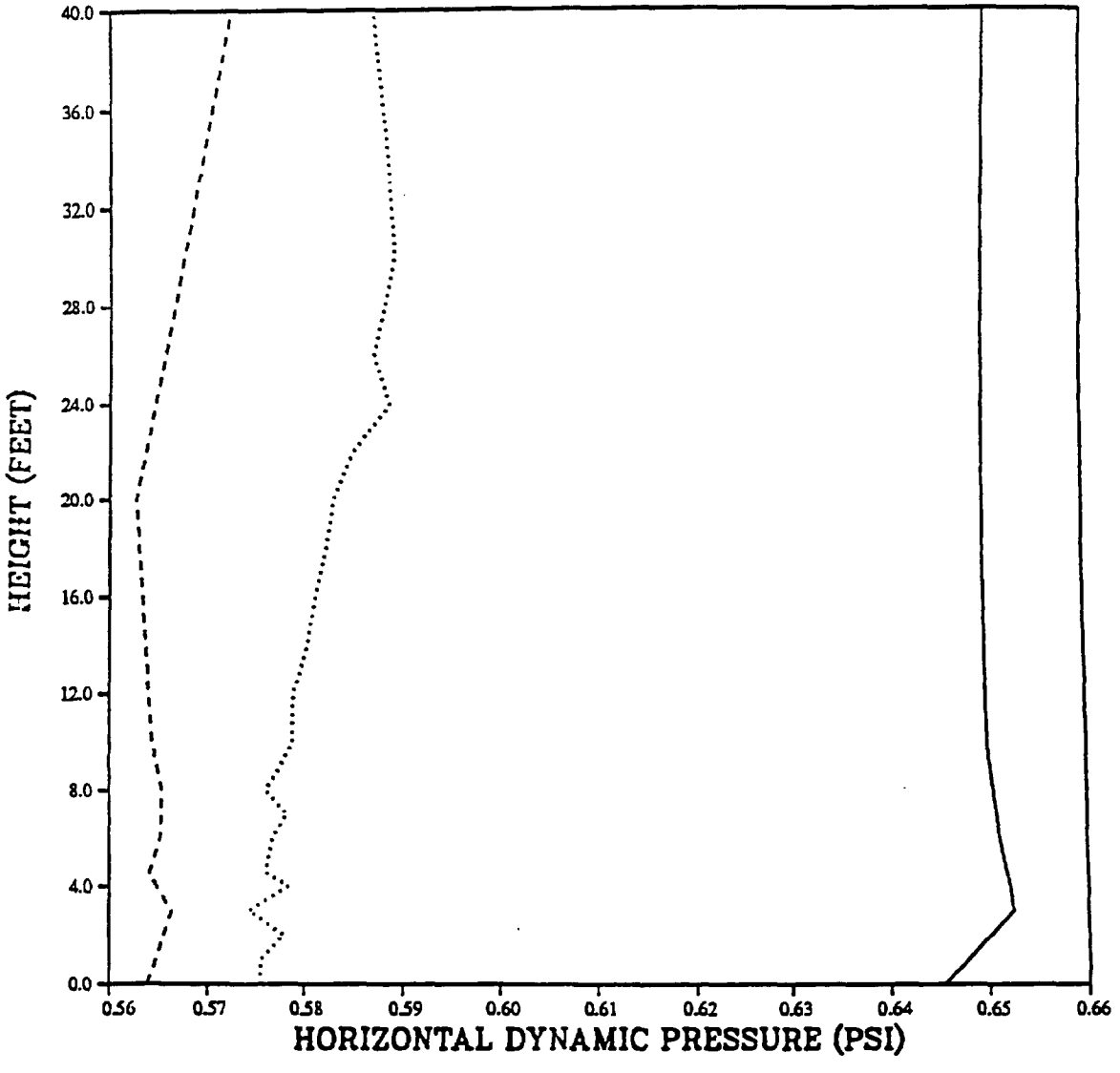

DESERT PRISCILLA
HORIZONTAL DYNAMIC PRESSURE IMPULSE
VERTICAL PROFILE AT 2100 FEET

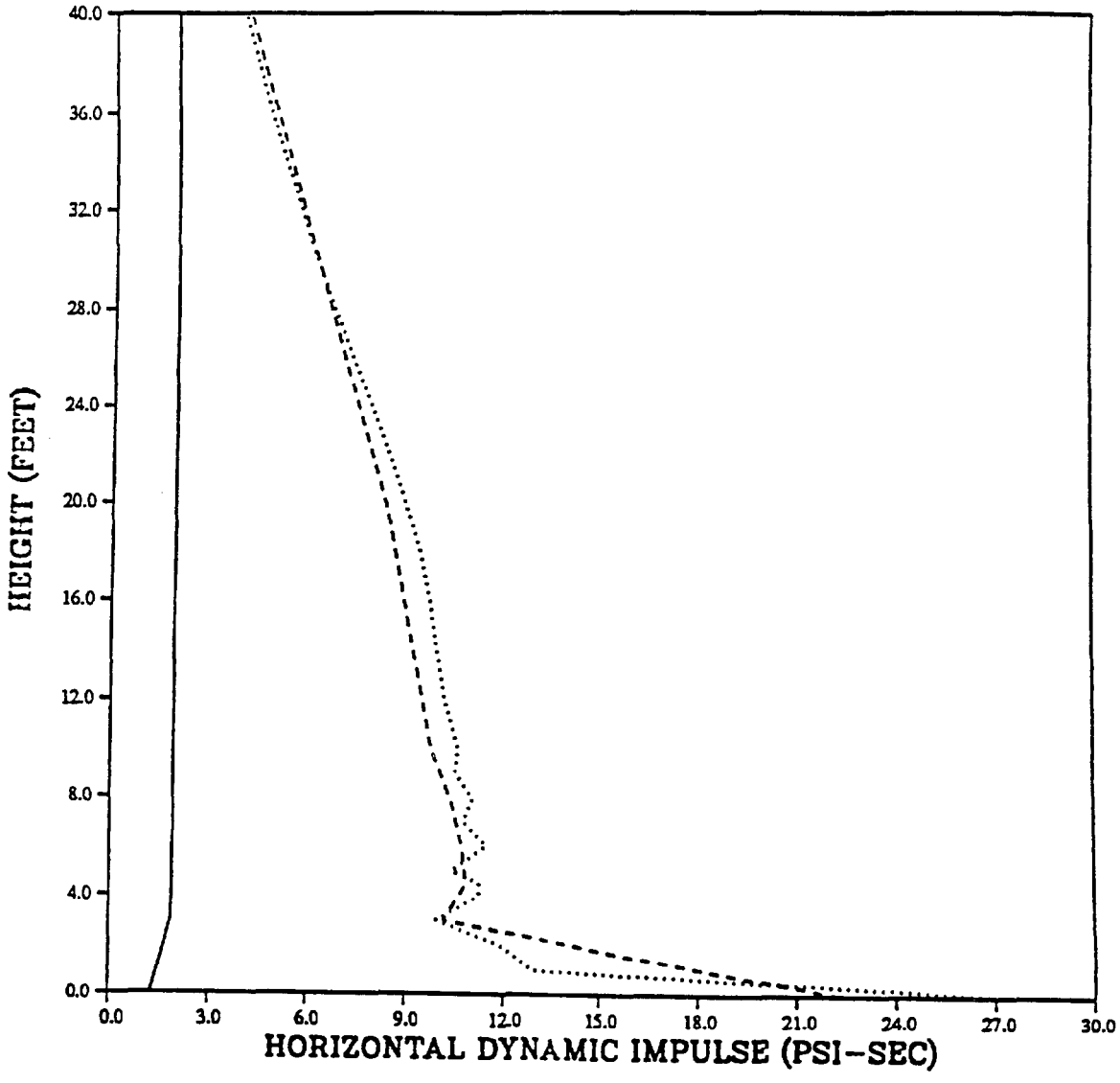

DESERT PRISCILLA
HORIZONTAL DYNAMIC PRESSURE IMPULSE
VERTICAL PROFILE AT 2300 FEET

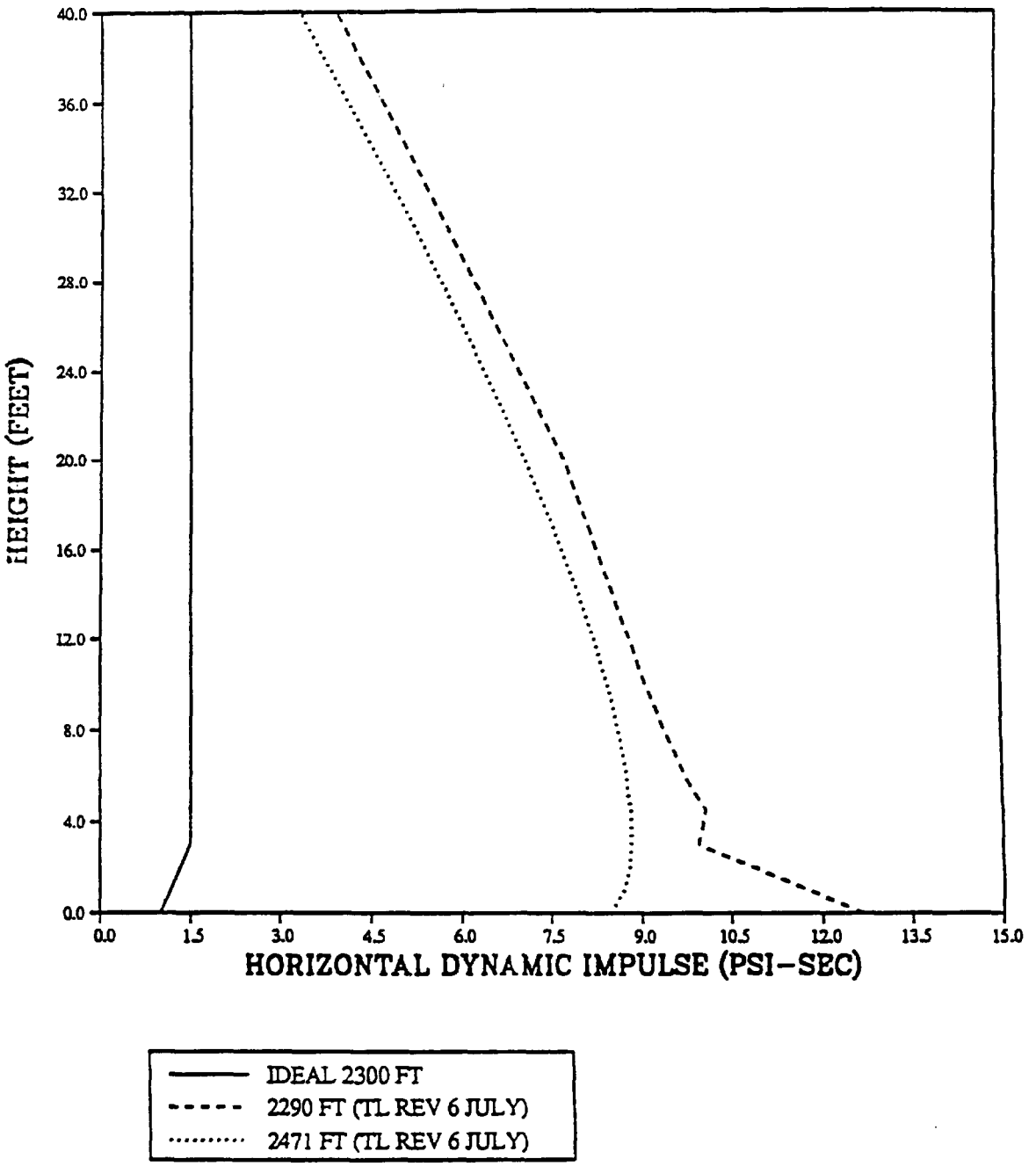

DESERT PRISCILLA
HORIZONTAL DYNAMIC PRESSURE IMPULSE
VERTICAL PROFILE AT 2550 FEET

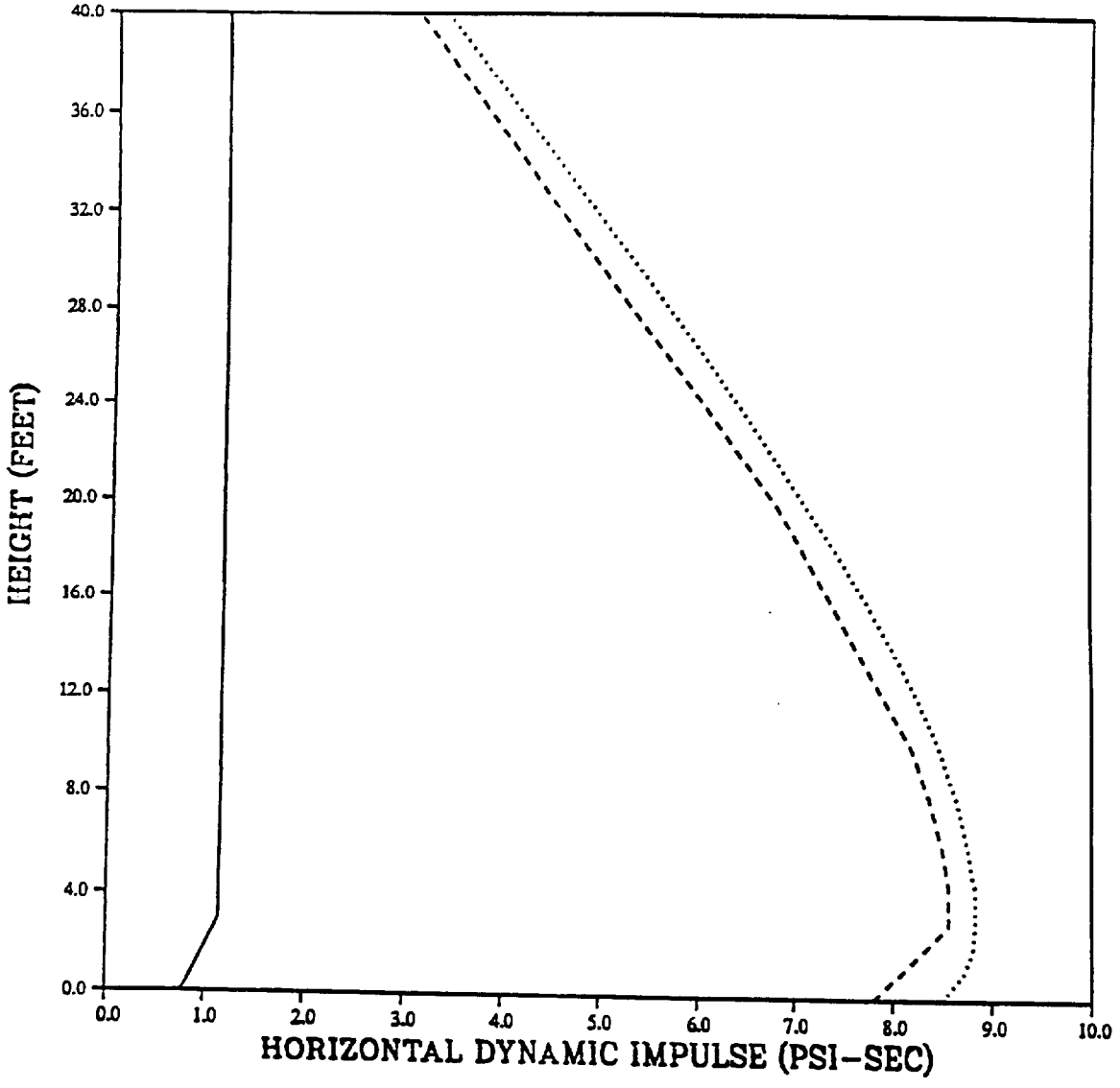

DESERT PRISCILLA
HORIZONTAL DYNAMIC PRESSURE IMPULSE
VERTICAL PROFILE AT 2950 FEET

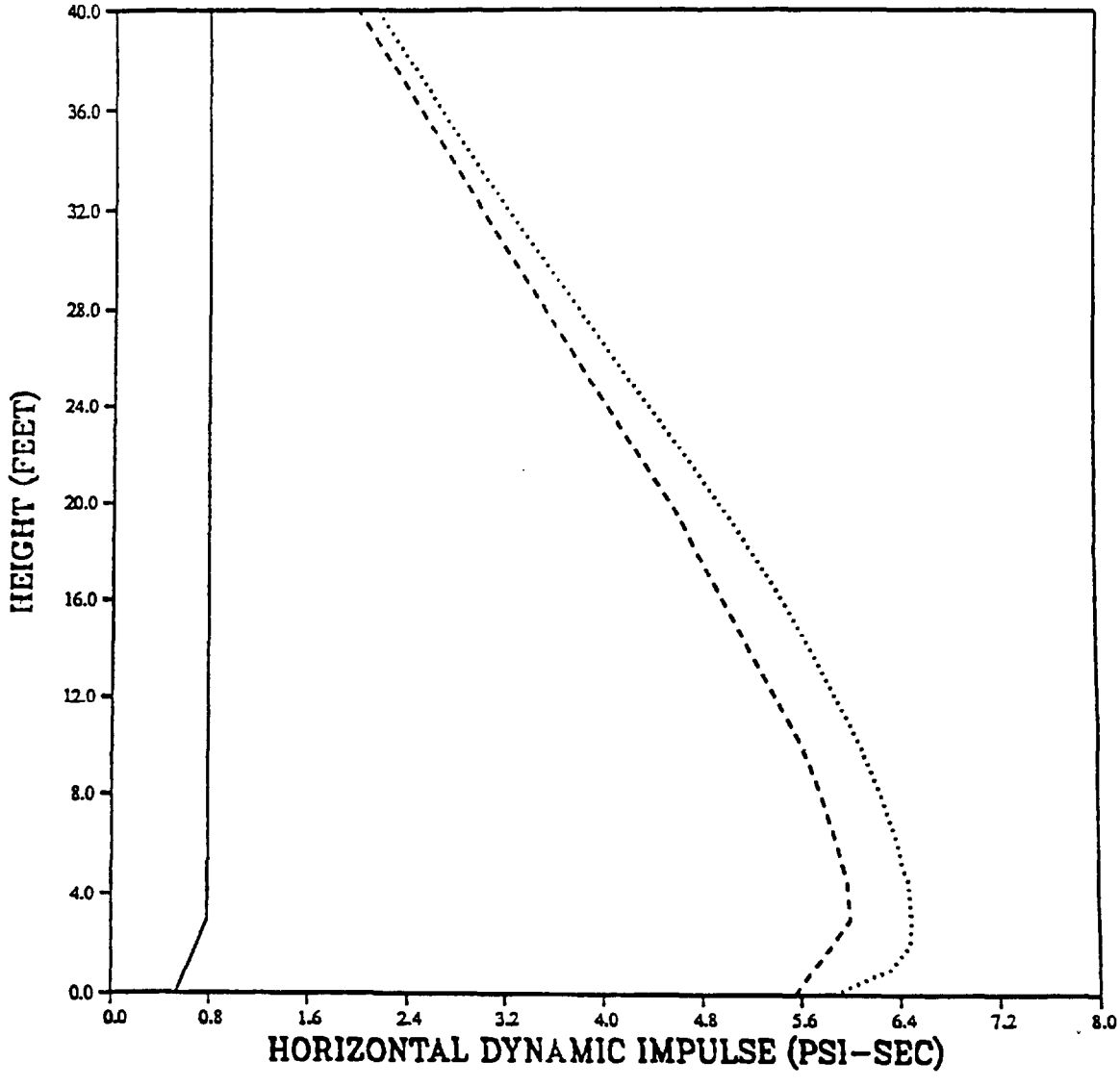

DESERT PRISCILLA
HORIZONTAL DYNAMIC PRESSURE IMPULSE
VERTICAL PROFILE AT 3250 FEET

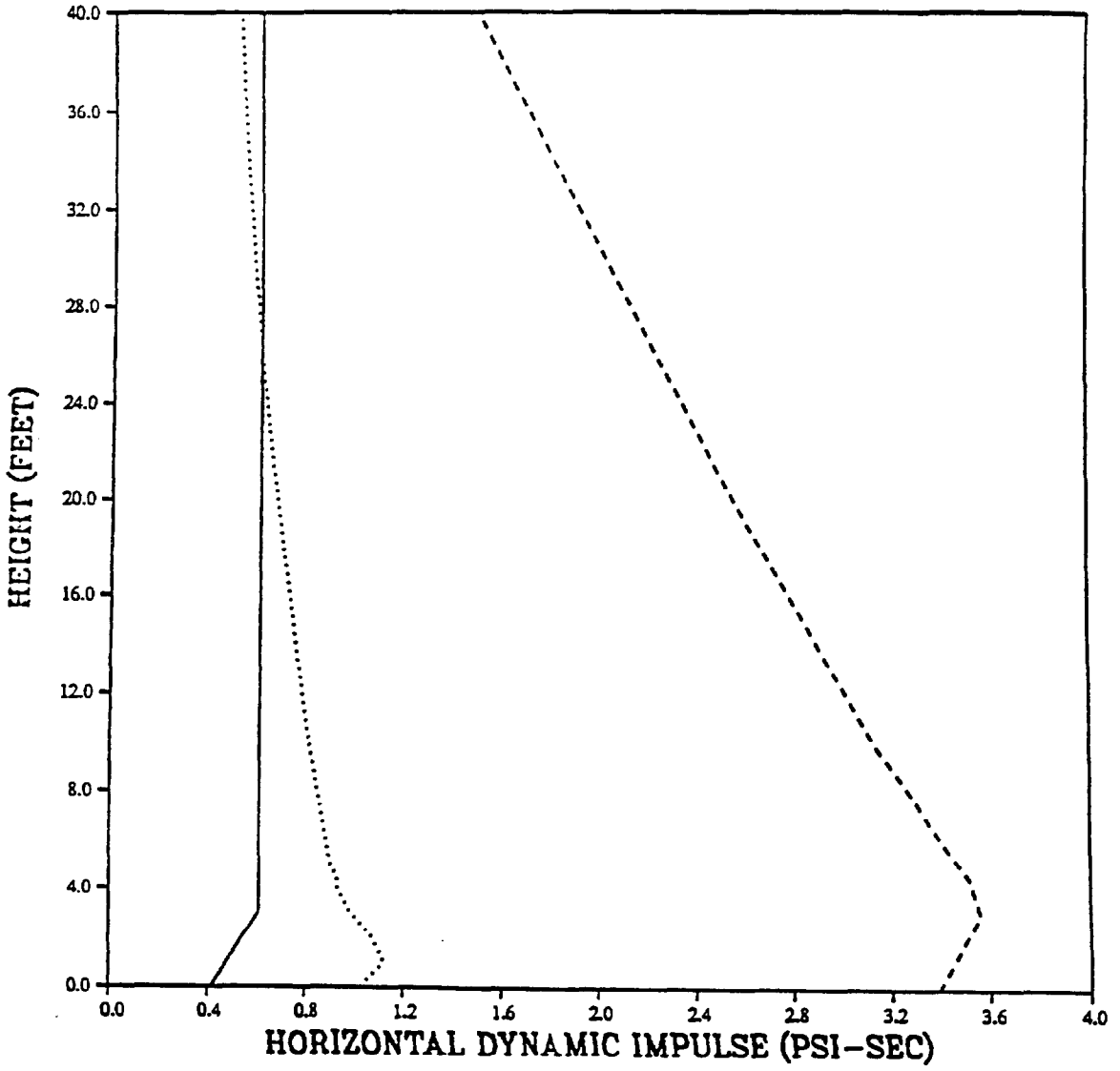

DESERT PRISCILLA
HORIZONTAL DYNAMIC PRESSURE IMPULSE
VERTICAL PROFILE AT 3650 FEET

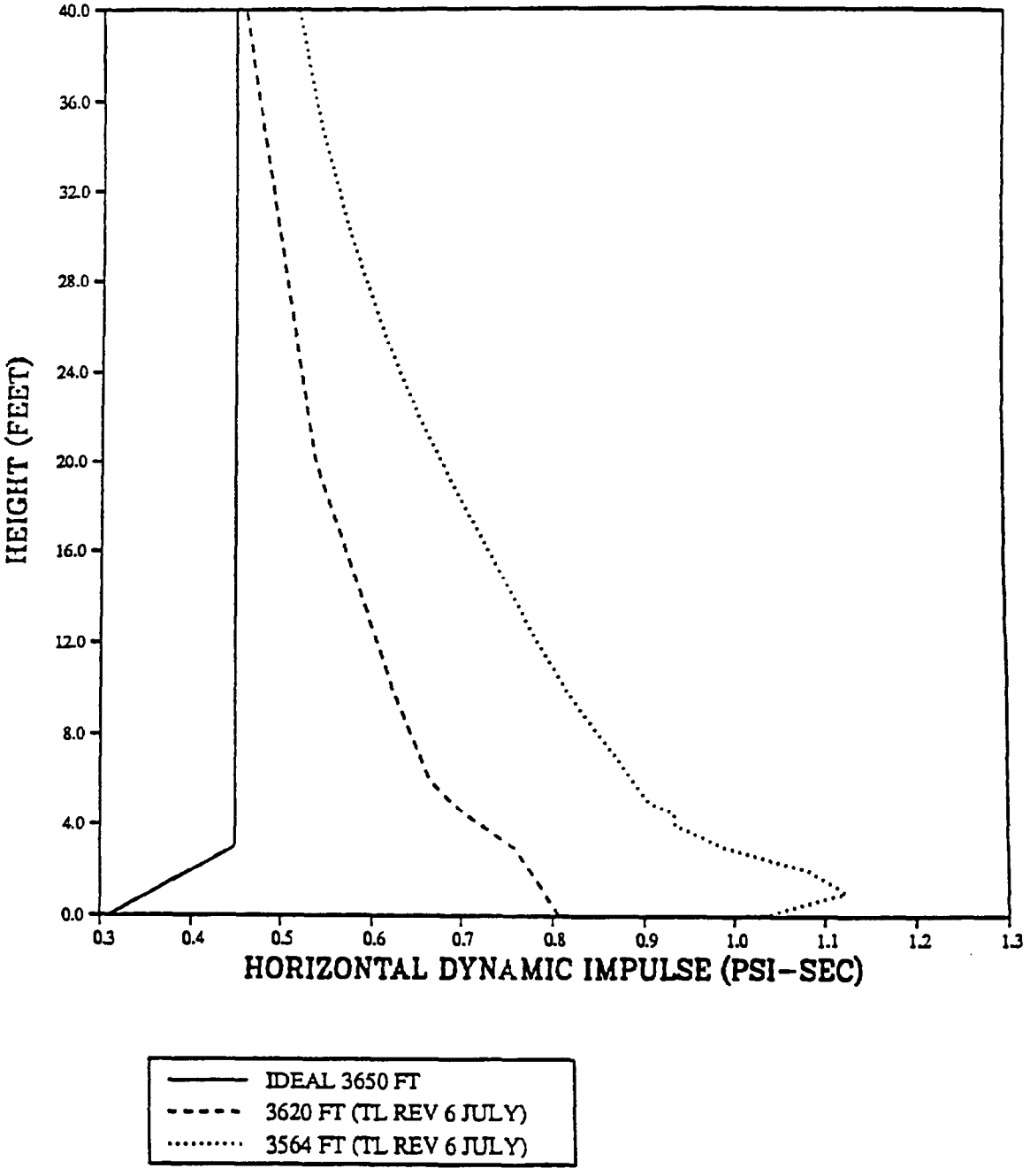

DESERT PRISCILLA
HORIZONTAL DYNAMIC PRESSURE IMPULSE
VERTICAL PROFILE AT 4100 FEET

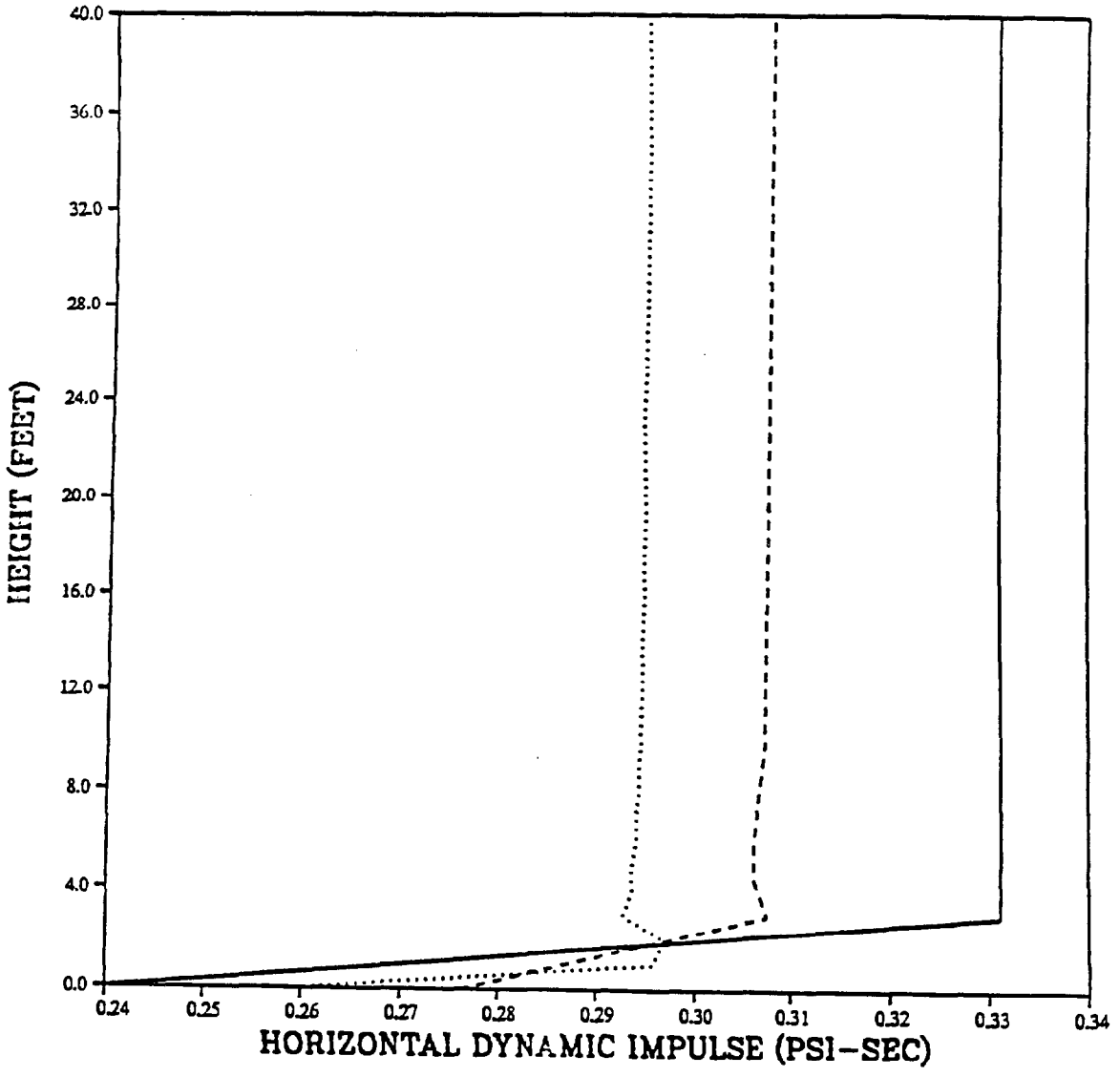

DESERT PRISCILLA
HORIZONTAL DYNAMIC PRESSURE IMPULSE
VERTICAL PROFILE AT 4900 FEET

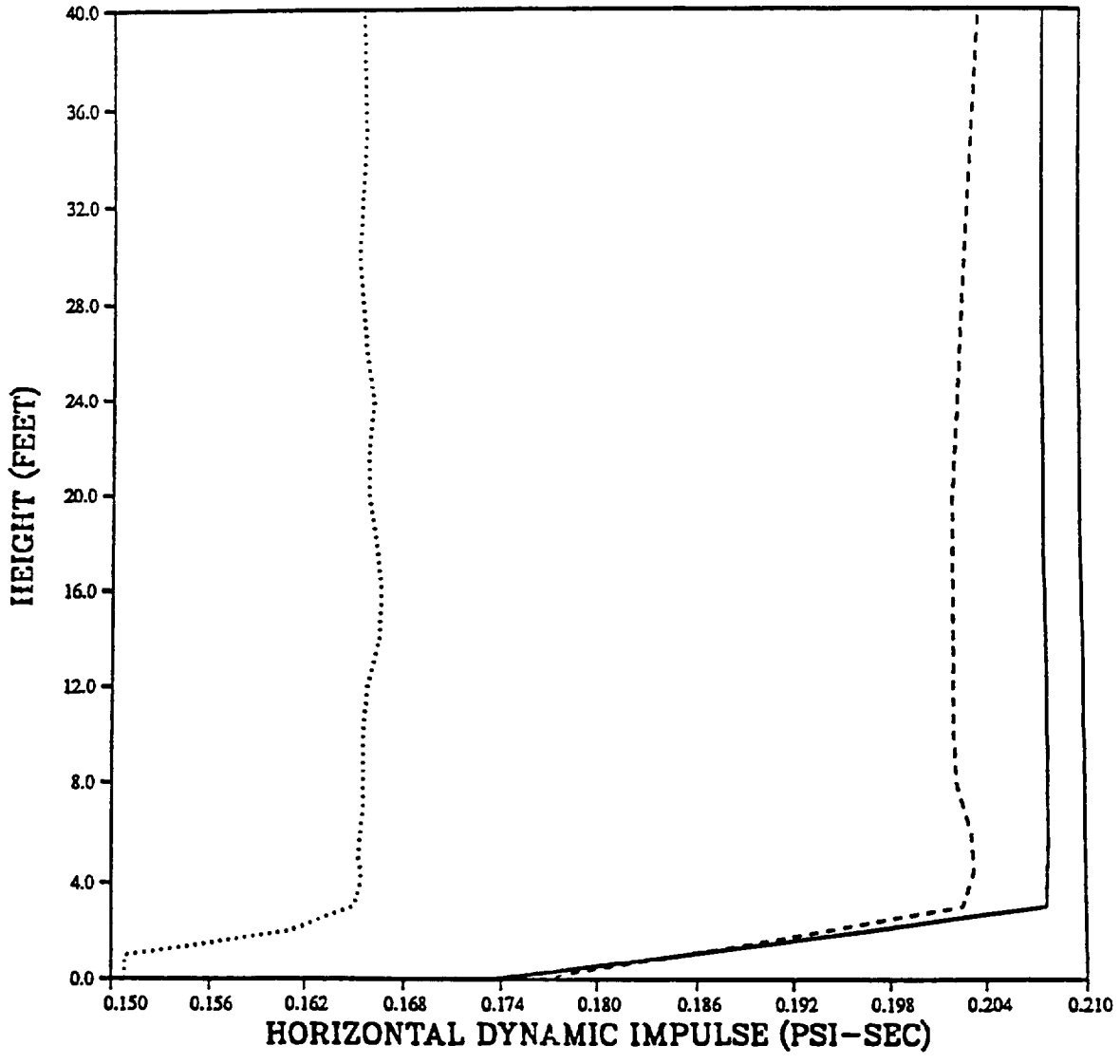

DESERT PRISCILLA
HORIZONTAL DYNAMIC PRESSURE IMPULSE
VERTICAL PROFILE AT 5350 FEET

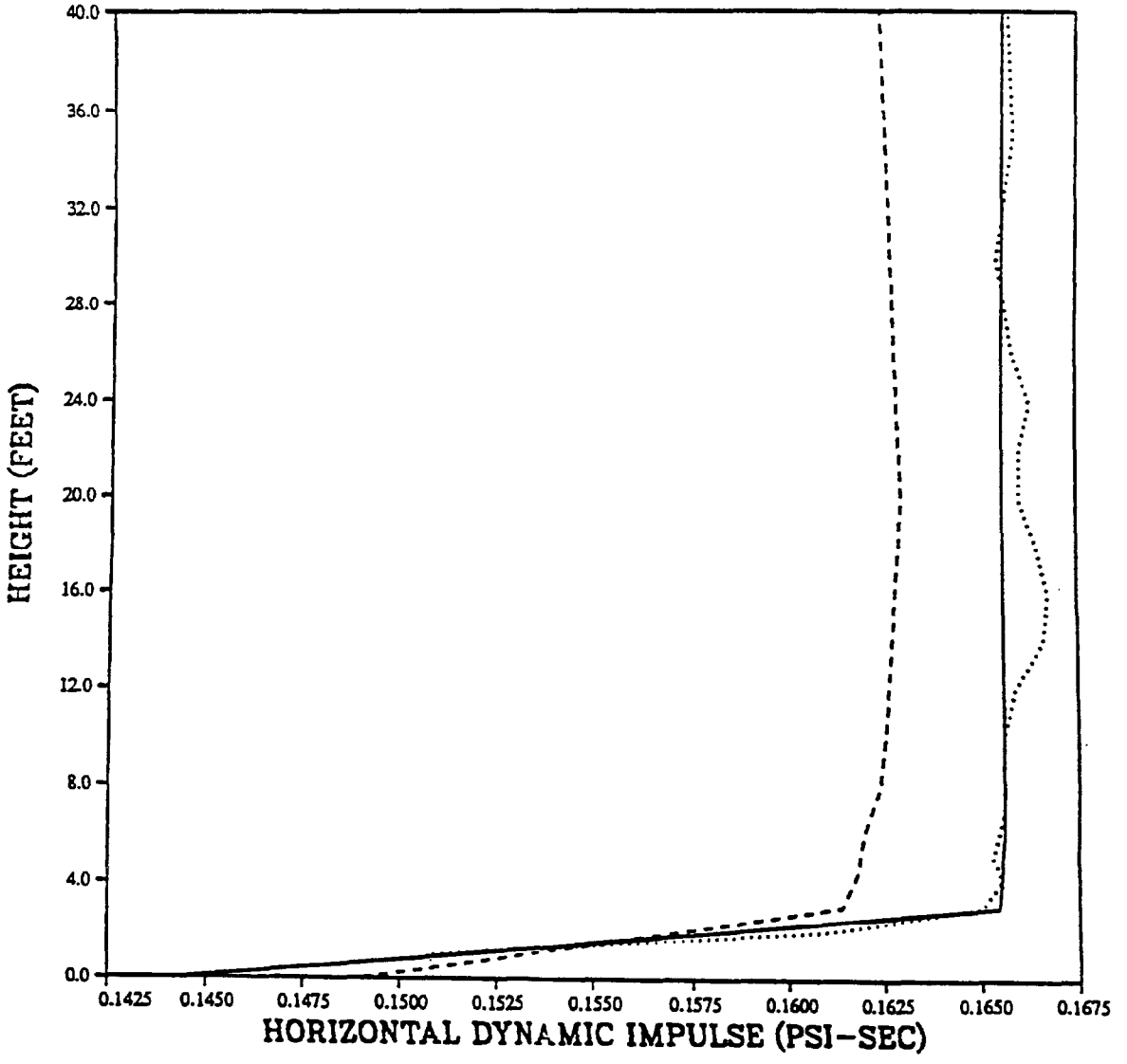

APPENDIX D

CONVERSION TABLE

Conversion factors for U.S. Customary to metric (SI) units of measurement

MULTIPLY →	BY →	TO GET
TO GET ←	BY ←	DIVIDE

angstrom	1.000 000 X E -10	meters (m)
atmosphere (normal)	1.013 25 X E +2	kilo pascal (kPa)
bar	1.000 000 X E +2	kilo pascal (kPa)
barn	1.000 000 X E -28	meter ^{2} (m^2)
British thermal unit (thermochemical)	1.054 350 X E +3	joule (J)
calorie (thermochemical)	4.184 000	joule (J)
cal (thermochemical)/cm^2	4.184 000 X E -2	mega joule/m^2 (MJ/m^2)
curie	3.700 000 X E +1	* giga becquerel (GBq)
degree (angle)	1.745 329 X E -2	radian (rad)
degree Fahrenheit	$t_K = (t\,^\circ f + 459.67)/1.8$	degree kelvin (K)
electron volt	1.602 19 X E -19	joule (J)
erg	1.000 000 X E -7	joule (J)
erg/second	1.000 000 X E -7	watt (W)
foot	3.048 000 X E -1	meter (m)
foot-pound-force	1.355 818	joule (J)
gallon (U.S. liquid)	3.785 412 X E -3	meter ^{3} (m^3)
inch	2.540 000 X E -2	meter (m)
jerk	1.000 000 X E +9	joule (J)
joule/kilogram (J/kg) (radiation dose absorbed)	1.000 000	Gray (Gy)
kilotons	4.183	terajoules
kip (1000 lbf)	4.448 222 X E +3	newton (N)
kip/inch ^{2} (ksi)	6.894 757 X E +3	kilo pascal (kPa)
ktap	1.000 000 X E +2	newton-second/m^2 ($N\text{-}s/m^2$)
micron	1.000 000 X E -6	meter (m)
mil	2.540 000 X E -5	meter (m)
mile (international)	1.609 344 X E +3	meter (m)
ounce	2.834 952 X E -2	kilogram (kg)
pound-force (lbs avoirdupois)	4.448 222	newton (N)
pound-force inch	1.129 848 X E -1	newton-meter (N•m)
pound-force/inch	1.751 268 X E +2	newton/meter (N/m)
pound-force/foot ^{2}	4.788 026 X E -2	kilo pascal (kPa)
pound-force/inch ^{2} (psi)	6.894 757	kilo pascal (kPa)
pound-mass (lbm avoirdupois)	4.535 924 X E -1	kilogram (kg)
pound-mass-foot ^{2} (moment of intertia)	4.214 011 X E -2	kilogram-meter ^{2} ($kg\cdot m^2$)
pound-mass/foot ^{3}	1.601 846 X E +1	kilogram/meter ^{3} (kg/m^3)
rad (radiation dose absorbed)	1.000 000 X E -2	** Gray (Gy)
roentgen	2.579 760 X E -4	coulomb/kilogram (C/kg)
shake	1.000 000 X E -8	second (s)
slug	1.459 390 X E +1	kilogram (kg)
torr (mm HG, 0°C)	1.333 22 X E -1	kilo pascal (kPa)

* The becquerel (Bq) is the SI unit of radioactivity; 1 Bq = 1 event/s.
** The Gray (GY) is the SI unit of absorbed radiation.

A more complete listing of conversions may be found in "Metric Practice Guide E 380-74," American Society for Testing and Materials.

INTENTIONALLY LEFT BLANK.

NO. OF COPIES	ORGANIZATION
2	ADMINISTRATOR ATTN DTIC DDA DEFENSE TECHNICAL INFO CTR CAMERON STATION ALEXANDRIA VA 22304-6145
1	DIRECTOR ATTN AMSRL OP SD TA US ARMY RESEARCH LAB 2800 POWDER MILL RD ADELPHI MD 20783-1145
3	DIRECTOR ATTN AMSRL OP SD TL US ARMY RESEARCH LAB 2800 POWDER MILL RD ADELPHI MD 20783-1145
1	DIRECTOR ATTN AMSRL OP SD TP US ARMY RESEARCH LAB 2800 POWDER MILL RD ADELPHI MD 20783-1145
	ABERDEEN PROVING GROUND
5	DIR USARL ATTN AMSRL OP AP L (305)

NO. OF COPIES	ORGANIZATION
2	HQDA ATTN SARD TR MS K KOMINOS DR R CHAIT PENTAGON WASHINGTON DC 20310-0103
2	HQDA ATTN SARD TT MS C NASH DR F MILTON PENTAGON WASHINGTON DC 20310-0103
1	DIR OF DEFNS RSRCH AND ENGRG ATTN DD TWP WASHINGTON DC 20301
1	ASST SECRETARY OF DEFNS ATTN DOCUMENT CONTROL ATOMIC ENERGY WASHINGTON DC 20301
1	CHAIRMAN ATTN J 5 R&D DIV JOINT CHIEFS OF STAFF WASHINGTON DC 20301
2	DA DCSOPS ATTN TECH LIB DIR OF CHEM & NUC OPS WASHINGTON DC 20310
1	EUROPEAN RSRCH OFC ATTN DR R REICHENBACH USARDSG UK PSC 802 BOX 15 FPO AE 09499-1500
1	DIR ATTN TECH LIB ADVNCD RSRCH PROJ AGCY 3701 N FAIRFAX DR ARLINGTON VA 22203-1714
2	CDR ATTN AMSEL RD AMSEL RO TPPO P US ARMY CECOM FT MONMOUTH NJ 07703-5301
1	MIT ATTN TECH LIB CAMBRIDGE MA 02139

NO. OF COPIES	ORGANIZATION
2	DIR ATTN PUBLIC RELATIONS OFC TECH LIB FED EMERG MGMT AGCY WASHINGTON DC 20472
1	CHAIRMAN DOD EXPLOSIVES SAFETY BOARD ROOM 856 C HOFFMAN BLDG 1 2461 EISENHOWER AVE ALEXANDRIA VA 22331-0600
1	DIR ATTN DT 2 WPNS & SYS DIV DEFNS INTLLGNC AGCY WASHINGTON DC 20301
8	DIR ATTN CSTI TECH LIB DDIR DFSP NANS OPNA SPSD SPTD DFTD DEFNS NUCLEAR AGENCY WASHINGTON DC 20305
3	CDR ATTN FCPR FCTMOF NMHE FIELD COMMAND DNA KIRTLAND ARB NM 87115
10	CIA ATTN GE 47 HQ DIR DB STANDARD WASHINGTON DC 20505
2	CDR ATTN AMSNA D DR D SIELING STRNC UE J CALLIGEROS US ARMY NRDEC NATICK MA 01762
1	CDR ATTN ASQNC ELC IS L R MYER CTR US ARMY CECOM R&D TECH LIB FT MONMOUTH NJ 07703-5000

NO. OF COPIES	ORGANIZATION
1	CDR ATTN SMCAR FSM W BARBER BLDG 94 US ARMY ARDEC PCTNY ARSNL NJ 07806-5000
1	DIR ATTN AIAMS YDL US ARMY MISSILE & SPACE INTLLGNC CTR REDSTONE ARSNL AL 35898-5500
1	DIR ATTN AMSMR ATL US ARMY RESEARCH LAB WATERTOWN MA 02172-0001
1	CDR ATTN HNDED FD US ARMY ENGINEER DIV PO BOX 1500 HUNTSVILLE AL 35807
1	CDR ATTN CESWF PM J US ARMY CORPS OF ENGRS FT WORTH DISTRICT PO BOX 17300 FT WORTH TX 76102-0300
1	CDR ATTN SLCRO D US ARMY RESEARCH OFFICE PO BOX 12211 RSCH TRI PK NC 27709-2211
1	DIR ATTN ATRC RPR RADDA HQ TRAC RPD FT MONROE VA 23651-5143
1	DIR ATTN ATRC WC KIRBY TRAC WSMR WSMR NM 88002-5502
1	CDR ATTN STEWS NED DR MEASON US ARMY WSMR WSMR NM 88002-5158

NO. OF COPIES	ORGANIZATION
2	CHIEF OF NAVAL OPERATIONS ATTN OP 03EG OP 985F DEPT OF THE NAVY WASHINGTON DC 20350
1	CDR ATTN RSRCH AND DATA BRANCH US ARMY NGIC 220 7TH STREET NE CHARLOTTESVILLE VA 22901-5396
1	DIR ATTN ATRC L MR CAMERON US ARMY TRAC FT LEE FORT LEE VA 23801-6140
2	CDR ATTN CSSD H MPL TECH LIB CSSD H XM DR DAVIES US ARMY STRATEGIC DEFENSE COMMAND PO BOX 1500 HUNTSVILLE AL 35807
3	CDR ATTN CEWES SS R J WATT CEWES SE R J INGRAM CEWES TL TECH LIBRARY US ARMY CORPS OF ENGINEERS WATERWAYS EXPERIMENT STATION PO BOX 631 VICKSBURG MS 39180-0631
3	CDR US ARMY NUCLEAR & CHEMICAL AGENCY 7150 HELLER LOOP, SUITE 101 SPRINGFIELD VA 22150-3198
1	DIR ATTN ATRC TRAC FLVN FORT LEAVENWORTH KS 66027-5200
1	CDR ATTN PME 117 21A NAVAL ELECTRONIC SYSTEMS COMMAND WASHINGTON DC 20360
2	OFFICE OF NAVAL RESEARCH ATTN DR A FAULSTICK CODE 23 800 N QUINCY STREET ARLINGTON VA 22217

NO. OF COPIES	ORGANIZATION
1	CDR ATTN CODE SEA 62R NAVAL SEA SYSTEMS COMMAND DEPARTMENT OF THE NAVY WASHINGTON DC 20362-5101
1	COMMANDING OFFICER CODE L51 ATTN J TANCRETO NAVAL CIVIL ENGINEERING LABORATORY PORT HUENEME CA 93043-5003
1	CIVIL ENGINEERING LABORATORY ATTN TECHNICAL LIBRARY CODE L31 NAVAL CONSTRUCTION BATTALION CTR PORT HUENEME CA 93041
1	CDR ATTN CODE E23 LIBRARY NAVAL SURFACE WARFARE CENTER DAHLGREN VA 22448-5000
1	WHITE OAK WARFARE CTR DETACHMENT ATTN CODE E232 TECHNICAL LIBRARY 10901 NEW HAMPSHIRE AVENUE SILVER SPRING MD 20903-5000
1	CDR ATTN DOCUMENT CONTROL NAVAL WEAPONS EVALUATION FAC KIRTLAND AFB NM 87117
1	AEDC ATTN R MCAMIS MAIL STOP 980 ARNOLD AFB TN 37389
1	OLAC PL TSTL ATTN D SHIPLETT EDWARDS AFB CA 93523-5000
2	AIR FORCE ARMAMENT LABORATORY ATTN AFATL DOIL AFATL DLYV EGLIN AFB FL 32541-5000
3	PHILLIPS LABORATORY (AFWL) ATTN NTE NTED NTES KIRTLAND AFB NM 87117-6008

NO. OF COPIES	ORGANIZATION
1	AFIT ATTN TECHNICAL LIBRARY BLDG 640 B WRIGHT PATTERSON AFB OH 45433
1	FTD NIIS WRIGHT PATTERSON AFB OH 45433
4	DIR ATTN R GUENZLER MS 3505 R HOLMAN MS-3510 R A BERRY W C REED IDAHO NATIONAL ENGINEERING LABORATORY EG&G IDAHO INC PO BOX 8757 BWI AIRPORT BALTIMORE MD 21240
3	KAMAN SCIENCES CORPORATION ATTN LIBRARY P A ELLIS F H SHELTON P O BOX 7463 COLORADO SPRINGS CO 80933-7463
2	DIR ATTN TH DOWLER MS F602 DOC CONTROL FOR REPORTS LIBRARY LOS ALAMOS NATIONAL LABORATORY PO BOX 1663 LOS ALAMOS NM 87545
1	DIR ATTN DOC CONTROL FOR TECH LIB SANDIA NATIONAL LABORATORIES LIVERMORE LABORATORY P O BOX 969 LIVERMORE CA 94550
1	DIR ATTN TECHNICAL LIBRARY NASA LANGLEY RESEARCH CENTER HAMPTON VA 23665
1	ADA TECHNOLOGIES INC ATTN JAMES R BUTZ HONEYWELL CENTER SUITE 110 304 INVERNESS WAY SOUTH ENGLEWOOD CO 80112

NO. OF COPIES	ORGANIZATION
1	ALLIANT TECHSYSTEMS INC ATTN ROGER A RAUSCH MN48 3700 7225 NORTHLAND DRIVE BROOKLYN PARK MN 55428
1	AEROSPACE CORPORATION ATTN TECH INFO SERVICES P O BOX 92957 LOS ANGELES CA 90009
1	THE BOEING COMPANY ATTN AEROSPACE LIBRARY P O BOX 3707 SEATTLE WA 98124
1	CALIFORNIA RES & TECH INC ATTN M ROSENBLATT 20943 DEVONSHIRE STREET CHATSWORTH CA 91311
1	DYNAMICS TECHNOLOGY INC ATTN D T HOVE G P MASON 21311 HAWTHORNE BLVD SUITE 300 TORRANCE CA 90503
1	EATON CORPORATION ATTN J WADA DEFENSE VALVE & ACTUATOR DIV 2338 ALASKA AVE EL SEGUNDO CA 90245-4896
5	DIR ATTN DOC CONTROL 3141 C CAMERON DIV 6215 A CHABAI DIV 7112 D GARDNER DIV 1421 J MCGLAUN DIV 1541 SANDIA NATIONAL LABORATORIES P O BOX 5800 ALBUQUERQUE NM 87185-5800
1	BLACK & VEATCH ENGINEERS - ARCHITECTS ATTN H D LAVERENTZ 1500 MEADOW LAKE PARKWAY KANSAS CITY MO 64114

NO. OF COPIES	ORGANIZATION
1	DIRECTOR ATTN DR T HOLTZ MS 202-14 NASA-AMES RESEARCH CENTER APPLIED COMPUTATIONAL AERO BRANCH MOFFETT FIELD CA 94035
2	APPLIED RESEARCH ASSOCIATES INC ATTN J KEEFER N H ETHRIDGE P O BOX 548 ABERDEEN MD 21001
1	CARPENTER RESEARCH CORPORATION ATTN H JERRY CARPENTER 27520 HAWTHORNE BLVD SUITE 263 ROLLING HILLS ESTATES CA 90274
1	GOODYEAR CORPORATION ATTN R M BROWN BLDG 1 SHELTER ENGINEERING LITCHFIELD PARK AZ 85340
2	FMC CORPORATION ATTN J DROTLEFF C KREBS MDP95 ADVANCED SYSTEMS CENTER BOX 58123 2890 DE LA CRUZ BLVD SANTA CLARA CA 95052
1	SVERDRUP TECHNOLOGY INC ATTN B D HEIKKINEN SVERDRUP CORPORATION AEDC MS 900 ARNOLD AFB TN 37389-9998
1	KTECH CORPORATION ATTN DR E GAFFNEY 901 PENNSYLVANIA AVE NE ALBUQUERQUE NM 87111
4	KAMAN AVIDYNE ATTN R RUETENIK (2 CYS) S CRISCIONE R MILLIGAN 83 SECOND AVENUE NORTHWEST INDUSTRIAL PARK BURLINGTON MA 01830

NO. OF COPIES ORGANIZATION

2 KAMAN SCIENCES CORPORATION
ATTN DASIAC (2 CYS)
P O DRAWER 1479
816 STATE STREET
SANTA BARBARA CA 93102-1479

1 LOCKHEED MISSILES & SPACE CO
ATTN J J MURPHY
DEPT 81 11 BLDG 154
P O BOX 504
SUNNYVALE CA 94086

1 ORLANDO TECHNOLOGY INC
ATTN D MATUSKA
60 SECOND STREET BLDG 5
SHALIMAR FL 32579

2 THE RALPH M PARSONS COMPANY
ATTN T M JACKSON
LB TS PROJECT MANAGER
100 WEST WALNUT STREET
PASADENA CA 91124

1 SAIC
ATTN N SINHA
501 OFFICE CENTER DRIVE APT 420
FT WASHINGTON PA 19034 3211

1 SAIC
ATTN J GUEST
2301 YALE BLVD SE
SUITE E
ALBUQUERQUE NM 87106

2 S CUBED
A DIVISION OF MAXWELL LABS INC
ATTN C E NEEDHAM
L KENNEDY
2501 YALE BLVD SE
ALBUQUERQUE NM 87106

1 TRW
BALLISTIC MISSILE DIVISION
ATTN H KORMAN
MAIL STATION 526 614
P O BOX 1310
SAN BERNADINO CA 92402

1 THERMAL SCIENCE INC
ATTN R FELDMAN
2200 CASSENS DR
ST LOUIS MO 63026

NO. OF COPIES ORGANIZATION

2 MCDONNELL DOUGLAS ASTRNTCS CORP
ATTN ROBERT W HALPRIN
K A HEINLY
5301 BOLSA AVENUE
HUNTINGTON BEACH CA 92647

1 MDA ENGINEERING INC
ATTN DR DALE ANDERSON
500 EAST BORDER STREET
SUITE 401
ARLINGTON TX 07601

2 PHYSICS INTERNATIONAL CORPORATION
P O BOX 5010
SAN LEANDRO CA 94577-0599

1 R&D ASSOCIATES
ATTN G P GANONG
P O BOX 9377
ALBUQUERQUE NM 87119

1 SCIENCE CENTER
ROCKWELL INTERNATIONAL CORPORATION
ATTN DR S CHAKRAVARTHY
DR D OTA
1049 CAMINO DOS RIOS
THOUSAND OAKS CA 91358

3 S CUBED
A DIVISION OF MAXWELL LABS INC
ATTN TECHNICAL LIBRARY
R DUFF
K PYATT
P O BOX 1620
LA JOLLA CA 92037-1620

1 SUNBURST RECOVERY INC
ATTN DR C YOUNG
P O BOX 2129
STEAMBOAT SPRINGS CO 80477

1 SVERDRUP TECHNOLOGY INC
ATTN R F STARR
P O BOX 884
TULLAHOMA TN 37388

1 SRI INTERNATIONAL
ATTN DR G R ABRAHAMSON
DR J GRAN
DR B HOLMES
333 RAVENWOOD AVENUE
MENLO PARK CA 94025

NO. OF COPIES	ORGANIZATION
1	BATTELLE TWSTIAC 505 KING AVENUE COLUMBUS OH 43201-2693
2	THINKING MACHINES CORPORATION ATTN G SABOT R FERREL 245 FIRST STREET CAMBRIDGE MA 02142-1264
1	CALIFORNIA INSTITUTE OF TECHNOLOGY ATTN T J AHRENS 1201 E CALIFORNIA BLVD PASADENA CA 91109
1	UNIVERSITY OF MINNESOTA ARMY OF HIGH PERF COMP RES CTR ATTN DR TAYFUN E TEZDUYAR 1100 WASHINGTON AVE SOUTH MINNEAPOLIS MN 55415
2	CDR ATTN SSCNC YSD J ROACH SSCNC WST A MURPHY US ARMY NRDEC KANSAS STREET NATICK MA 10760-5018
3	SOUTHWEST RESEARCH INSTITUTE ATTN DR C ANDERSON S MULLIN A B WENZEL P O DRAWER 28255 SAN ANTONIO TX 78228-0255
1	STATE UNIVERSITY OF NEW YORK MECHANICAL & AEROSPACE ENGRG ATTN DR PEYMAN GIVI BUFFALO NY 14260
2	DENVER RESEARCH INSTITUTE ATTN J WISOTSKI TECHNICAL LIBRARY P O BOX 10758 DENVER CO 80210
2	UNIVERSITY OF MARYLAND INSTITUTE FOR ADV COMPUTER STUDIES ATTN L DAVIS G SOBIESKI COLLEGE PARK MD 20742

NO. OF COPIES	ORGANIZATION
1	NORTHROP UNIVERSITY ATTN DR F B SAFFORD 5800 W ARBOR VITAE STREET LOS ANGELES CA 90045
1	STANFORD UNIVERSITY ATTN DR D BERSHADER DURAND LABORATORY STANFORD CA 94305

ABERDEEN PROVING GROUND

1	CDR USATACOM ATTN AMSTE-TE-F (L TELETSKI)
1	CDR USATHAMA ATTN AMSTH-TE
1	CDR USACSTA ATTN STEC-LI
5	DIR USARL ATTN AMSRL-SL-CM (BLDG E3331) AMSRL-WT-NC (R LOTTERO)(2 CP) AMSRL-WT-NC (A. MIHALCIN)(2 CP)

INTENTIONALLY LEFT BLANK.